UNIVERSITY OF CALIFORNIA, SAN DIEGO

Mechanisms of Regulation of Protein Kinase C and Its Tumor Suppressor Function in Cancer

A dissertation submitted in partial satisfaction of the requirements for the degree Doctor of Philosophy

in

Biomedical Sciences

by

Corina Elena Antal

Committee in charge:

Professor Alexandra C. Newton, Chair
Professor Seth J. Field
Professor Tony Hunter
Professor Renate Pilz
Professor Jing Yang

2015

The Dissertation of Corina Elena Antal is approved, and it is acceptable in quality and form for publication on microfilm and electronically:

_____

_____

_____

_____

_____

Chair

University of California, San Diego

2015

TABLE OF CONTENTS

LIST OF FIGURES

LIST OF TABLES

ACKNOWLEDGEMENTS

I would like to foremost express my sincere gratitude to my mentor, Alexandra Newton, for her guidance, support, and countless insightful discussions. I have been fortunate to have such a caring advisor who has been instrumental in my scientific development. I am very grateful for a *plethora* of opportunities she has bestowed upon me.

I would like to acknowledge my thesis committee members for all their helpful comments and suggestions. I would like to thank past and present members of the Newton Lab for their guidance and helpful discussions, particularly Maya Kunkel for her mentorship and invaluable input. I thank all my collaborators for their contributions, especially Tony Hunter and John Brognard for their critical scientific feedback. I express my appreciation to members of Jack Dixon's lab for scientific as well as career advice and for their generous sharing of their lab equipment.

Chapter 1, in part, is an adaptation of material that appears in "Tuning the signalling output of protein kinase C", as published in *Biochemical Society Transactions* 2014, and "Spatiotemporal dynamics of phosphorylation in lipid second messenger signaling" in *Molecular & Cellular Proteomics* 2013*,* both by Corina E. Antal and Alexandra C. Newton. The dissertation author was the primary author of these literature reviews.

Chapter 2, in full, is a reprint of the material as it appears in "Intramolecular Conformational Changes Optimize Protein Kinase C Signaling" by Corina E. Antal, Jonathan D. Violin, Maya T. Kunkel, Søs Skovsø, and Alexandra C. Newton, as published in *Chemistry & biology* in 2014. The dissertation author was the primary investigator and author of this paper.

Chapter 3, in full, has been submitted for publication of the material as it may appear in Cell, 2015, by Corina E. Antal, Julia A. Callender, Alexandr M. Kornev, Susan S. Taylor, and Alexandra C. Newton. The dissertation author was the primary investigator and author of the material.

Chapter 4, in full, is a reprint of material that appears in "Cancer-associated Protein Kinase C Mutations Reveal Kinase's Role as Tumor Suppressor" by Corina E. Antal, Andrew M. Hudson, Emily Kang, Ciro Zanca, Christopher Wirth, Natlaie N. Stephenson, Emily W. Trotter, Lissa L. Gallegos, Crispin J. Miller, Frank B. Furnari, Tony Hunter, John Brognard, and Alexandra C. Newton as published in *Cell in* 2015. The dissertation author was the primary investigator and author of the material.

VITA

2015 Doctor of Philosophy, University of California, San Diego

2009 Bachelor of Science, University of Miami

PUBLICATIONS

Antal, C.E., Hudson, A.M., Kang, E., Zanca, C., Wirth, C., Stephenson, N.L., Trotter, E.W., Gallegos, L.L., Miller, C.J., Furnari, F.B., Hunter, T., Brognard, J., and Newton, A.C. (2015) Cancer-associated Protein Kinase C Mutations Reveal Kinase's Role as Tumor Suppressor. ***Cell*** 160, 489-502

Antal, C. E., and Newton, A. C. (2014) Tuning the signalling output of protein kinase C. ***Biochemical Society transactions*** 42, 1477-1483

Antal, C. E., Violin, J. D., Kunkel, M. T., Skovso, S., and Newton, A. C. (2014) Intramolecular conformational changes optimize protein kinase C signaling. ***Chemistry & biology*** 21, 459-469

Antal, C. E., and Newton, A. C. (2013) Spatiotemporal dynamics of phosphorylation in lipid second messenger signaling. ***Molecular & cellular proteomics : MCP*** 12, 3498-3508

Scott, A. M., **Antal, C. E.**, and Newton, A. C. (2013) Electrostatic and hydrophobic interactions differentially tune membrane binding kinetics of the C2 domain of protein kinase Calpha. ***The Journal of biological chemistry*** 288, 16905-16915

de Lichtervelde, L., **Antal, C. E.**, Boitano, A. E., Wang, Y., Krastel, P., Petersen, F., Newton, A. C., Cooke, M. P., and Schultz, P. G. (2012) Euphohelioscopin A is a PKC activator capable of inducing macrophage differentiation. ***Chemistry & biology*** 19, 994-1000

Everett, M. V., **Antal, C. E.**, and Crawford, D. L. (2012) The effect of short-term hypoxic exposure on metabolic gene expression. ***Journal of experimental zoology. Part A, Ecological genetics and physiology*** **317**, 9-23

Gould, C. M., **Antal, C. E.**, Reyes, G., Kunkel, M. T., Adams, R. A., Ziyar, A., Riveros, T., and Newton, A. C. (2011) Active site inhibitors protect protein kinase C from dephosphorylation and stabilize its mature form. *The* ***Journal of biological chemistry*** 286, 28922-28930

ABSTRACT OF THE DISSERTATION

Mechanisms of Regulation of Protein Kinase C
and Its Tumor Suppressor Function in Cancer

by

Corina Elena Antal

Doctor of Philosophy in Biomedical Sciences

University of California, San Diego, 2015

Professor Alexandra C. Newton, Chair

The serine/threonine protein kinase C (PKC) family has been extensively studied over the last 35 years, yet fundamental questions regarding the regulation of its signaling and its dysregulation in disease remain unanswered. PKC is involved in a multitude of cellular processes and precise control of the amplitude of PKC signaling is essential for maintaining cellular homeostasis. This thesis expands on the knowledge of PKC at the molecular level by unveiling how intramolecular conformational changes tune the affinity of PKC for its ligands, and at the pathophysiological level by overturning a 30-year-old scientific dogma on the role

of PKC in cancer. First, mechanistic studies reveal that processing phosphorylations promote intramolecular interactions that clamp PKC in a closed conformation to prevent signaling in the absence of agonists, but allow efficient activation in response to small changes in agonist levels. These studies offer novel means of therapeutically targeting PKC with molecules or peptides that can either disrupt these interactions to activate PKC or maintain them closed to inhibit PKC activity. Second, analysis of PKC gene family mutations in human cancers reveals that they are loss-of-function, and that this loss-of-function confers a growth advantage, both *in vitro* and *in vivo*. These data suggest that therapies should focus on restoring, not inhibiting, PKC activity in the treatment of cancer. Taken together, this thesis identifies novel strategies to modulate PKC activity in therapies and, most importantly, establishes that PKC is a tumor suppressor.

CHAPTER 1 − INTRODUCTION

DIACYLGLYCEROL PATHWAY

The alteration of protein structure by phosphorylation is one of the most effective ways to transduce extracellular signals into cellular actions. Phosphorylation can alter enzyme activity, regulate protein stability, affect protein interactions or localization, or influence other post-translational modifications. A plethora of cellular processes, including cell proliferation, differentiation, and migration, are tightly regulated by phosphorylation. Cellular homeostasis is achieved by a precisely regulated balance between phosphorylation and dephosphorylation, with disruption of this balance resulting in pathophysiologies. Protein kinases and phosphatases are antagonist effector enzymes that mediate phosphorylation/dephosphorylation events.

Some kinases become activated upon binding lipid second messengers, which are signaling molecules produced in response to extracellular stimuli. A prominent lipid second messenger pathway is that mediated by diacylglycerol (DAG) (Figure 1A). DAG is produced upon activation of receptor tyrosine kinases (RTKs), non-receptor tyrosine kinases, and G-protein-coupled receptors (GPCRs) by agonists. These in turn activate phospholipase C (PLC), which hydrolyzes phosphatidylinositol 4,5-bisphosphate (PIP_2) found at the plasma membrane into the second messengers DAG and inositol 1,4,5-trisphosphate (IP_3) (Berridge, 1987). DAG recruits proteins that contain C1 domains, small globular DAG-binding domains, to membranes (Sharkey et al., 1984), while IP_3 freely diffuses inside the cell and binds to the IP_3 receptor in the endoplasmic reticulum (ER). This releases another second messenger, Ca^{2+}, which induces further production of DAG at the Golgi (Kunkel and Newton, 2010). Two main classes of proteins that bind DAG are protein kinase C (PKC) and protein kinase D (PKD), and the Rac-GAPs chimerins. DAG can also be generated from phosphatidic acid (PA) by phosphatidic acid phosphatases (PAPs) or sphingomyelin synthases (SMSs) (Figure 1B).

Removal of DAG and thus termination of its signaling is achieved by diacylglycerol kinases (DGK) that convert it into PA.

PKC AS AN EFFECTOR

The PKC family, effector kinases of DAG, transduces a multitude of signals that control diverse cellular processes such as proliferation, migration, invasion, differentiation, apoptosis, transcription, and translation. Therefore, aberrant PKC activity or localization has been linked to numerous diseases, most notably cancer, neurodegeneration, and diabetes (Dempsey et al., 2000). This serine/threonine kinase family belongs on the AGC kinase branch of the kinome (Manning et al., 2002) and comprises 9 genes that are divided into 3 categories based on the domain structure of the enzymes they encode, and hence the second messengers they require for activation. They all share a similar architecture with an N-terminal regulatory moiety and a C-terminal kinase domain (Figure 2). Conventional PKCs (cPKCs: α, β and γ) contain tandem C1 domains that bind DAG and phosphatidylserine (PS) and a C2 domain that binds anionic phospholipids, including phosphatidylinositol 4,5-bisphosphate (PIP_2) and PS, in a Ca^{2+}-dependent manner. Novel PKCs (nPKCs: δ, ε, η, θ) contain tandem C1 domains that bind DAG and a novel C2 domain that is Ca^{2+}-unresponsive and does not assist in membrane binding. Atypical PKCs (aPKCs: ι and ζ) have an atypical C1 domain that does not bind DAG and lack a C2 domain altogether, but instead contain a PB1 domain that mediates protein-protein interactions (Lamark et al., 2003). Atypical PKCs and PKCα also contain a C-terminal PDZ ligand that mediates protein-protein interactions and thus affects scaffolding and localization of these isozymes.

Regulation by priming phosphorylation

Phosphorylation is critical in 1] rendering PKC in a catalytically competent

conformation and 2] protecting PKC from degradation (Newton, 2003). In contrast to many other kinases, the phosphorylation of PKC is constitutive and thus, its activity is not acutely regulated by phosphorylation. Rather, cellular levels of PKC are directly regulated by its phosphorylation. Conventional and novel PKCs are constitutively phosphorylated at 3 conserved residues: the activation loop, the turn motif, and the hydrophobic motif (Keranen et al., 1995) (Figure 2). Atypical PKCs are also phosphorylated at the activation loop and turn motif, but contain a phosphomimetic glutamic acid at the hydrophobic motif. The first priming phosphorylation on PKC occurs at the activation loop within the kinase domain and is catalyzed by the phosphoinositide-dependent kinase, PDK-1 (Dutil et al., 1998a; Le Good et al., 1998). Phosphorylation at this site properly aligns residues within the active site for catalysis, an event that induces two tightly-coupled and ordered phosphorylations on the C-terminal tail: phosphorylation at the turn motif and intramolecular autophosphorylation at the hydrophobic motif. For conventional and novel PKCs such as PKCε, but not PKCδ, these phosphorylation events require mTORC2; however, whether mTOR is the direct kinase for this site in cells remains controversial (Behn-Krappa and Newton, 1999; Facchinetti et al., 2008; Guertin et al., 2006; Ikenoue et al., 2008). Phosphorylation at the hydrophobic motif controls the stability of the enzyme. Indeed, dephosphorylation of this site is the first step in the degradation of PKC as it destabilizes PKC and promotes its degradation. The PH domain leucine-rich repeat protein phosphatase (PHLPP) directly dephosphorylates the hydrophobic motif of PKCs, an event that requires the PH domain of PHLPP (Gao et al., 2008). Thus, loss of PHLPP in the cell leads to an increase in steady state PKC levels. Conversely, PKC levels are low in cells in which any of the phosphorylation steps have been perturbed, such as by loss of mTORC2 or PDK-1 (Balendran et al., 2000; Guertin et al., 2006). Thus, priming phosphorylations regulate the steady state levels of PKC but not its activity in an acute,

agonist-dependent manner; instead, the spatial and temporal dynamics of PKC signaling are regulated by second messengers.

Regulation by second messengers

Although phosphorylated PKC is catalytically competent, an N-terminal autoinhibitory pseudosubstrate binds the substrate-binding cavity intramolecularly, to maintain PKC in an inactive conformation until the appropriate second messengers bind. Conventional PKCs are allosterically activated by binding to two second messengers: Ca^{2+} and diacylglycerol (Figure 3A). Binding of Ca^{2+} to the C2 domain targets the kinase to the plasma membrane through 1] hydrophobic interactions that drive binding to the membrane and 2] electrostatic interactions with anionic phospholipids that contribute to retention of the C2 domain onto membranes (Scott et al., 2013b). This relocalization reduces the dimensionality in which the C1 domain has to probe for its membrane-embedded ligand, DAG, thus increasing the effectiveness of this search by several orders of magnitude (Nalefski and Newton, 2001). Once at the membrane, one of the C1 domains of PKC is positioned to find and bind DAG, an event that provides the necessary energy to expel the pseudosubstrate segment and activate PKC (Orr et al., 1992). Novel PKCs are activated solely by DAG (Figure 3B), whereas atypical PKCs do not respond to either of these second messengers and their activity is instead regulated by protein-protein interactions.

Differential binding of second messengers to conventional *vs*. novel PKCs leads to substantial differences in their spatiotemporal dynamics of signaling. Firstly, conventional and novel PKCs predominantly translocate to different membranes (Figure 3). Conventional PKCs translocate to, and are active at, the plasma membrane because their Ca^{2+}-bound C2 domain pre-targets them to the plasma membrane-localized lipid PIP_2, where they are retained following DAG binding (Scott et al., 2013b). Novel PKCs do not have a Ca^{2+}-sensing C2

domain to pre-target them to the plasma membrane; instead, their C1B domain has an approximately 100-fold higher affinity for DAG due to the presence of a Trp (W) at position 22 in the domain, compared to the C1B domain of conventional PKCs that contains a Tyr (Y) at that position (Figure 2) (Dries et al., 2007). Consequently, nPKCs translocate to DAG-rich endomembranes such as the Golgi. Indeed, impairing the Ca^{2+}-binding ability of the C2 domain of PKCα forces it to the Golgi instead, as the C1 domain interaction becomes the dominant force (Scott et al., 2013b). Secondly, the kinetics of activation differ between conventional and novel PKCs. Conventional PKCs display rapid but transient activity at the plasma membrane that tracks with the initial Ca^{2+} release (Gallegos et al., 2006). In fact, the kinetics of cPKC activation closely follow Ca^{2+} levels (Violin et al., 2003). PKCβII exhibits oscillatory translocation to the plasma membrane in response to Ca^{2+} oscillations produced by histamine stimulation of HeLa cells. This, in turn, leads to oscillatory phosphorylation of membrane-localized substrates that are phase locked with Ca^{2+} oscillations with a slight lag. Novel PKCs, on the other hand, are activated with slower kinetics because they do not respond to this fast Ca^{2+} release (Gallegos et al., 2006). Thirdly, the duration of PKC activity, which is partially controlled by the persistence of the second messengers at a particular subcellular location, also differs among the PKCs. For example, DAG levels are more sustained at the Golgi than the plasma membrane, leading to prolonged nPKC activity at the Golgi compared to the short-lived cPKC activity at the plasma membrane (Gallegos et al., 2006). Thus, second messengers precisely dictate the kinetics, magnitude, duration, and location of conventional and novel PKC activity and are responsible for the apparent differences between them.

PKC levels, and thus PKC activity, are exquisitely controlled by various mechanisms both under basal conditions and after agonist stimulation. Under basal conditions, the E3 ligase for PKC, RING-finger protein that interacts with C kinase (RINCK), controls the

amplitude of PKC signaling by regulating its levels (Chen et al., 2007). RINCK interacts with the C1A domain of PKC and induces its ubiquitination and thus its degradation. PKCα activity was also shown to be regulated, under basal conditions, through an interaction with diacylglycerol kinase ζ, which prevents its activation by locally metabolizing DAG (Luo et al., 2003). Only under stimulated conditions in which enough DAG is locally produced is PKCα activated, allowing it to phosphorylate diacylglycerol kinase ζ, thereby causing disassociation of the two proteins. However, agonist stimulation ultimately leads to termination of PKC signaling through various mechanisms. For example, PKC signaling is quickly terminated by the clearance of the respective second messengers, but also by agonist-induced downregulation of the enzyme. Several mechanisms control this downregulation. First, the peptidyl-prolyl isomerase Pin1 controls the isomerization of the turn motif (LTP), an event that is required to allow dephosphorylation of this site (Abrahamsen et al., 2012). Thus, Pin1 converts PKC into a downregulation-capable species. Second, this species of active PKC can be dephosphorylated by PHLPP (hydrophobic motif) causing it to be shunted to the detergent-insoluble fraction where it is further dephosphorylated by okadaic acid-sensitive phosphatases such as protein phosphatase 2A (activation loop and turn motif), ubiquitinated, and ultimately degraded by the proteasome (Lu et al., 1998). Agonist-induced proteasome-mediated degradation of PKCα can, however, also occur via ubiquitination of plasma membrane-localized, fully-primed PKC (Leontieva and Black, 2004; Lum et al., 2013a). Additionally, phosphorylated PKCα can also be internalized through lipid raft-mediated endocytic pathways and degraded by the lysosome (Leontieva and Black, 2004; Lum et al., 2013b). These mechanisms desensitize PKC signaling by regulating its levels, thus providing another means of exquisite control.

Regulation independent of second messengers

Particular conventional and novel PKCs can also be activated independently of second messengers, adding to the complexity of PKC signaling. For example, certain PKCs can be activated by the accumulation of reactive oxygen species, which are often elevated in diseases such as cancer, cardiovascular disease, and neurodegeneration (Rahman, 2007). Specifically, H_2O_2 causes oxidation of cysteine residues within the C1B domain of PKCγ, inducing conformational changes that release PKCγ from its scaffold, leading to its translocation to the plasma membrane and subsequent DAG-independent activation (Lauer et al., 2010; Lin and Takemoto, 2005). PKCδ is phosphorylated at multiple tyrosine residues by Src family kinases in response to acute stimulation of cells by H_2O_2, epidermal growth factors, or platelet-derived growth factor. Tyrosine phosphorylation can induce the DAG-independent activation of PKCδ, in the absence of membrane translocation, and can alter its subcellular localization (Konishi et al., 1997; Konishi et al., 2001). For example, tyrosine phosphorylation of PKCδ at Tyr64 and Tyr155 in response to apoptotic stimuli, such as H_2O_2 and etoposide, induces a conformational change that exposes its nuclear localization sequence and chaperone-binding site, allowing its import into the nucleus where it can induce apoptosis (Adwan et al., 2011). H_2O_2-induced tyrosine phosphorylation at Tyr311 has also been proposed to activate PKCδ by inducing caspase-3 cleavage between its regulatory and catalytic domains, resulting in a nuclear-localized, uninhibited catalytic domain (Kaul et al., 2005). Therefore, these agonist-induced phosphorylations and conformational changes can activate PKCs independently of second messengers by either releasing PKCs from scaffolds or by exposing binding sites for scaffolds to bind.

Regulation by scaffolding

Scaffolding also plays an integral part in determining the precise location, duration,

and amplitude of PKC activity, as well as in establishing substrate specificity. Even though lipid second messengers acutely regulate the activity of PKC, scaffolds can mediate access to particular substrates. Considering that there are multiple PKC isozymes expressed in the same cell that are activated by the same stimuli, scaffolds provide a level of functional selectivity. Protein scaffolds coordinate and allow specificity and fidelity by compartmentalizing kinases and their downstream substrates, as well as the phosphatases that can rapidly terminate the signal (Scott and Newton, 2012). Among the PKC scaffolds are receptors for activated C kinase (RACK) (Ron et al., 1994; Ron et al., 1995; Stebbins and Mochly-Rosen, 2001), 14-3-3 proteins (Kostelecky et al., 2009; Nguyen et al., 2004), and A-kinase anchoring proteins (AKAPs) (Akakura et al., 2010; Hoshi et al., 2010).

Although multiple PKC isozymes respond to the same second messengers, there is some specificity in their function and signaling mediated in part by their cell-specific pattern of expression, their differential affinities for certain lipids, and by protein scaffolds. PKC is anchored to numerous protein scaffolds through interactions mediated by its regulatory domain, pseudosubstrate, or, in the case of PKCα and the aPKCs, a PDZ ligand. Particular scaffolds augment PKC signaling whereas others inhibit it. The first PKC scaffolds were identified by Mochly-Rosen and colleagues as receptors for activated C kinase (RACKs), which are proposed to selectively bind active PKC and enhance its activity towards substrates anchored at that location (Csukai et al., 1997; Ron et al., 1994). For PKCβII, this interaction occurs via its C2 domain and C-terminal tail and it stabilizes PKC's active conformation, thus enhancing its activity towards co-scaffolded substrates (Ron et al., 1994; Ron et al., 1995; Stebbins and Mochly-Rosen, 2001). The phosphoserine/threonine binding protein 14-3-3 binds to a pair of phosphoserines within the hinge region of PKCε, leading to its activation (Kostelecky et al., 2009). However, scaffolds can also be inhibitory towards PKC by

sequestering it away from its substrates or maintaining it in an inactive conformation. For example, in lens epithelial cells, 14-3-3ε binds PKCγ's C1B domain and controls both its activity and localization, thus regulating gap junction activity (Nguyen et al., 2004). A subset of (AKAPs), which were first identified as PKA scaffolds (Hirsch et al., 1992), also anchor PKC in proximity to its targets, but in its inactive state, thus enabling rapid downstream signaling upon PKC activation. For example, AKAP12 binds to and attenuates PKCα and PKCδ signaling, thereby preventing senescence (Akakura et al., 2010). Similarly, AKAP5 inhibits PKC activity by binding to its catalytic pocket (Hoshi et al., 2010).

PKCα, ζ, and ι also bind PDZ domain-containing scaffolds through their distinct PDZ ligands. In the case of PKCα, scaffolding by its PDZ ligand is required for cerebellar long-term depression (Leitges et al., 2004). One likely PDZ domain-binding partner involved in this is protein interacting with Cα kinase (PICK1), which interacts specifically with the PDZ ligand of PKCα (Staudinger et al., 1997; Staudinger et al., 1995). Interestingly, PICK1 can have opposing roles in PKCα function in neurons, where it can act as either a mediator or an inhibitor of phosphorylation of downstream targets. PICK1 targets activated PKCα to synapses to phosphorylate the glutamate receptor subunit GluR2 leading to its endocytosis (Perez et al., 2001), but can also act as a barrier to phosphorylation of the metabotropic glutamate receptors mGluR7a by PKCα (Dev et al., 2000). More recently, a family of Discs large homolog (DLG) scaffolds that interacts with the PDZ ligand of PKCα to facilitate cellular migration has also been identified (O'Neill et al., 2011).

Scaffolds can also regulate the duration of PKC activity towards a substrate by co-scaffolding a phosphatase of the substrate. The phosphatase can thus rapidly dephosphorylate and attenuate signaling downstream of PKC substrates. Such an example is the coordination of PKC and protein phosphatase 2B/calcineurin on AKAP79/150 at the postsynaptic density in

neurons (Klauck et al., 1996). Another AKAP (AKAP350/AKAP450) was proposed to act as a scaffold for the maturation of PKC (Takahashi et al., 2000). This AKAP only associates with nascent PKCε at the Golgi/centrosome and this complex disassembles after PKCε maturation by phosphorylation. Interestingly, this complex also contains protein phosphatase 2A (Takahashi et al., 1999), which dephosphorylates PKC leading to its degradation. Perhaps PKC levels are dynamically controlled on this scaffold through regulation of its phosphorylation. Scaffolding of PKC also has clinical relevance because scaffolds have been shown to change the pharmacological prolife of PKC. Specifically, ATP-competitive inhibitors were found to be ineffective against scaffolded PKC (Hoshi et al., 2010). To explain how scaffolds amplify, accelerate, and insulate PKC signaling, Greenwald et al. (Greenwald et al., 2014) proposed a stochastic state-switching model. In this model, the complex containing PKC, its substrate, and its scaffold alters between inactive and active intermediate states, thus allowing phosphorylation of the substrate, even in the presence of active-site PKC inhibitors. Accordingly, scaffolds are able to precisely control PKC activity and to confer functional selectivity.

MONITORING PKC ACTIVITY IN LIVE CELLS

Genetically encoded reporters allow the visualization of the spatiotemporal dynamics of kinase activity in individual cells. These reporters can be targeted to various subcellular localizations and to protein scaffolds to measure localized activity, which can be more physiologically relevant than simply measuring bulk activity in the cytosol.

Because cPKCs and nPKCs are constitutively phosphorylated at the C-terminal sites, and because the phosphate at the activation loop does not modulate activity once the C-terminal tail is phosphorylated (Keranen et al., 1995), their activity cannot be measured with phosphorylation-specific antibodies, as is done for most other kinases. However, PKC activity

can be monitored using activity reporters such as the C Kinase Activity Reporter (CKAR; Figure 4A), which is composed of a CFP-YFP FRET pair flanking a PKC specific substrate and an FHA2 phosphothreonine-binding domain (Violin et al., 2003). Upon phosphorylation of this substrate by PKC, the reporter undergoes a conformational change that decreases FRET. As phosphorylation of the reporter is reversible (i.e. phosphatases can dephosphorylate the reporter), it provides a real-time read-out of PKC activity.

CKAR has been targeted to various intracellular locations to specifically monitor PKC activity at these regions. Using these targeted reporters, Gallegos et al. (Gallegos et al., 2006) found that activation of PKC with the natural agonist UTP, leads to rapid and relatively sustained PKC activity at the Golgi, driven by the persistence of DAG at this membrane. UTP-dependent PKC activity in the cytosol is, however, quickly terminated by phosphatases, whereas activity in the nucleus is low because of high phosphatase suppression in this compartment. The mitochondria also has little UTP-stimulated activity; however, using a mitochondrially-targeted PKCδ-specific activity reporter, Mito-δCKAR, Wu-Zhang et al. (Zheng et al., 2012) revealed that PKCδ translocates to, and is active at, the outer membrane of mitochondria upon stimulation with phorbol esters, and that its intrinsic catalytic activity is required for its interaction with the mitochondria.

The Schultz lab has developed a reporter for nPKCs and aPKCs, KCP-1 (Figure 4B), that is based on the PKC substrate pleckstrin (Schleifenbaum et al., 2004). This reporter does not utilize a phosphopeptide-binding domain; rather, phosphorylation of residues between its PH and DEP (Dishevelled, Egl-10, pleckstrin) domains causes a conformational change in the reporter, resulting in a change in FRET. Thus, interactions between the phosphorylated sites and other endogenous proteins are reduced.

CONCLUSIONS

Considering the involvement of PKC in prominent diseases such as cancer, neurodegeneration, cardiomyopathies, and diabetes, PKC has been a sought after drug target. Therefore, understanding its regulation at the molecular level and its role in these diseases could lead to novel means of targeting this enzyme for therapeutic purposes. This thesis discusses a novel mode of regulation of PKC signaling: conformation changes. In Chapters 2 and 3, we show that conformational changes and intradomain interactions maintain PKC in a closed conformation until the proper second messengers are present. These studies provide novel means of modulating PKC through regulating its intradomain interactions. In Chapter 4, we present a surprising role of PKC in cancer. We show evidence that PKC acts as a tumor suppressor and should, therefore, be inhibited in the treatment of cancer.

ACKNOWLEDGMENTS

We thank members of the lab for helpful suggestions. This work was supported by the National Institutes of Health (GM43154) to A.C.N. C.E.A. was supported in part by the National Science Foundation Graduate Research Fellowship (DGE1144086) and by the UCSD Graduate Training Program in Cellular and Molecular Pharmacology through an institutional training grant from the National Institute of General Medical Sciences (T32 GM007752).

Chapter 1, in part, is an adaptation of material that appears in "Tuning the signalling output of protein kinase C", as published in *Biochemical Society Transactions* 2014, and "Spatiotemporal dynamics of phosphorylation in lipid second messenger signaling" in *Molecular & Cellular Proteomics* 2013, both by Corina E. Antal and Alexandra C. Newton. The dissertation author was the primary author of these literature reviews.

FIGURES

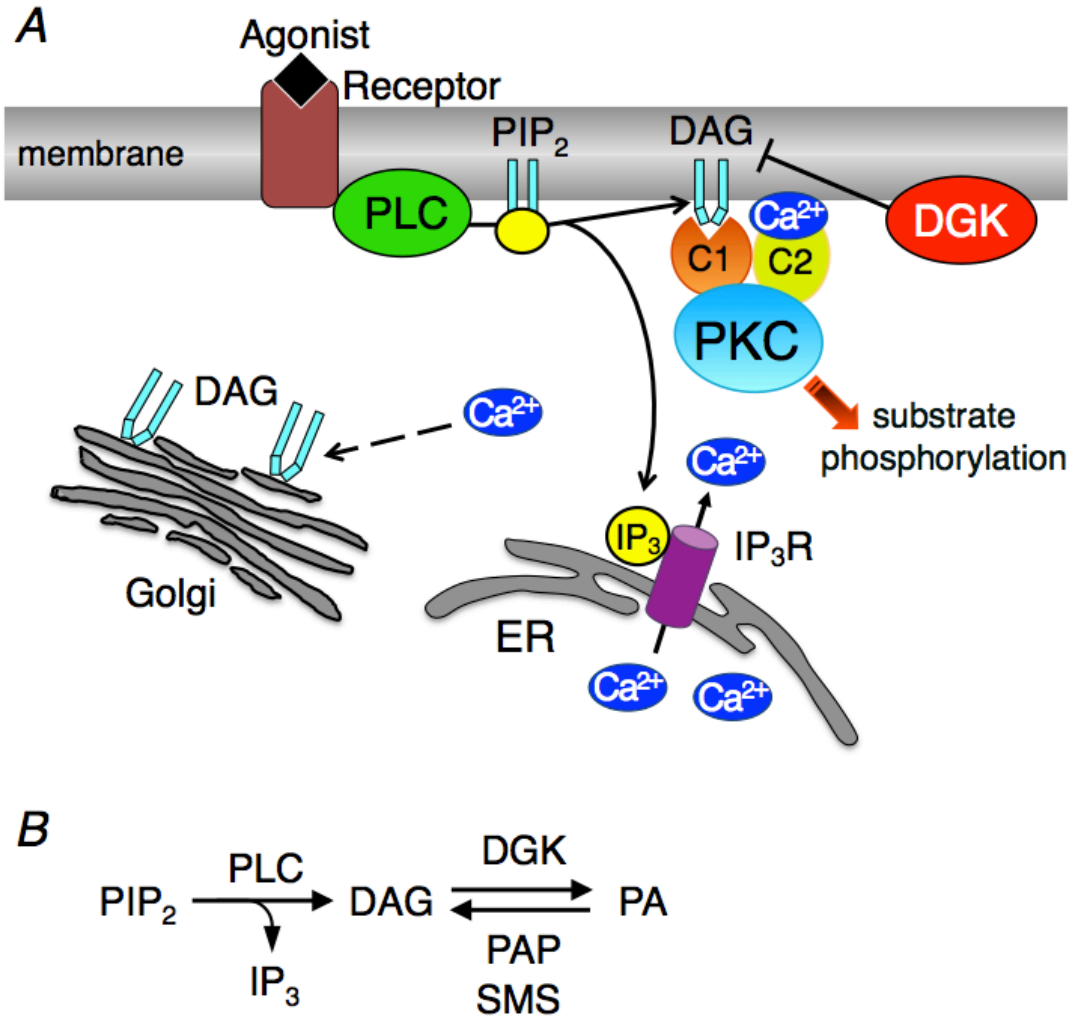

Figure 1. Diagram of diacylglycerol and PIP_3 signaling pathways
(A) Agonist stimulation activates cell surface receptors such as receptor tyrosine kinases or G-protein coupled receptors, which active phospholipase C (PLC), which acts on phosphatidylinositol 4,5-bisphosphate (PIP_2). PLC hydrolyzes PIP_2 to produce diacylglycerol (DAG) and inositol triphosphate (IP_3). IP_3 binds to the IP_3 receptor (IP_3R) at the endoplasmic reticulum (ER), releasing Ca^{2+}. DAG and Ca^{2+} recruit conventional protein kinase C (PKC) to the plasma membrane (via its C1 and C2 domains, respectively) and activate it. Ca^{2+} release also leads to the production of DAG at the Golgi. Diacylglycerol kinase (DGK) suppresses DAG-mediated signaling by converting DAG to phosphatidic acid (PA). (B) Enzymes involved in DAG production and removal. PIP_2 can be converted to DAG and IP_3 by PLC. DAG can then be removed by DGKs as it gets converted to PA. Phosphatidic acid phosphatases (PAPs) and sphingomyelin synthases (SMSs) convert PA back to DAG.

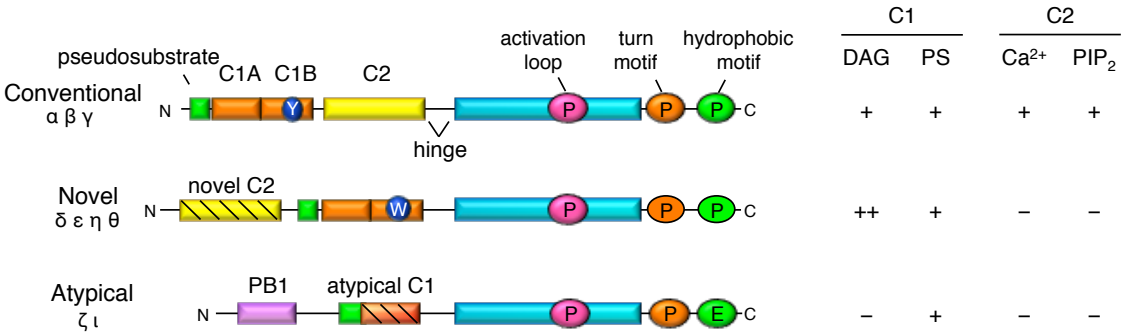

Figure 2. Schematic showing domain composition of three classes of protein kinase C

Conventional PKCs (α, β, and γ) contain an N-terminal pseudosubstrate (green), tandem C1 domains (orange) that bind diacylglycerol (DAG) and phosphatidylserine (PS), a C2 domain (yellow) that binds anionic phospholipids, including phosphatidylinositol 4,5-bisphosphate (PIP_2), in a Ca^{2+}-dependent manner, and a C-terminal kinase domain (cyan). Novel PKCs (δ, ε, η, and θ) have a similar domain composition except that their C2 domain cannot bind Ca^{2+} or PIP_2 and their C1B domain has ~100-fold higher affinity for DAG due to having a Trp (W) at position 22 in the domain, as opposed to a Tyr (Y) as the C1B domain of cPKCs has. Atypical PKCs (ζ and ι) have a protein-binding module, the PB1 domain, and an atypical C1 domain that cannot bind DAG. All PKCs are phosphorylated at 3 conserved sites: the activation loop within the kinase domain and the turn and hydrophobic motifs within the C-terminal tail (except for atypical PKCs which have a phosphomimetic Glu at the hydrophobic motif). The table on the right summarizes the second messengers bound by each of the classes of PKC, with + representing binding, ++ representing binding with ~100-fold higher affinity, and – representing lack of binding.

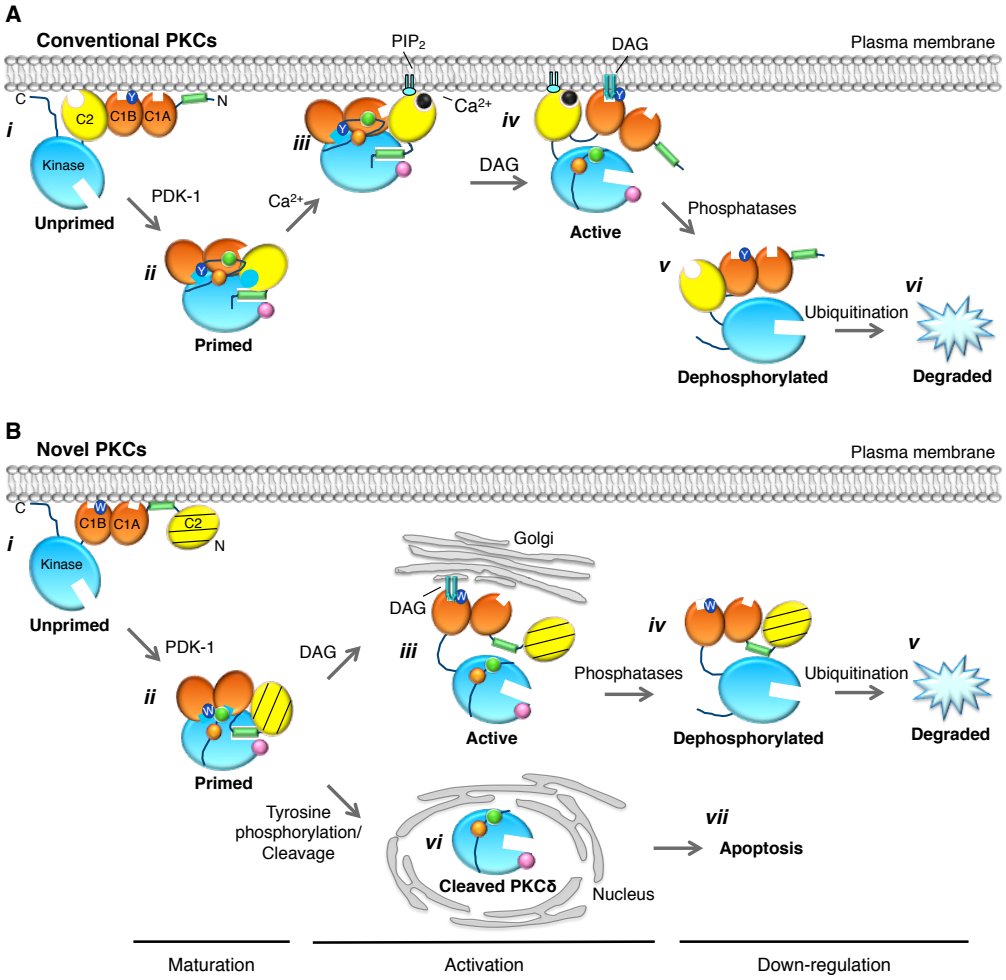

Figure 3. Regulation of conventional and novel protein kinase C

(A) Model showing life cycle of conventional PKC (cPKC). *i* Unprimed cPKC is in a membrane-associated, open conformation in which both its C1A and C1B domains are fully exposed. *ii* Upon priming phosphorylation at its activation loop (pink circle) by PDK-1, followed by phosphorylation at the turn motif (orange circle) and the hydrophobic motif (green circle), cPKC matures into a closed conformation in which both the C1A and C1B domains become masked, the pseudosubstrate binds the substrate-binding site, and the primed enzyme localizes to the cytosol. This masking of the C1 domains prevents pretargeting of cPKC to membranes in the absence of agonist-evoked increases in DAG, thus preventing basal signaling. *iii* In response to agonists that promote PIP_2 hydrolysis, cPKC is recruited to the plasma membrane in a Ca^{2+}-dependent manner. *iv* This pretargeting to the plasma membrane facilitates binding to DAG, predominantly via the C1B domain, which expels the pseudosubstrate from the substrate-binding cavity, thereby activating PKC. *v* Dephosphorylation of activated cPKC allows it to regain the open conformation of unprimed PKC. *vi* Ubiquitination of cPKCs leads to its proteasome-mediated degradation, thus terminating signaling. (B) Model showing life cycle of novel PKC (nPKC). Unprimed nPKC is also in an open conformation that associates with membranes. *ii* Priming phosphorylations induce a closed conformation with both C1 domains masked. *iii* In response to agonists that produce DAG, nPKC is recruited to and activated at the DAG-rich Golgi via its higher DAG affinity C1B domain (due to the presence of a Trp (W) at position 22 within the domain). *iv* Activated nPKC is dephosphorylated, *v* ubiquitinated and degraded. *vi* The novel PKCδ can also be activated by tyrosine phosphorylation and caspase cleavage. *vii* Nuclear-localized PKCδ can induce apoptosis.

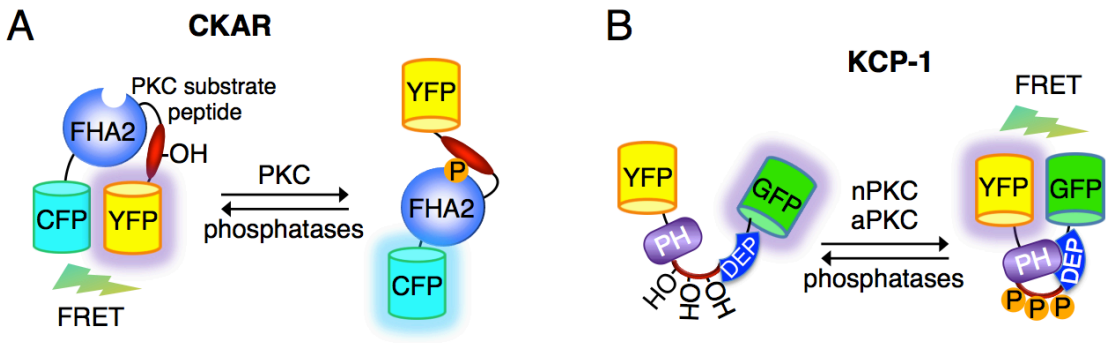

Figure 4. Genetically encoded reporters for measuring PKC activity
(A) The PKC reporter, CKAR, is made up of an FHA2 domain, a PKC specific substrate peptide, and a CFP-YFP FRET pair. When phosphorylated, the substrate sequence binds the FHA2 domain and this conformational change results in a decrease in FRET. (B) The nPKC and aPKC reporter KCP-1 is based on the PKC substrate pleckstrin. PKC phosphorylation at three sites between the PH and DEP domains of pleckstrin results in a conformational change that increases FRET between enhanced YFP and GFP2.

CHAPTER 2 − INTRAMOLECULAR CONFORMATIONAL CHANGES OPTIMIZE PROTEIN KINASE C SIGNALING

ABSTRACT

Optimal tuning of enzyme signaling is critical for cellular homeostasis. We use fluorescence resonance energy transfer reporters in live cells to follow conformational transitions that tune the affinity of a multi-domain signal transducer, protein kinase C, for optimal response to second messengers. This enzyme comprises two diacylglycerol sensors, the C1A and C1B domains, whose intrinsic affinity for ligand is sufficiently high that the enzyme would be in a ligand-engaged, active state if not for mechanisms that mask its domains. We show that both diacylglycerol sensors are exposed in newly-synthesized protein kinase C and that conformational transitions following priming phosphorylations mask the domains such that the lower affinity sensor, the C1B domain, is the primary diacylglycerol binder. Protein kinase C's conformational rearrangements serve as a paradigm for how multi-module transducers optimize their dynamic range of signaling.

INTRODUCTION

The use of modules to build recognition in signal transducing proteins is at the crux of signaling networks (Pawson, 1995, 2007). The serine/threonine kinase, protein kinase C (PKC), epitomizes the use of multiple modules to effectively respond to second messengers. Intramolecular interactions control both the accessibility of the active site to substrate and of the regulatory modules to the second messengers (Oancea and Meyer, 1998; Orr and Newton, 1994; Stensman and Larsson, 2007). PKC isozymes are critical in processing signals that drive cellular functions such as proliferation, apoptosis, and differentiation (Griner and Kazanietz, 2007a; Newton, 2010). Correctly tuning PKC output is essential for cellular homeostasis and, as such, its dysregulation is associated with a myriad of diseases, including cancer, metabolic disorders, and neurodegeneration. Key to regulation of the signaling output of most PKC isozymes is the ability of cytosolic enzyme to respond to the membrane-embedded lipid

second messenger, diacylglycerol (DAG), in a dynamic range that prevents signaling in the absence of agonists but allows efficient signaling in response to small changes in DAG.

PKC isozymes are classified based on their membrane-targeting domains (Newton, 2010). cPKCs (Figure 5A; PKCα, PKCβ, and PKCγ) contain tandem C1 domains (cysteine-rich zinc finger domains), that bind DAG or their functional analogs, phorbol esters (Sharkey et al., 1984), and a C2 domain that requires phosphatidylinositol-4,5-bisphosphate (PIP_2) as well as phosphatidylserine for Ca^{2+}-dependent plasma membrane targeting (Corbalan-Garcia et al., 2003; Corbin et al., 2007; Evans et al., 2006; Konig et al., 1985a). Novel PKC (nPKC) isozymes (PKCδ, PKCε, PKCη, PKCθ) also have tandem C1 domains, but lack a functional C2 domain (Cho and Stahelin, 2006). nPKC isozymes efficiently respond to DAG production without the need for Ca^{2+}-dependent pre-targeting to the plasma membrane because their affinity for DAG is almost two orders of magnitude higher than that of cPKCs. The C2 domains of the novel PKCδ and PKCθ bind proteins containing phosphotyrosine, which for PKCθ is an activating event (Benes et al., 2005; Stahelin et al., 2012). Atypical PKCs (PKCι/λ and PKCζ) respond to neither Ca^{2+}, nor DAG, and protein scaffold interactions likely regulate their function (Kazanietz et al., 1994).

When first synthesized, PKC is in an open conformation, with its autoinhibitory pseudosubstrate out of the substrate-binding cavity (Dutil and Newton, 2000). This species of PKC is membrane-associated (Borner et al., 1989; Sonnenburg et al., 2001), but inactive. Catalytic competence requires maturation of PKC by ordered phosphorylation at three highly conserved sites: the activation loop, the turn motif, and hydrophobic motif (Newton, 2003). The first phosphorylation occurs at the activation loop by PDK-1 and positions the active site for catalysis (Dutil et al., 1998; Grodsky et al., 2006; Le Good et al., 1998). This phosphorylation triggers phosphorylation at the turn motif, which anchors the C-terminal tail

onto the N-lobe of the kinase, conferring stability (Hauge et al., 2007). Turn motif phosphorylation, which is necessary for catalytic function, triggers intramolecular autophosphorylation of the hydrophobic motif (Behn-Krappa and Newton, 1999; Edwards et al., 1999). Phosphorylation at this site is not required for activity but helps align the αC helix of the kinase domain for catalysis and thus supports optimal activity and stability (Gao et al., 2008; Yang et al., 2002). Processing by phosphorylation depends on a conserved PXXP motif (P616/P619 in PKCβII; Figure 5B) within PKC that binds the chaperone heat shock protein 90 (Gould et al., 2009); mutation of either of these Pro residues results in a kinase that is not phosphorylated and is thus inactive. Processing phosphorylations are also absent in other kinase-inactive PKC mutants, presumably because autophosphorylation is prevented (Behn-Krappa and Newton, 1999). Lastly, processing phosphorylations depend on the integrity of the mTORC2 kinase complex by an unknown mechanism (Facchinetti et al., 2008; Ikenoue et al., 2008).

Mature PKC is released to the cytosol, where it adopts an autoinhibited conformation with the pseudosubstrate bound within the substrate-binding site. Membrane engagement of the C1 and C2 domains of cPKCs, or just the C1 domain for nPKCs, induces a conformational change that expels the pseudosubstrate, activating PKC (Orr and Newton, 1994). Why PKC has two tandem C1 domains is not clear considering that only one of the C1 domains engages the membrane at a time (Kikkawa et al., 1983; Konig et al., 1985b). Several studies have shown that for the novel PKCδ, the C1B domain is the predominant membrane-binding domain (Pu et al., 2009; Szallasi et al., 1996; Wu-Zhang et al., 2012). However, it remains to be elucidated which C1 domain of PKCβII is the predominant membrane binder.

Here we use fluorescence energy transfer (FRET)-based imaging to visualize conformational transitions of cPKCs and nPKCs in live cells. Using a PKC conformation

reporter, Kinameleon, we show that PKCβII undergoes conformational transitions as it matures, becomes activated, and downregulated. In addition, analysis of membrane translocation kinetics reveals that the ligand-binding surface of the C1 domains of PKC become masked during the maturation of the enzyme. This occurs through intramolecular interactions and tunes the affinity of mature PKC for optimal response to second messengers. This mechanism is commonly employed by other enzymes to optimize their dynamic range of signaling, and thus visualization of conformational rearrangements within PKC serves as a paradigm for signaling by other multi-module transducers.

RESULTS

Maturation of cPKC retards agonist-dependent membrane translocation kinetics

We have previously shown that the integrity of a PXXP motif in PKCβII (P616/P619) is required for the proper phosphorylation and folding of PKC (Gould et al., 2009). In imaging studies co-expressing PKCβII-RFP and PKCβII-P616A/P619A-YFP in the same cell, we observed that the kinase-dead PKC translocated to the plasma membrane more rapidly than wild-type in response to phorbol dibutyrate (PDBu), a PKC agonist (Figure 5C, left panels). To determine whether this accelerated translocation was caused by lack of catalytic activity, we examined the translocation of two additional constructs whose active site had been altered to inhibit catalysis (Figure 5B). In PKCβII-K371R, the conserved Lys that coordinates the α-β phosphates of ATP was mutated (Buechler et al., 1989; Ohno et al., 1990) and in PKCβII-D466N, the conserved Asp that serves as the catalytic base in the phosphorylation reaction was mutated. This latter construct retains the ability to autophosphorylate weakly but cannot phosphorylate substrates (Gould et al., 2011; Shi et al., 2010). As observed for the PXXP mutant, both catalytically impaired constructs fully translocated to plasma membrane after 2.5

min PDBu treatment, whereas the wild-type enzyme, in the same cell, was primarily cytosolic and required 12.5 min for membrane translocation (Figure 5B). All three kinase-dead mutants were partially localized at the plasma membrane prior to stimulation. Thus, impairing PKCβII activity by three independent mechanisms resulted in pretargeting to the plasma membrane and accelerated agonist-induced membrane translocation compared to wild-type.

To assess whether phosphorylation per se, or the ordered conformation changes that accompany maturation caused the delayed translocation kinetics of wild-type PKCβII, we evaluated the phosphorylation state of the constructs used in the translocation assays. We took advantage of the mobility shift on Western blots induced by quantitative phosphorylation at the C-terminal tail (Keranen et al., 1995). Under the conditions of our experiments, PKCβII migrated predominantly (67%) as an upper mobility band, reflecting phosphorylation at the two C-terminal priming sites (Figure 5D, lane 1, asterisk); approximately a third of the protein was not phosphorylated (lower band, dash). The kinase-inactive mutants PKCβII-K371R and PKCβII-P616A/P619A were completely unphosphorylated (Figure 5D, lanes 2 and 4). In contrast to these kinase-dead PKC mutants, the PKCβII-D466N showed equal amounts of phosphorylated (52%) and unphosphorylated (48%) species (Figure 5D, lane 3). Thus, the translocation kinetics of PKC were unrelated to the state of processing phosphorylations: wild-type PKCβII, with 67% phosphorylated species, and PKCβII-D466N, with 52% phosphorylated species, translocated with significantly different kinetics. These data reveal that the conformation of the kinase-impaired PKCβII-D466N does not recapitulate the ordered conformational transitions accompanying the maturation of wild-type PKC, despite permissive phosphorylation. In summary, catalytically-inactive constructs of PKC have accelerated membrane translocation, independently of their phosphorylation state.

Kinameleon: a probe for conformational transitions of PKC in cells

One possibility for the accelerated membrane association of kinase-inactive PKC compared with wild-type is that unprimed PKC is in a different conformation from mature PKC. To probe for conformational differences between these two species, we engineered a FRET-based conformational reporter we named Kinameleon (for the changing colors depending on conformation). Kinameleon (Figure 6A) comprises a CFP and YFP flanking the N- and C-terminus, respectively, of wild-type PKCβII (Kinameleon-WT) or the kinase-inactive PKCβII-K371R (Kinameleon-K371R). A similar approach has been used for PKCδ, and this construct was shown to behave like untagged PKCδ (Braun et al., 2005). When expressed in MDCK (Madin-Darby canine kidney) cells, unphosphorylated, kinase-dead Kinameleon-K371R, exhibited a significantly lower basal FRET ratio than mature, phosphorylated Kinameleon-WT, as illustrated by the raw pseudocolor FRET ratio image (Figure 6B). Upon 15 min stimulation with PDBu, Kinameleon-WT translocated to plasma membrane and FRET increased further, consistent with an additional conformational rearrangement upon activation. Following 12 hours PDBu treatment to promote dephosphorylation of PKC, FRET decreased to levels similar to those of Kinameleon-K371R. Quantitation of the FRET ratios (FRET/CFP) as a function of time revealed that the FRET ratio for Kinameleon-WT approached that of the unprimed Kinameleon-K371R following 12 hours of PDBu stimulation (Figure 6C). The FRET increase resulted, in part, from intermolecular FRET between Kinameleons concentrated at the plasma membrane; however, this only accounted for a small portion of the increase observed because control cells co-expressing YFP-PKCβII-YFP and CFP-PKCβII-CFP displayed a more modest increase (Figure 6D; compare upper to lower panel). These data are consistent with a model (Figure 6A) in which the N- and C-termini of PKC are oriented for low FRET in unprimed

PKC, they re-orient to yield intermediate FRET upon maturation of PKC, they are repositioned for high FRET upon activation of PKC, and they regain their original orientation (low FRET) following dephosphorylation.

Translocation kinetics of isolated C1A-C1B domains of PKC can be tuned by a single residue

We have previously shown that a Trp at position 22 within the C1A or C1B domain (Figures 5A and 7A) confers an almost two orders of magnitude higher affinity for DAG than a Tyr at that position (Dries et al., 2007). In cPKCs, Trp is present in the C1A (Trp 58; high affinity for DAG) and Tyr in the C1B (Tyr 123; low affinity for DAG). Here we take advantage of this toggle to selectively tune the affinity of the C1A and/or C1B domains within cPKCs as a tool to differentiate between them. We monitored the rate of translocation of the isolated C1A-C1B domain to membranes as a function of whether Tyr or Trp was present at position 22. We used our previously developed Diacylglycerol Reporter, DAGR (Violin et al., 2003) that contains the tandem C1A-C1B domain of PKCβ flanked by CFP and YFP. Translocation of this reporter to the plasma membrane can be quantified by the increase in intermolecular FRET from CFP to YFP as the DAGR reporters become concentrated at the membrane. In response to PDBu, the isolated C1A-C1B domain translocated to the plasma membrane with a half-time of 0.82 ± 0.02 min (Figure 7B). Reducing the C1A domain's affinity for ligand by mutating Trp58 to a Tyr (C1A-C1B-W58Y) resulted in a 5-fold reduction in the rate of translocation of the C1A-C1B domain to the plasma membrane ($t_{½}$ = 3.69 ± 0.04 min) compared to wild-type. This effect could be rescued by increasing the affinity of the C1B domain for ligand: the double mutant C1A-C1B-W58Y/Y123W displayed similar translocation kinetics to wild-type. Increasing the C1B domain's affinity for ligand (C1A-C1B-Y123W) while leaving the high affinity of the C1A domain unchanged, resulted in

pretargeting of the domain to the plasma membrane and Golgi (Dries et al., 2007). It was previously shown that the Y123W mutation does not perturb the structure of the C1B domain (Stewart et al., 2011), indicating that the domain is not pretargeted to membranes and unable to translocate because it is misfolded; rather its intrinsic affinity for membranes is so high that it likely binds basal levels of DAG. Moreover, the isolated C1A-C1B domain has a relatively high affinity for phorbol esters since sub-saturating levels of PDBu (50 nM) that were insufficient to maximally translocate full length PKCβII (see Figure 8D) were sufficient to cause full translocation of the C1A-C1B domain to the plasma membrane (Figure 7D*)*. These data are consistent with the C1A and C1B moieties of the C1A-C1B module being fully accessible for membrane engagement: Tyr at the toggle position of either domain reduces the rate of translocation, whereas Trp at either position increases the rate of translocation. Moreover, constructs with Tyr in one moiety and Trp in the other moiety have similar translocation kinetics, independently of whether the Tyr is in the C1A or C1B.

Unprimed PKC has an exposed C1A-C1B domain that is masked upon proper maturation

Using FRET, we quantified the translocation kinetics of YFP-tagged cPKCs towards plasma membrane-targeted CFP. PKCβII translocated to the plasma membrane in response to PDBu with significantly slower kinetics than the isolated C1A-C1B domain (Figure 8A; t½ = 3.56 ± 0.02 min versus 0.82 ± 0.02 min). In contrast, the unphosphorylated PKCβII-K371R and PKCβII-P616A/P619A mutants translocated with rates that matched those of the isolated C1A-C1B domain (t½ = 0.35 ± 0.07 min and t½ = 0.63 ± 0.05 min, respectively). These data are consistent with both C1A and C1B moieties being fully exposed in these mutants, whereas one or the other (or both) becomes masked in the properly primed wild-type PKCβII. PKCβII-D466N (t½ = 0.53 ± 0.07 min) also translocated with kinetics similar to those of the isolated C1A-C1B domain, suggesting that even though about 52% of the pool of PKCβII-D466N is

phosphorylated, it is not properly folded. Next we examined whether the C1A-C1B domain of another cPKC, PKCα, was also masked during maturation. The corresponding PKCα kinase-dead mutant, PKCα-K368M, migrated as an unphosphorylated species on a PAGE gel (Figure 8B, lanes 2 and 4, dash) whereas 52% of the pool of PKCα-D463N was phosphorylated at the C-terminal sites (Figure 8B, compare lanes 1 and 3), same as for PKCβII-D466N. Yet both of these kinase-dead PKCα mutants (PKCα-K368M t½ = 0.82 ± 0.02 min; PKCα-D463N t½ = 1.26 ± 0.01 min) responded more rapidly to PDBu than wild-type (t½ = 9.18 ± 0.01 min) (Figure 8C), showing that the trend of fast translocation of kinase-dead PKCs is a common phenomenon among cPKCs. These data corroborate that the kinase-dead PKCβII-D466N and PKCα-D463N do not adopt the conformation of wild-type enzyme despite being partially phosphorylated. Thus, cPKCs undergo a conformational change upon proper PKC maturation, which masks the ligand-binding surface of the C1A-C1B domain, leading to a slower translocation of primed PKC compared to unprocessed PKC or to the isolated C1A-C1B domain.

As an additional measure of whether the C1A-C1B domain becomes masked upon maturation we examined membrane binding induced by sub-saturating concentrations of phorbol esters (50nM). Whereas the C1A-C1B domain fully translocated to the plasma membrane upon 50 nM PDBu, less than 50% of the pool of monitored full-length, wild-type PKCβII translocated (Figure 8C compared to Figure 7D). However, all the kinase-dead PKCβIIs maximally translocated, (Figure 7D), suggesting that these unprimed or improperly primed mutants have a lower threshold for PDBu activation resulting from fully exposed ligand-binding surfaces on their C1A-C1B domains.

Both the C1A and C1B domains of unphosphorylated PKC are exposed and become masked upon priming

Conventional and novel PKCs have two functional C1 domains, yet only one of the domains is engaged on the membrane at a time (Giorgione et al., 2003; Kikkawa et al., 1983). To dissect the respective contribution of each domain on driving translocation of PKCβII, we addressed the effect of altering the ligand affinity of the C1A and C1B domains on ligand-dependent membrane translocation. We first examined the phorbol ester-dependent membrane translocation, and then the DAG-dependent translocation (see below), as the differences in affinity for these two ligands vary greatly between the domains. Specifically, the affinity of the C1A domain for DAG is almost two orders of magnitude higher than that of the C1B domain, whereas for PDBu, the difference in affinity is only 6-fold (Dries et al., 2007). To this end, we altered the affinity of the C1A or C1B domain by mutating the residue at position 22 within full-length PKCβII. A Trp to Tyr mutation in the C1A domain (PKCβII-W58Y) did not affect translocation kinetics (Figure 9A), which consistent with the ligand-binding surface of the C1A domain being occluded within primed PKCβII. In contrast, the translocation kinetics of the kinase-dead PKCβII-W58Y/K371R (Figure 9B; t½ = 1.38 ± 0.04 versus 0.35 ± 0.07 min) and PKCβII-W58Y/D466N (Figure 9C; t½ = 1.55 ± 0.04 versus 0.52 ± 0.04 min) were sensitive to mutation of the C1A domain, revealing that the C1A domain is exposed in these mutants. To further show that this single residue can dictate the translocation kinetics of full-length kinase-dead PKC, we inverted the DAG affinities of the C1A (from high to low) and C1B domains (from low to high) in a kinase inactive construct. This PKCβII-W58Y/Y123W/D466N mutant translocated with similar kinetics to that of PKCβII-D466N (Figure 9C; t½ = 0.49 ± 0.06 min vs. 0.52 ± 0.04 min), supporting the finding that both domains are exposed in this improperly processed PKC and revealing that these mutations do

not affect the folding of the C1 domains. Moreover, these results show that it does not matter whether the higher affinity domain is positioned before or after the lower affinity domain. Curiously, the PKCβII-W58Y/P616A/P619A (0.71 ± 0.03 min) mutant did not display slower kinetics of translocation than PKCβII-P616A/P619A (0.63 ± 0.05 min) (Figure 9D), suggesting that this mutant may be folded differently from the other kinase-inactive ones. These data reveal that the ligand-binding surface of both C1A and C1B domains are exposed in unprocessed PKC and that the C1A domain becomes occluded during maturation.

We next addressed whether the C1B domain is exposed in matured PKCβII. There was no difference between PKCβII and PKCβII-Y123W (Figure 9A), indicating that the ligand-binding surface of the C1B domain is also masked in the fully matured PKC. However, the C1B domain is fully exposed in the kinase dead mutants, as evidenced by the mutants constitutive association with the plasma membrane and the Golgi (Figure 9E, top panels), similarly to the C1A-C1B-Y123W domain mutant (Figure 7C). These mutants displayed no further translocation to the plasma membrane with PDBu treatment (Figure 9E, bottom panels).

To further validate that both the C1A and C1B domains are exposed in unprocessed PKC, we examined the effect of preventing processing of the novel PKCδ, which contains two high-affinity C1 domains as it has Trp at position 22 in both domains (Figure 5A). The kinase-dead PKCδ-K376R and PKCδ-D471N were constitutively associated with the plasma membrane and Golgi (Figure 9E), consistent with exposure of two high affinity DAG binders causing constitutive membrane interaction. These data reveal that unprimed mutants of both conventional and novel PKCs have exposed ligand-binding surfaces in their C1A and C1B domains and that these surfaces become occluded through intramolecular conformational changes as PKC matures.

Both the C1A and C1B domains are involved in membrane binding, but the C1B domain dominates

The insensitivity of mature PKC towards changes in ligand affinity of the C1A or C1B domain toward PDBu could reflect the use of saturating concentrations of this potent ligand, such that 6-fold differences in ligand affinity between Trp versus Tyr at position 22 might be undetectable. To address this, we used a much lower affinity ligand, DAG, to test whether stimulation with sub-saturating levels of the synthetic DAG, 1,2-Dioctanoyl-sn-glycerol (DiC8) could reveal a difference between PKCβII and PKCβII in which the affinity of either the C1A or C1B domain has been altered. Modifying the affinity of either the C1A or C1B domain altered the steady-state levels of PKCβII bound to the DiC8-containing plasma membrane (and thus the amplitude of translocation): decreasing the affinity of the C1A domain (PKCβII-W58Y) lowered the amplitude of translocation by 13%, whereas increasing the affinity of the C1B domain (PKCβII-Y123W) increased the amplitude by 20% (Figure 10). In comparison, the unprimed PKCβII-D466N mutant translocated maximally and with much faster kinetics than wild-type enzyme upon DiC8 treatment, reflecting two highly exposed C1 domains. These data further sustain that properly primed PKCβII has its ligand-binding surfaces on both its C1A and C1B domains masked and that the improperly primed PKCβII-D466N mutant's translocation does not mimic that of WT PKCβII.

DISCUSSION

Here we use genetically-encoded reporters to show that maturation of PKCβII by phosphorylation triggers conformational changes that set the ligand affinity of the enzyme for optimal signaling. The paradigm of intramolecular interactions tuning the ligand binding affinity to increase the dynamic range of a signaling molecule is employed by numerous

multi-domain enzymes. For example, the Src family of tyrosine kinases displays intramolecular interactions between its kinase domain and its phospho-Tyr binding SH2 domain and PXXP-recognizing SH3 domain to maintain the kinase in an inactive conformation (Boggon and Eck, 2004; Hof et al., 1998). In this case, the enzyme's affinity for its domains is sufficiently low to allow intermolecular ligands to effectively compete and allow signal transduction. Similarly, intramolecular interactions of the PH and Ras-association domains of the Rap1-interacting adapter molecule restrain their ability to bind membranes (Wynne et al., 2012). This also seems to be the case for the PH domain of Akt (Astoul et al., 1999), consistent with intramolecular interactions lowering the affinity of its PH domain for membranes to optimize its signaling.

Extensive studies have established that PKC is matured by phosphorylation, but the role of phosphorylation in structuring the enzyme for signaling is not known. Partial crystal structures of PKC have been solved (Grodsky et al., 2006; Guerrero-Valero et al., 2009; Leonard et al., 2011; Xu et al., 1997); however, little information exists on conformational rearrangements. Using Kinameleon, we show that unprocessed PKC and PKC that has been dephosphorylated following prolonged activation are both in an open conformation that is distinct from the closed conformation of mature, but inactive, PKC. Analysis of translocation kinetics reveal that the ligand-binding surfaces of the C1A and C1B domains are fully exposed in this open conformation but become masked upon maturation by phosphorylation. Our data are consistent with the partial PKCβII structure, which shows that phosphorylation anchors the carboxyl-terminal tail of PKC onto the top of its N-lobe where it interacts with the C1B domain (Leonard et al., 2011), preventing this domain from easily accessing DAG. Our data also corroborate work from Larsson and colleagues showing that the membrane translocation of kinase-dead PKCα-K368M is much more sensitive to DAG than wild-type PKCα

(Stensman et al., 2004). They propose that only the C1A domain of PKCα is masked through intramolecular interaction between the C-terminal tail and the C2 domain (Stensman and Larsson, 2007), whereas our data are more consistent with both C1A and C1B domains of PKCβII becoming masked. This masking of the C1 domains likely occurs in all cPKCs and some of the nPKCs; the C1 domains of PKCγ were also shown to be occluded in the full length protein (Oancea and Meyer, 1998) and here we show PKCδ's C1 domains are also masked, consistent with a study by Stahelin et al. (Stahelin et al., 2004). We also demonstrate that species of PKC with impaired catalytic activity remain in the open conformation regardless of phosphorylation status: although half of the pool of PKCβII-D466N or PKCα-D463N is phosphorylated, the translocation kinetics of these kinase-dead mutants are identical to those of the isolated C1A-C1B domain, not those of wild-type PKC, suggesting that these kinase-inactive PKCs are not folded like wild-type PKC. We note caution should be taken when using kinase-dead mutants because they do not provide the same scaffolding structure as wild-type, their translocation is much more sensitive to DAG and, in the case of nPKCs, they are localized differently from wild-type, a finding consistent with work from the Steinberg lab (Guo et al., 2010). It is also noteworthy that gross overexpression of PKC allows a pool of PKC to remain unprocessed and thus more readily associate with membranes. In summary, our data are consistent with a model in which phosphorylation triggers a series of ordered conformational transitions, by a mechanism that requires the intrinsic catalytic activity of PKC, that masks the C1 domains such that the lower affinity DAG sensor, the C1B domain, is used for PKCβII.

The stoichiometry of ligand binding of full length PKC is one mole DAG/phorbol ester per mole PKC (Kikkawa et al., 1983; Konig et al., 1985b), and kinetic studies have established that there is no cooperativity in binding DAG (Hill coefficient = 1), as would be

expected from the reduction in dimensionality of engaging the second C1 domain once the first one has engaged on the membrane (Hannun and Bell, 1986; Mosior and Newton, 1998a; Newton and Koshland, 1989). Yet whether the C1A or C1B dominates as the DAG sensor in PKCβII has not been well established. To distinguish between the contributions of these domains, we engineered PKCβII mutants in which we toggled the affinity of each C1 domains for ligand. Inverting the affinities of the C1A and C1B domains for ligand had no apparent effect on PDBu-induced PKC translocation rates (Figure 9A), likely because this switch has a modest effect on phorbol ester binding and because saturating concentrations of PDBu were used. Importantly, stimulation with sub-saturating levels of DAG, which exhibits an almost two orders of magnitude higher affinity for the C1A versus C1B domain (Dries et al., 2007), uncovered a difference (Figure 10). Decreasing the affinity of the C1A domain for ligand lowered the steady-state levels of PKCβII bound to the plasma membrane, whereas increasing the affinity of the C1B domain increased the steady-state levels bound to the membrane, suggesting that both domains can be involved in membrane binding. The altered membrane affinities are likely caused by changes in the membrane dissociation rate, as we have previously shown that mutants with lower affinities for DAG have increased membrane dissociation rate constants (Dries and Newton, 2008). However, reducing the affinity of the C1A domain for DAG by almost 100-fold only decreased steady-state binding by two-fold. If this were the dominant binding domain, the steady-state levels should have decreased by at least an order of magnitude more. This suggests that the C1B is the predominant binding domain for PKCβII. Here, increasing the membrane affinity by 100-fold increased steady-state levels also by two-fold; this is less than expected but consistent with the C1B domain being masked in the full-length wild-type enzyme. Moreover, our data show that both the C1A and

C1B domains are exposed in kinase-dead PKCs, because toggling the affinity of either domain had a significant effect on their translocation kinetics.

Based on these studies on PKC conformation, we build on the model for PKC maturation (Figure 11). We propose that unprimed PKC is in an open conformation that associates with membranes (Sonnenburg et al., 2001) through weak interactions with the pseudosubstrate (Mosior and McLaughlin, 1991), C1 and C2 domains (Johnson et al., 2000), and C-terminal tail (Yang and Igumenova, 2013). Both the C1A and C1B domains are exposed and the pseudosubstrate is out of the active site (Dutil and Newton, 2000; Johnson et al., 2000) (Figure 11A). Upon ordered phosphorylation of PKC at its three priming sites, PKC matures into its closed conformation in which the ligand-binding surface of both the C1A and C1B domains becomes masked and the pseudosubstrate occupies the substrate-binding cavity (Figure 11B). Thus PKCs are maintained in an inactive, closed conformation by intramolecular interactions induced by phosphorylation. Upon activation, cPKCs translocate to membranes by a two-step mechanism (Nalefski and Newton, 2001): first, binding of Ca^{2+} to the C2 domain mediates its binding to the membrane through electrostatic and hydrophobic interactions (Scott et al., 2013) (Figure 11C). Since the C2 domain of cPKC has a high affinity for PIP_2, which is enriched within the plasma membrane compared to other membranes, cPKCs preferentially translocate to this membrane (Evans et al., 2006; Ferrer-Orta et al., 2009; Guerrero-Valero et al., 2009; Marin-Vicente et al., 2005). Engagement of the C2 domain in the membrane not only reduces the dimensionality of the C1A or C1B domain search for DAG, but also leads to intramolecular conformational changes (Stahelin and Cho, 2001) that allow the C1A and C1B domains to become slightly more exposed (Bittova et al., 2001). Secondly, binding of either the C1A or the C1B domain, but predominantly the C1B domain for PKCβII (Figure 11D), to DAG, expels the pseudosubstrate and activates PKC. Use of this

lower affinity C1B domain as the primary membrane localization module for cPKCs allows PKC to respond accordingly to a wider range of DAG levels at the plasma membrane. Upon activation, PKC is quickly dephosphorylated and thus transitions back to its exposed (open) conformation of unprimed PKC (Figure 11E).

In summary, our data reveal an elegant mechanism by which intramolecular conformational transitions tune the affinity of mature PKC for its allosteric activator, DAG, as a regulatory mechanism to allow ultrasensitivity in the signaling output of PKC (Figure 12). We have previously shown that the binding of PKC to membranes displays high cooperativity with respect to phosphatidylserine (Newton and Koshland, 1989; Orr and Newton, 1992). Thus, by reducing the affinity of both conventional and novel PKCs for membranes through conformational transitions induced during maturation, basal signaling of these isozymes is minimized. Indeed, without this masking by maturation, isozymes such as the novel PKCδ that has two high affinity C1 domains would be constitutively pretargeted to the plasma membrane and the Golgi; for these isozymes, masking of the C1 domains is necessary to prevent constitutive association of PKC with membranes and thus constitutive activity. The mature enzyme conformation does, however, enable PKCs to respond effectively to very small changes in DAG. Moreover, basal signaling of PKCβII is further attenuated through the preferential use of the lower affinity DAG sensor, the C1B domain, which allows cPKCs to signal at different membranes from nPKCs. The affinity of the C1B domain for DAG is too low to allow cPKCs to sense agonist-evoked changes in this second messenger without pre-targeting by the Ca^{2+}-regulated C2 domain (Dries et al., 2007); therefore, cPKCs are directed to the plasma membrane via the PIP_2-sensing C2 domain where they can then find DAG. In contrast, nPKCs, which have a higher affinity C1B domain, translocate to the most DAG-enriched membrane, the Golgi, without the need for pre-targeting. Thus, masking of the C1A

domain in cPKCs tunes the affinity of PKC to reduce basal signaling, increase the dynamic range of the PKC signal, and determine the membrane to which PKC is recruited.

SIGNIFICANCE

In this manuscript, we follow conformational transitions in living cells to unveil a key regulatory mechanism in cell signaling: tuning of ligand affinity by intramolecular conformational changes. Specifically, we use FRET-based reporters, in live cells, to show how a multi-domain signal transducer, PKC, undergoes conformational transitions upon phosphorylation-induced maturation that tune the affinity of its DAG-binding C1A and C1B domains for optimal signaling. Importantly, we show that these conformational transitions keep PKC inactive under basal conditions, but allow ultrasensitivity in responses to small changes in agonist-evoked levels of DAG. Conformational rearrangements that optimize the dynamic range of signaling will likely serve as a paradigm for signaling by many other multi-module transducers. Our FRET-based methods to visualize these changes in living cells are applicable to the vast array of multi-module signal transducers.

EXPERIMENTAL PROCEDURES

Plasmid Constructs

C-terminally tagged rat PKCβII-YFP (Dries et al., 2007), rat PKCβII-RFP (Gould et al., 2009), mouse PKCδ-YFP (Wu-Zhang et al., 2012), DAGR, bovine PKCα-HA, and membrane-targeted CFP were described previously (Violin et al., 2003). Kinameleon was cloned into pcDNA3 as YFP-PKCβII-CFP and Kinameleon-K371R was generated by QuikChange site-directed mutagenesis (Stratagene). A C1A-C1B construct containing the N-terminus of rat PKCβII (residues 1-156) was subcloned into DAGR. Bovine YFP-PKCα was

generated by subcloning PKCα into pcDNA3 with YFP at the N-terminus. All mutants were generated by QuikChange site-directed mutagenesis (Stratagene).

Antibodies and Materials

The mouse monoclonal anti-HA antibody (HA.11, clone 16B12) was purchased from Covance, the mouse monoclonal anti-β-actin antibody (A2228) was purchased from Sigma-Aldrich, and the mouse monoclonal anti-PKCβ antibody (610128) was from BD Transduction Laboratories. Phorbol 12,13-dibutyrate (PDBu) and 1,2-Dioctanoyl-sn-glycerol (DiC8) were obtained from Calbiochem. The 1X Hanks' Balanced Salt Solution was purchased from Cellgro. All other materials and chemicals were reagent grade.

Cell Culture, Transfection, and Immunoblotting

COS7 cells were maintained in DMEM (Cellgro) containing 5% or 10% fetal bovine serum (Gibco) and 1% penicillin/streptomycin (Gibco) at 37 °C in 5% CO_2. MDCK cells were cultured in DMEM/F-12 50/50 (Cellgro) containing 10% FBS and 1% penicillin/streptomycin. Transient transfection of COS7 was carried out using the jetPRIME transfection reagent (PolyPlus Transfection) or the FuGENE 6 transfection reagent (Roche Applied Science) for ~24h. MDCK cells were transiently transected using PolyFect (Qiagen) for ~36h. Cells were lysed in 50 mM Tris, pH 7.4, 1% Triton X-100, 50 mM NaF, 10 mM $Na_4P_2O_7$, 100 mM NaCl, 5 mM EDTA, 1 mM Na_3VO_4, 1 mM PMSF, and 50 nM Okadaic acid. Whole cell lysates were analyzed by SDS-PAGE and Western blotting via chemiluminescence on a FluorChem imaging system (Alpha Innotech).

FRET Imaging and Analysis

Cells were plated onto glass coverslips in 35 mm dishes, transfected with the indicated constructs, and imaged in Hanks' Balanced Salt Solution supplemented with 1 mM $CaCl_2$.

CFP, YFP, and FRET images were acquired with a 40X objective with a Zeiss Axiovert microscope (Carl Zeiss Microimaging) using a MicroMax digital camera (Roper-Princeton Instruments) controlled by MetaFluor software version 6.1r6 (Universal Imaging Corporation) as described previously (Gallegos et al., 2006). Pseudocolor images were acquired at the indicated times before and after treatment with 200 nM PDBu and normalized to the same min and max values. For the translocation experiments, base-line images were acquired every 7 or 15 sec for 3 or more min before ligand addition. Because the maximal amplitude of translocation of the mutants varied, possibly due to changes in the orientation or distance of the fluorophores caused by differential folding of the kinase, the data were normalized to the maximal amplitude of translocation for each cell. Normalization was achieved by dividing by the average base-line FRET ratio, and then scaled from 0 to 100 % of maximal translocation using the equation: $X = (Y-Y_{min})/(Y_{max}-Y_{min})$, where Y = normalized FRET ratio, Y_{min} = minimum value of Y, and Y_{max} is maximum value of Y. Data from at least three different imaging dishes were referenced around the ligand addition time point and the average of these normalized values ± SEM were plotted and curve fitted. Curve fitting was performed using Graph Pad Prism 6.0a (GraphPad Software Inc., CA, USA). The half-time of translocation was calculated by fitting the data to a non-linear regression using a one-phase exponential association equation.

ACKNOWLEDGMENTS

We thank Alyssa Wu-Zhang, Emily Kang, and Timothy R. Baffi for technical assistance. This work was supported by NIH GM43154 to ACN. CEA and JDV were supported in part by the UCSD Graduate Training Program in Cellular and Molecular Pharmacology (T32 GM007752). CEA was supported in part by the NSF Graduate Research Fellowship (DGE1144086).

Chapter 2, in full, is a reprint of the material as it appears in "Intramolecular Conformational Changes Optimize Protein Kinase C Signaling" by Corina E. Antal, Jonathan D. Violin, Maya T. Kunkel, Søs Skovsø, and Alexandra C. Newton, as published in *Chemistry & biology* in 2014. The dissertation author was the primary investigator and author of this paper.

FIGURES

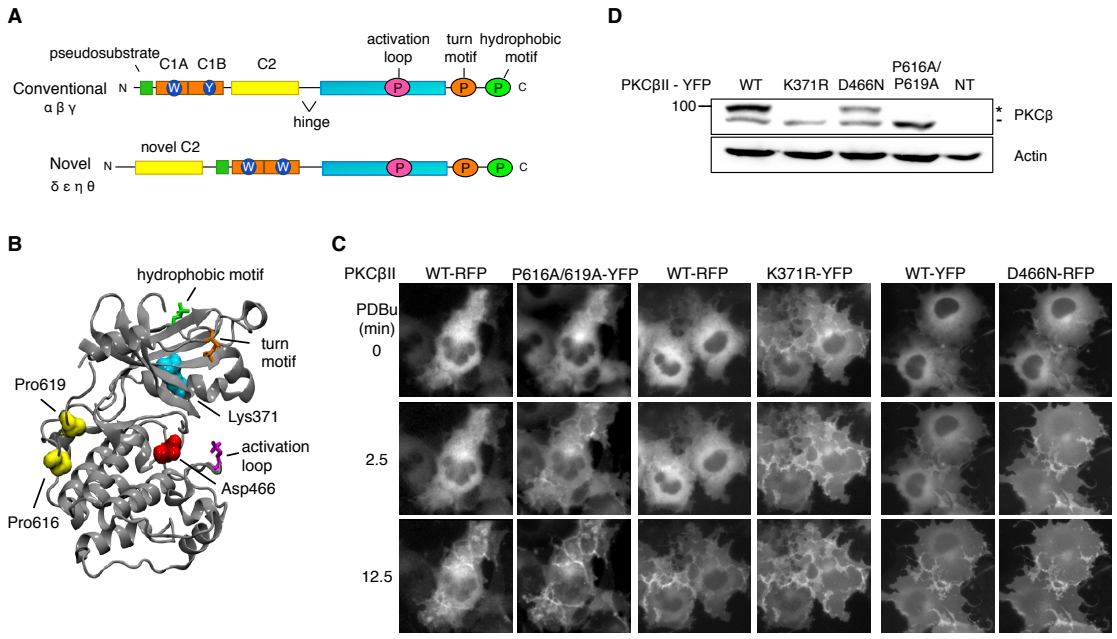

Figure 5. Maturation of PKC retards agonist-dependent membrane translocation kinetics.
(A) Schematic of cPKCs and nPKCs showing domain composition with the C1A and C1B domains (orange) and the C2 domain (yellow). The W and Y are the Trp and Tyr residues at position 22 within the C1A (W58 in PKCβII) or C1B (Y123 in PKCβII) domains of cPKCs that dictate membrane affinity. nPKCs contain Trp at both of these sites. The kinase domain (cyan) and the three priming phosphorylations are shown: the activation loop, turn motif, and hydrophobic motif. (B) Ribbon structure of the kinase domain of PKCβII (PDB ID 2I0E) showing the three priming phosphorylations in stick form (Thr500, activation loop; Thr641, turn motif; Ser600, hydrophobic motif) and the kinase-inactivating mutations (Lys371 and AspD466 in the active site and Pro616 and Pro619 in the PXXP motif) in ball form. (C) Representative images displaying localization of the indicated YFP- and RFP-tagged PKCs, co-transfected into COS7 cells, before (top), after 2.5 min (middle), or after 12.5 min (bottom) of PDBu treatment are shown. (D) Western blot displaying whole-cell lysates of COS7 cells transfected with the indicated PKCβII constructs. The *asterisk* denotes the position of mature, fully phosphorylated PKCβII, and the *dash* denotes the position of unphosphorylated PKCβII.

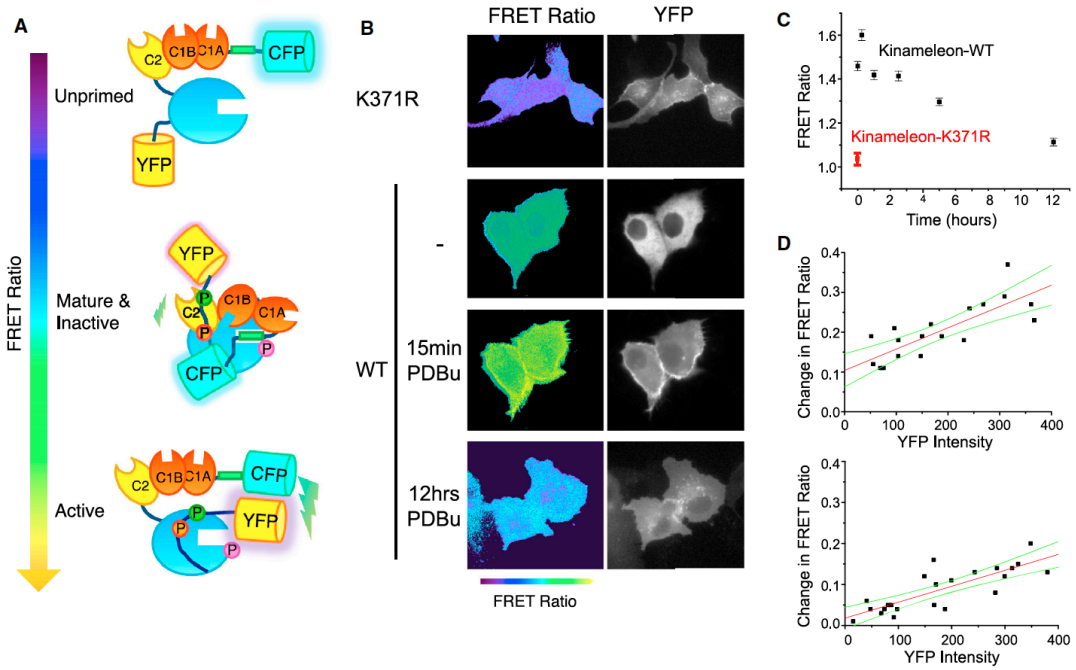

Figure 6. An intramolecular FRET reporter reads conformational transitions of PKC in live cells. (A) Diagram of Kinameleon showing CFP on N-terminus and YFP on C-terminus of PKC; schematic of how very low FRET reflects an unprimed conformation (upper panel), intermediate FRET reflects a mature (phosphorylated at the activation loop in pink, turn motif in orange, and hydrophobic motif in green) but inactive conformation (middle panel), and high FRET reflects an active conformation (lower panel). (B) Pseudocolor FRET ratio images (left) and localization (right) of MDCK cells transiently expressing Kinameleon-K371R (representing unprocessed PKC), Kinameleon-WT (representing mature, phosphorylated, but inactive PKC), Kinameleon-WT after 15 min of PDBu treatment (representing mature, active PKC), and Kinameleon-WT after 12 hrs of PDBu treatment (representing dephosphorylated PKC), report different PKC conformations. (C) Quantitation of the FRET ratios ± SEM of Kinameleon-WT post PDBu treatment of cells and of Kinameleon-K371R in the absence of PDBu treatment. (D) Kinameleon expressed in MDCK cells and stimulated with 200 nM PDBu results in increased FRET, shown as a change in the FRET ratio (upper panel). The increasing FRET change with higher expression levels (linear regression in red, with 95% confidence bands in green) indicates an intermolecular (concentration dependent) interaction. The non-zero y-intercept indicates an intramolecular (concentration-independent) interaction, consistent with a conformational change upon translocation. In contrast, co-expression of CFP-PKCβII-CFP and YFP-PKCβII-YFP show only an intermolecular interaction after 200 nM PDBu (lower panel).

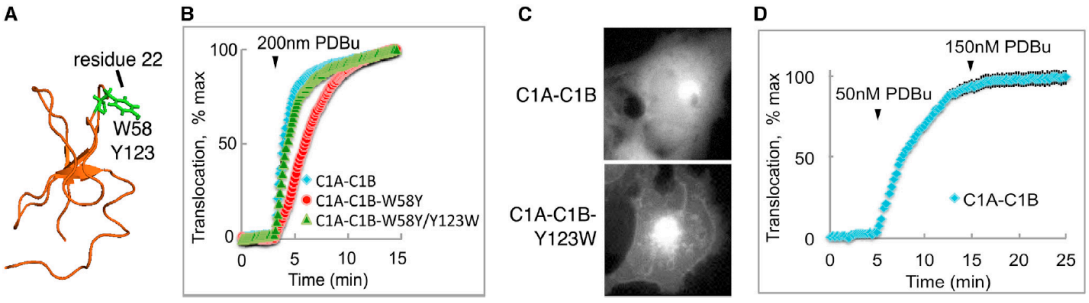

Figure 7. Translocation kinetics of the isolated C1A-C1B domain of PKCβII can be tuned by a single residue.

(A) Ribbon structure of the C1B domain of PKCα (PDB ID 2ELI) showing the DAG affinity toggle, Tyr at position 22 in the domain (Tyr123 in PKCα and PKCβ). This residue is present as Trp (Trp58) in the C1A domain of PKCα and PKCβ. (B) COS7 cells transfected with the indicated C1A-C1B constructs flanked by CFP and YFP were monitored for their intermolecular FRET ratio ± SEM upon PDBu stimulation. (C) Representative YFP images of the basal localization of wild-type or mutant C1A-C1B domains. (D) Trace showing translocation kinetics of the C1A-C1B domain ± SEM with sub-saturating levels of phorbol esters (50 nM PDBu), followed by saturating amounts of PDBu to yield a final concentration of 200 nM.

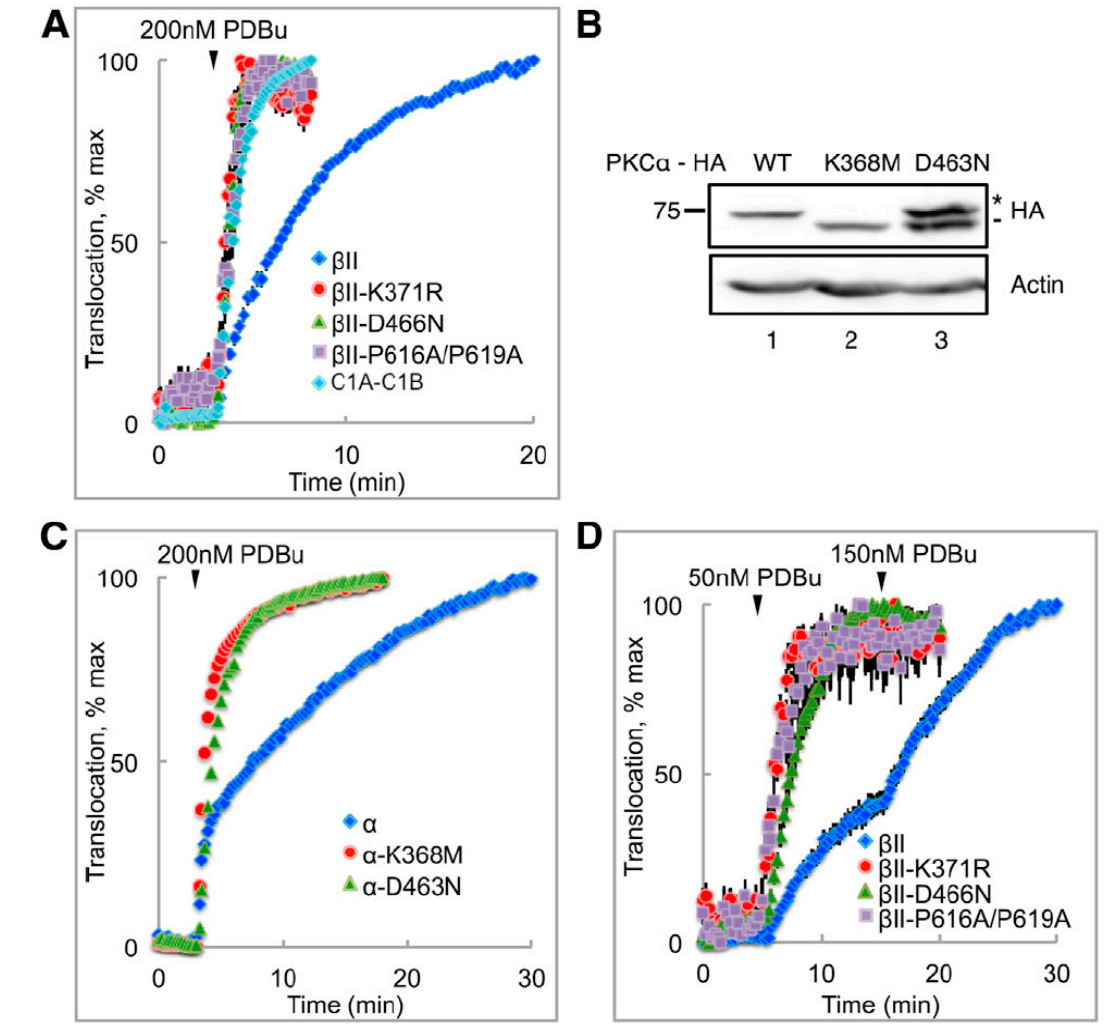

Figure 8. Unprimed cPKCs have an exposed C1A-C1B tandem module that is masked upon maturation. (A) The FRET ratios of COS7 cells co-transfected with membrane-targeted CFP and the indicated full-length, YFP-tagged PKCβII constructs were monitored upon PDBu treatment. Plots show data normalized to 100% for the maximal FRET response ± SEM. (B) Western blot of whole-cell lysates of COS7 cells transfected with the indicated HA-PKCα constructs. The asterisk denotes the position of mature, fully phosphorylated PKCα, and the dash denotes the position of unphosphorylated PKCα. (C) FRET ratios ± SEM of COS7 cells co-transfected with membrane-targeted CFP and the indicated full-length, YFP-tagged PKCα constructs were monitored upon PDBu stimulation. (D) FRET ratios ± SEM of COS7 cells co-transfected with membrane-targeted CFP and the indicated full-length, YFP-tagged PKCβII constructs were monitored upon stimulation with a sub-saturating PDBu concentration for wild-type PKCβII (50 nM), followed by treatment with another 150 nM PDBu to evoke a maximal response.

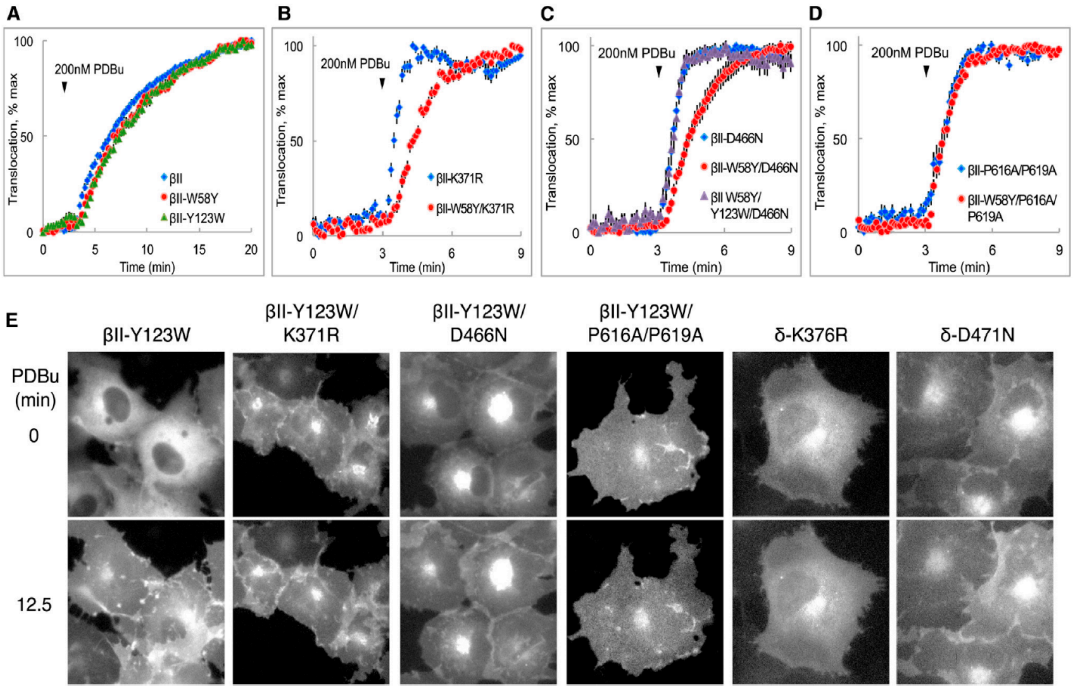

Figure 9. Both the C1A and C1B domains of unphosphorylated PKCs are exposed and become masked upon priming of PKC.
(A-D) FRET ratios ± SEM of COS7 cells co-transfected with membrane-targeted CFP and the indicated full-length, YFP-tagged PKCβII constructs were monitored upon PDBu treatment. (E) Representative YFP images of localization of the indicated PKCβII or PKCδ mutants before (top) or after (bottom) PDBu treatment.

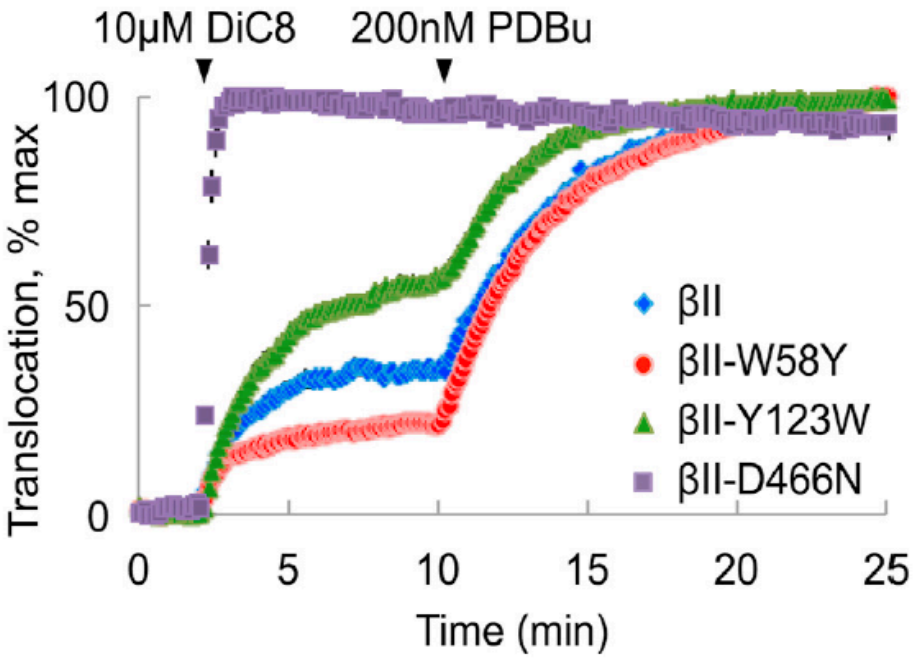

Figure 10. Both the C1A and C1B domains are involved in membrane binding, but the C1B domain dominates.
The FRET ratios ± SEM of COS7 cells co-transfected with membrane-targeted CFP and the indicated full-length, YFP-tagged PKCβII constructs were monitored upon stimulation with the PKC agonists DiC8 and PDBu.

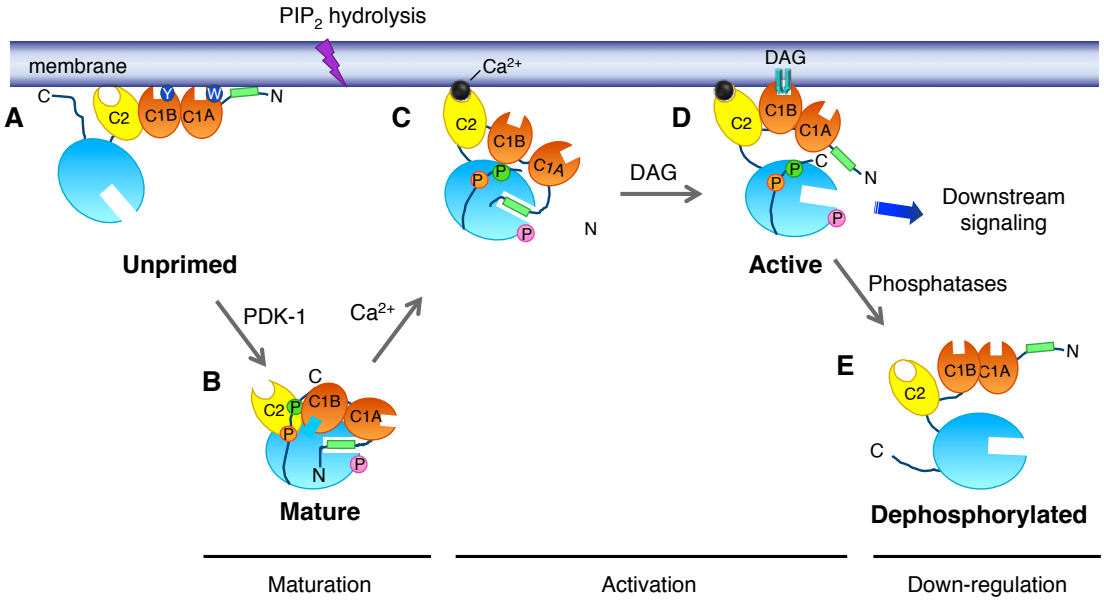

Figure 11. Model showing how maturation of cPKC masks C1 domains to increase the dynamic range of DAG sensing and thus PKC output.
(A) Unprimed PKC is in an open conformation that associates with membranes via weak interactions from the C2 domain, both C1A and C1B domains, the exposed pseudosubstrate, and the C-terminal tail. In this conformation, both C1A and C1B domains are fully exposed. (B) Upon ordered phosphorylation of PKC at its activation loop (pink), turn motif (orange), and hydrophobic motif (green) sites, PKC matures into its closed conformation, in which both the C1A and C1B domains become masked, the pseudosubstrate binds the substrate binding site, and the enzyme localizes to the cytosol. This masking of the C1 domains prevents pretargeting of PKC to membranes in the absence of agonist-evoked increases in DAG, thus decreasing basal signaling. (C) In response to agonists that promote PIP_2 hydrolysis, Ca^{2+}-dependent binding of the C2 domain of cPKCs to the plasma membrane allows the low-affinity DAG sensor to find its membrane-embedded ligand, DAG. (D) Binding of DAG, predominantly to the C1B domain of PKCβII, expels the pseudosubstrate from the substrate-binding cavity and activates PKC. Use primarily of the lower-affinity C1B domain increases the dynamic range of PKC output as the signal does not saturate as readily using the lower affinity module and allows cPKCs to signal at the plasma membrane as opposed to the Golgi. (E) Dephosphorylation of activated PKC allows it to regain the exposed (open) conformation of unprimed PKC.

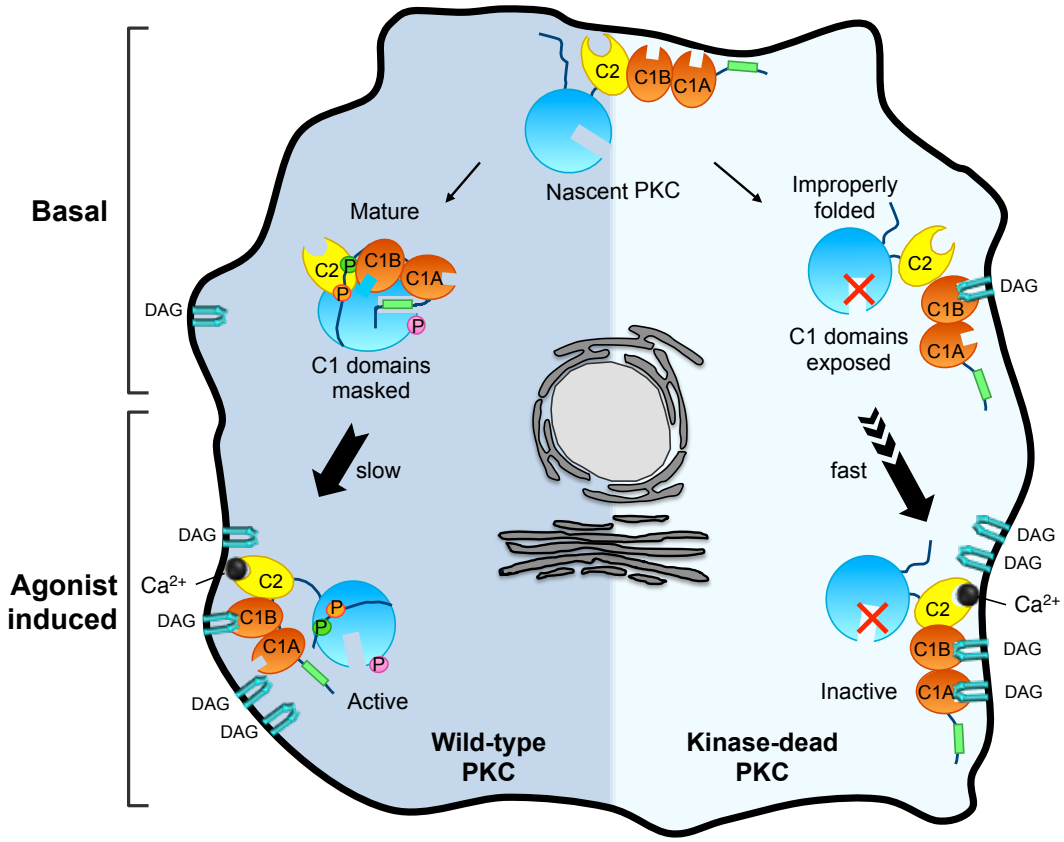

Figure 12. Model comparing the conformation, localization, and translocation kinetics of wild-type and a kinase-dead PKC.
Nascent PKC is in an open conformation and associated with the plasma membrane. Maturation induces conformational changes that mask its C1 domains, therefore keeping the enzyme inactive under basal conditions, but allowing it to respond to increases in Ca^{2+} and DAG levels. Kinase-dead PKC is not primed by phosphorylation and, therefore, remains in an open conformation, allowing basal levels of DAG to recruit a pool of PKC to the plasma membrane. Agonist-induced increases in DAG result in rapid translocation of the remaining PKC to membranes.

CHAPTER 3 − INTRAMOLECULAR C2 DOMAIN-MEDIATED AUTOINHIBITION OF PROTEIN KINASE C βII

ABSTRACT

The signaling output of protein kinase C (PKC) is exquisitely controlled, with disruption of the output resulting in pathophysiologies. Identifying the structural basis for autoinhibition is central to developing effective therapies for cancer, where PKC activity needs to be enhanced, or degenerative diseases, where PKC activity needs to be inhibited. Here, we reinterpret a previously reported partial crystal structure of PKCβII and propose a new structure, which we validate biochemically, and a model that is consistent with extensive literature on PKC regulation. Mutagenesis of predicted contact residues establishes that the Ca^{2+}-sensing C2 domain forms an intramolecular clamp with the kinase domain and carboxyl-terminal tail, locking PKC in an inactive conformation. Ca^{2+}-dependent bridging of the C2 domain to membranes provides the first step in the activation of PKC via conformational selection. Elucidation of the structural basis for autoinhibition of PKCβII unveils a unique direction for therapeutically targeting PKC.

INTRODUCTION

Protein kinase C isozymes transduce a myriad of signals that result in phospholipid hydrolysis. As such, they play key roles in a multitude of cellular processes, including controlling the balance between cell survival and death, and their dysregulation has been implicated in numerous diseases. Mounting evidence suggests that PKC activity suppresses survival signaling (Reyland, 2007); thus, it functions as a tumor suppressor and cancer-associated mutations are generally loss-of-function (Antal et al., 2015). In marked contrast, its activity is elevated in degenerative diseases such as spinocerebellar ataxia 14 (Ji et al., 2014; Verbeek et al., 2005), ischemic neurodegeneration (Sieber et al., 1998), and in cardiomyopathies (Belin et al., 2007; Bowling et al., 1999; Takeishi et al., 2000). From a

therapeutic standpoint, identifying intramolecular interactions between the different PKC domains is essential for the designing of small molecules or peptides that can either disrupt these contacts to open up and activate PKC or clamp the domains closed to prevent PKC activation.

The PKC family consists of 9 genes that are grouped according to their regulatory domains and thus the second messengers that regulate them (Parker and Murray-Rust, 2004). Conventional PKC isozymes (α, β, γ) contain tandem C1 domains, C1A and C1B, that bind diacylglycerol (DAG) and a C2 domain that binds anionic phospholipids in a Ca^{2+}-dependent manner (Figure 13A); the C2 domain also contains phosphatidylinositol-4,5-bisphosphate (PIP_2)-binding determinants that direct conventional PKC isozymes to the plasma membrane. Novel PKC (δ, ε, η, θ) isozymes lack a functional C2 domain, and thus are activated solely by DAG binding to the C1 domain. Atypical PKC (ι, ζ) isozymes bind neither of these second messengers and are regulated by protein-protein interactions. Conventional and novel PKC isozymes are constitutively phosphorylated at three priming sites (activation loop, turn motif, and hydrophobic motif), that trigger a series of conformational changes that allow PKC to adopt an autoinhibited conformation that is catalytically competent but unable to signal in the absence of agonists (Antal et al., 2015; Feng et al., 2000; Stensman et al., 2004). Specifically, the C1 domains become masked to prevent basal recognition of DAG, and the pseudosubstrate binds the substrate-binding cavity to prevent substrate phosphorylation. Signals that result in phospholipid hydrolysis activate conventional PKC isozymes by a two-step mechanism: generation of Ca^{2+} recruits PKC to the plasma membrane where it binds its membrane-embedded ligand, DAG. This latter event releases the pseudosubstrate, thus activating PKC.

Elucidation of the structure of PKC has been challenging given that it is a highly dynamic, multi-module protein that undergoes large conformational changes. The structures of

the isolated C1, C2, and kinase domains of conventional PKC isozymes have been previously solved (Grodsky et al., 2006; Guerrero-Valero et al., 2009; Hommel et al., 1994). The most complete PKCβII crystal structure to date is that of a protein in which three cysteine residues were mutated within the C1A domain, C2 domain, and C-terminal tail (C70S/C217S/C622S) and electron density is only evident for the C1B, C2, and kinase domains, and the C-terminal tail (Leonard et al., 2011). Because the structure lacks adequate electron density for the pseudosubstrate, the C1A domain, or any of the regions connecting the domains to one another, the assignment of which domains belong to a particular polypeptide, as opposed to other neighboring polypeptides, was challenging. Consequently, in the crystal packing of this structure, the C2 domain that interfaced with the kinase domain and C-terminal tail was dismissed, despite extensive literature establishing the existence of intramolecular contacts between the C2 domain and C-terminal tail of conventional PKC isozymes (Banci et al., 2002; Conrad et al., 1994; Corbalan-Garcia et al., 2003; Edwards and Newton, 1997a, b; Feng et al., 2000; Kheifets and Mochly-Rosen, 2007). Furthermore, one of the mutated residues, Cys70, is a key Zn^{2+}-coordinating residue and its mutation to Ser prevents the folding of the C1A domain (Kazanietz et al., 1995; Ono et al., 1989), likely explaining the lack of electron density for this domain and raising uncertainties regarding the placement of the C1B domain. Consequently, the structure proposed for PKCβII, as well as the model suggested for its multistep activation, are inconsistent with extensive biochemical analyses (Newton, 2001; Nishizuka, 1995). Most notably, the structure and model are inconsistent with the literature establishing that 1] interactions between the C2 domain and C-terminal tail maintain the enzyme in a closed, inactive, DAG and PIP_2-insensitive conformation until Ca^{2+} binds, 2] only one C1 domain engages ligand, and 3] binding of the C2 domain to membranes results in large movements of the hinge region separating the C2 domain from the kinase domain. This raises

the question as to whether the dismissed structure, with a different assignment of intradomain contacts, is the biologically relevant structure.

Here we use structure/function analysis to test whether the C2 domain clamps over the kinase domain to provide a previously undescribed mechanism of autoinhibition in which not only is the pseudosubstrate in the substrate-binding cavity, but the C2 domain clamps this autoinhibited conformation. From the crystal packing, we identify key ion pairs between the C2 domain and kinase domain or C-terminal tail and show that reversal of one charge unfolds PKC and that reversal of both charges re-clamps PKC in a closed conformation. Furthermore, we show that the mutation of C70S, which allowed crystals to defract well, results in constitutively active PKC, accounting for the absence of the pseudosubstrate in the substrate-binding cavity and suggesting that unfolding of the C1A domain was critical in allowing crystallization. Finally, we propose a model for the two-step activation of PKC in which 1] Ca^{2+} binding to the C2 domain pushes the equilibrium towards the open conformation (C2 removed from kinase domain) because the C2 domain is now retained at the plasma membrane via Ca^{2+}-bridging to anionic phospholipids and 2] binding of DAG to the C1B domain repositions the pseudosubstrate-C1A moiety to relieve autoinhibition. Our findings reveal activation of PKC by conformational selection. Additionally, they open new avenues for therapeutically targeting PKC with small molecules or peptides that could disrupt or strengthen intramolecular contacts in order to modulate PKC activity.

RESULTS

PKCβII Crystal Structure Packing Reveals that the C2 Domain Interfaces with the Kinase Domain

Given the inconsistencies in the PKCβII structure and model of activation (Leonard et

al., 2011) with PKC biology, we examined the reported crystal packing to determine whether there were any other conformations that were more consistent with the literature. The crystal packing revealed a number of possible positions of the C2 domain in relation to the kinase domain, one of which interfaced with the C-terminal tail and kinase domain by binding between the amino- and carboxyl-terminal lobes (Figure 13B; mode *ii*). These mode *ii* contacts were attributed to a different PKC molecule (Leonard et al., 2011) because of speculation that these contacts were only possible in the absence of the pseudosubstrate segment and, therefore, did not represent a physiologically relevant structure. However, docking of the C2 domain onto a complex of the kinase domain with a modeled pseudosubstrate (Figure 13C) showed that the C2 domain can be bound to the kinase domain with the pseudosubstrate present in its active site in a way that is very similar to the mode *ii* with the RMSD being 13Å (1095 atoms) (Figure 13D). In this model, an opening between the catalytic and C2 domains would readily accommodate the presence of the linker between the pseudosubstrate and C1A domain (Figures 13E). If this interaction were biologically relevant, it would unveil yet another mechanism of autoinhibition, with the C2 domain clamping over the kinase domain to maintain the pseudosubstrate in the substrate-binding cavity.

Mutational Analysis Corroborates a C2:Kinase Domain Interface

To test whether the C2 domain of PKCβII interfaces with the kinase domain and the C-terminal tail in the closed, autoinhibited conformation, we determined which residues were involved in this interaction. Based on the crystal packing, Asp382 within the kinase domain and Lys209 within the C2 domain were predicted to form hydrogen bonds (Figure 14A). To test this potential point of contact, we mutated the negatively charged Asp382 to a positively charged Lys and assessed whether this induced an open conformation of the enzyme by displacing regulatory moieties from the kinase domain. Note, we refer to an open

conformation of PKC as one in which the C1 and/or C2 domains of PKC are displaced from the kinase domain and the pseudosubstrate is out of the substrate-binding site, and to a closed conformation as one in which PKC is autoinhibited through intramolecular interactions with its pseudosubstrate and regulatory domains. We have previously shown that unphosphorylated PKCβII adopts an open conformation that, because of unmasked C1A and C1B domains, translocates more rapidly to the plasma membrane upon treatment with the C1 ligand, phorbol dibutyrate (PDBu), compared with matured (phosphorylated) PKC that has undergone conformational transitions to mask its C1 domains (Antal et al., 2014). Indeed, when the Asp382-Lys209 interaction was disrupted by a D382K mutation, the protein translocated more rapidly (Figure 14B; $t_{1/2}$= 1.7 ± 0.1 min versus 3.5 ± 0.2 min), indicating that it was in a more open conformation with its C1 domains exposed. Simultaneously inverting the charges of both Asp382 and Lys209 (D382K/K209D) rescued the translocation kinetics ($t_{1/2}$=3.4 min ± 0.2 min), corroborating the interpretation that these residues interact with each other. Glu655 and Lys205 are also positioned in proximity such that they could interact electrostatically (Figure 14A). Similar to the Asp382-Lys209 pair, mutating Glu655 to a Lys also increased the translocation rate ($t_{1/2}$=1.6 min ± 0.1 min) induced by PDBu, and simultaneously reversing the charges of both Glu655 and Lys205 rescued the translocation kinetics (Figure 14C; $t_{1/2}$=2.9 min ± 0.2 min). As a negative control, mutating the nearby Glu657 within the C-terminal tail to a Lys had no effect on the translocation kinetics (Figure 14C; $t_{1/2}$=4.0 min ± 0.2 min) because this residue does not interface with the C2 domain. Furthermore, mutating both residues involved in the interaction with the C2 domain (D382K and E655K) resulted in a more open conformation, as it further increased the rate of translocation (Figure 14D; $t_{1/2}$=1.1 min ± 0.1 min) induced by phorbol dibutyrate (PDBu). However, this conformation was not as open as that of unprocessed, kinase-dead PKCβII (Antal et al., 2014), suggesting that there are

other contributing points of contact within the regulatory domain. Note that all the mutants were processed by phosphorylation (Figure 15).

To ensure that the mutations that disrupted the C2:kinase domain interface indeed disengaged the C2 domain to allow it to favor Ca^{2+}-dependent lipid binding, we monitored the steady-state levels of binding of the PKCβII-D382K/E655K mutant enzyme to the plasma membrane upon elevation of Ca^{2+} with thapsigargin, a sarco/endoplasmic reticulum Ca^{2+}-ATPase inhibitor (Rogers et al., 1995). Elevation of intracellular Ca^{2+} resulted in an approximately 2-fold increase in the steady-state binding of the PKCβII-D382K/E655K to the plasma membrane (Figure 14E), consistent with disruption of these ion pairs favoring an open conformation with an exposed C2 domain. Moreover, this mutant translocated to membranes with much faster kinetics upon subsequent stimulation with PDBu, corroborating this open conformation. Kinase-dead PKCβII-D466N, which has fully exposed C1A and C1B domains (Antal et al., 2014; Gould et al., 2011; Shi et al., 2010), translocated rapidly and more completely to the membrane upon elevation of Ca^{2+} (Figure 14E), revealing that the C2 domain, similar to the C1A and C1B domains, is highly exposed in unprimed PKC. Thus, the C2 domain of the PKCβII-D382K/E655K favors a more open conformation than that of wild-type, but not as open as that of the kinase-dead PKC, likely because of additional points of contact between the C2 and kinase domains.

The C2:Kinase Domain Interaction is Intramolecular

To exclude the possibility that the C2:kinase domain interaction is intermolecular, as opposed to intramolecular, we examined whether an intermolecular interaction between a YFP-tagged PKCβII E655K mutant and a RFP-tagged PKCβII K205E mutant could rescue the fast translocation kinetics of the E655K mutant (Figure 16A). In contrast to the rescue by introducing a complementary C2 domain mutation into the same polypeptide as the kinase

domain mutation (see Figure 14C; $t_{1/2}$=1.0 min ± 0.1 min versus 2.9 min ± 0.2 min), the presence of a C2 domain mutation on another PKCβII molecule did not rescue the fast translocation kinetics for the C-terminal tail mutant (Figure 16B). These data are consistent with an intramolecular, and not intermolecular, C2:kinase domain interaction and support biophysical studies showing that cellular PKCβII translocates to plasma membranes as a monomer (L. Kaestner and P. Lipp, personal communication) and biochemical studies showing that pure PKC is fully active as a monomer (Hannun and Bell, 1986).

Mutation of Cys70 in the C1A Domain Dysregulates PKC by Releasing Its Pseudosubstrate

C1 domains are characterized by a highly conserved motif of six Cys and two His that binds two atoms of Zn^{2+} (Quest et al., 1992), thus maintaining the fold of the domain (Newton, 1995). The motif is $HX_{12}CX_2CX_nCX_2\underline{C}X_4HX_2CX_7C$ (n=13 or 14), where X is a variable amino acid residue (Kazanietz et al., 1995; Ono et al., 1989). The underlined Cys corresponds to Cys70 in the C1A domain of PKCβII (Figure 17A), which is one of three residues Leonard et al. (2011) mutated to Ser to improve diffraction of the crystals. Mutation of this residue, including to Ser, unfolds the domain as assessed by loss of ability to bind ligand (Kazanietz et al., 1995; Ono et al., 1989). To test how mutation of this key Cys altered the basal activity of PKC in cells, we measured the effect of the PKC inhibitor Gö6983 on the basal phosphorylation of our PKC activity sensor, CKAR (Violin et al., 2003), in cells expressing equal amounts of either wild-type PKCβII, the C70S construct, or a RFP control construct. The magnitude of the drop in the FRET ratio reflects the degree of basal activity in the absence of agonist stimulation (Gallegos and Newton, 2011). Figure 17B shows that the C70S mutation caused constitutive activation of PKCβII, revealing that the unfolded C1A domain resulted in dysregulation of PKC by releasing the pseudosubstrate. Furthermore, the lack of a folded C1A domain casts a doubt on the position of the C1B domain within the structure.

Lastly, we tested the allosteric activation model proposed by Hurley and coworkers postulating that Phe629 of the NFD helix controls the activity of PKC (Leonard et al., 2011). Specifically, the authors proposed that the C1B clamps the NFD in a low activity conformation in which the Phe is displaced from the active site, with binding of the C1B domain to membranes releasing the Phe to interact with the adenine ring of ATP. Mutation of Phe629 to Ala resulted in a kinase whose activation kinetics and magnitude were indistinguishable from that of the wild-type enzyme, both in response to natural agonists and phorbol esters (Figure 17C). Thus, this Phe is not a key regulator of the physiological activation of PKC.

DISCUSSION

Re-analysis of the crystal packing of PKCβII (Leonard et al., 2011) reveals intramolecular inhibition of the kinase domain by the Ca^{2+}-sensing C2 domain (mode *ii* in Figure 13B), a structure that we validate by mutagenesis of interacting surfaces. Using this structure, we propose a model (Figure 18) for the activation mechanism of PKC that is consistent with the vast body of literature on PKC structure, function, and regulation. Based on mode *i* in Figure 13B, Hurley and coworkers proposed three steps in the activation of PKC: 1] Ca^{2+}-dependent translocation in the absence of conformational changes, 2] binding of DAG to the C1A domain accompanied by conformational changes, including release of the pseudosubstrate, and 3] binding of a second molecule of DAG to the C1B domain accompanied by large conformational changes in the hinge connecting the C2 domain and kinase domain and rearrangement of the conserved NFD motif helix (residues 628–630) into a catalytically-competent state. Each of these steps is in conflict with the literature or with data in this contribution. Our re-examination of the structure allows us to present a model

consistent with the literature that explains how conformational selection regulates the first step in the activation of PKC.

To assess whether the C2:kinase domain interaction observed in the crystal packing of PKCβII is intramolecular or, as proposed by Hurley and coworkers, intermolecular, we tested whether mutations predicted to disrupt ion pairs of the C2:kinase domain interface would shift the equilibrium toward a more open PKC conformation. We have previously shown that unprimed PKC is in an open conformation in which both C1 domains are exposed, resulting in significantly faster membrane translocation than the matured enzyme (Antal et al, 2014). We now show that disruption of ion pairs at the C2:kinase domain/C-terminal tail interface unclamp the C2 domain and that reversal of charges in this ion pair maintain the clamped conformation. Additionally, we show that disruption of an ion pair is not rescued by introducing the opposite charge in a separate molecule of PKC, establishing that monomeric PKC binds its own C2 domain. These data support a model in which the C2 domain forms an intramolecular clamp with the kinase domain and C-terminal tail.

One reason Leonard et al. (2011) dismissed the pose of the C2 domain interfacing with the kinase domain (Figure 13B; mode *ii*) is because they reasoned that Ca^{2+} would not bind the C2 domain in this conformation. However, the affinity of the C2 domain for Ca^{2+} is over three-orders of magnitude lower in the absence of anionic lipids compared to their presence (Nalefski and Newton, 2001). This is because anionic lipids are required to stabilize Ca^{2+} binding such that Ca^{2+} bridges the C2 domain with anionic lipids (Nalefski and Falke, 1996). Stopped flow kinetic experiments are consistent with a model in which PKC collides with membranes at the diffusion-controlled limit but rapidly dissociates because of unfavorable electrostatic interactions between the C2 domain and the anionic membrane surface. Following elevation of intracellular Ca^{2+}, weak binding of Ca^{2+} to the C2 domain

allows anionic lipids to retain the Ca^{2+}-bound C2 domain on membranes, increasing the lifetime of the membrane-bound complex by several orders of magnitude. It is relevant that engaging the C2 domain on membranes results in a two orders of magnitude increase in proteolytic sensitivity of the hinge connecting the C2 domain and kinase domain (Keranen and Newton, 1997; Kishimoto et al., 1983; Young et al., 1988). This supports a model in which Ca^{2+} provides conformational selection by favoring an equilibrium in which the C2 domain is pulled away from the kinase domain via bridging to the membrane.

A second reason why Leonard et al. (2011) dismissed the structure of the C2 domain interfacing with the kinase domain is that they reasoned the pseudosubstrate would be excluded from the substrate-binding cavity in this conformation. However, molecular modeling of residues 16 – 26 of the pseudosubstrate in the substrate-binding cavity reveals that there is no steric hindrance (Figure 13C). Indeed, a clear opening is present that would accommodate threading of the segment following the pseudosubstrate to allow it to connect to the C1A domain that begins 10 residues past the pseudosubstrate (Figures 13E).

A third reason for dismissal of the structure in which the C2 domain binds intramolecularly with the kinase domain is that the authors considered this mode of interaction at odds with the elongated shape obtained by SAXS data. The authors used the program AutoGNOM to determine maximum linear dimension (D_{max}) of the complex, although rounds of manual fitting in GNOM were made with no details of the procedure presented in the paper. Fitting of the theoretical curve to the experimental data were provided, with no statistical measure of the fitting quality. The D_{max} obtained by the authors is 100Å, which is close to their proposed model of PKCβII. However, the D_{max} parameter is well recognized as a "soft" parameter as its value strongly depends on suggestions made prior to its calculation (Jacques and Trewhella, 2010). Additional experiments, like sedimentation studies or electron

microscopy, are required for the independent estimate of D_{max} (Moore, 1980). Our model of the kinase domain and C2 in mode *ii* is approximately 83Å (Figure 13E); however, we did not include the C1A and C1B domains, which would increase the D_{max}, because their exact placement within the full-length structure is yet to be determined owing to the unfolded C1A domain. Finally, the major limitation of SAXS analysis is that it considers proteins as rigid bodies; however, our model of PKCβII suggests that the C2 domain is a highly dynamic domain that alternates between various conformations until Ca^{2+}-binding drives the equilibrium towards the membrane-bound, open conformation. It is known that interdomain dynamics can significantly alter SAXS profiles and lead to misinterpretation of SAXS data (Bernado, 2010).

Our structure and model are consistent with prior biochemical studies that established that the C2 domain of PKC interfaces with the C-terminal tail and that these interactions maintain PKC in a closed, inactive conformation. Specifically, the C-terminal tail of PKCβII has been previously suggested to interface with the C2 domain because Ca^{2+} affinity, mediated by the C2 domain, is sensitive to the composition of the C-terminal tail: PKCβI and PKCβII splice variants differ only in the last 50 amino acids, yet the concentration of Ca^{2+} required for half-maximal activation is an order of magnitude higher for PKCβII compared to PKCβI (Edwards and Newton, 1997b). Similarly, phosphorylation of the hydrophobic motif within the C-terminal tail of PKCβII increases Ca^{2+} affinity by an order of magnitude (Edwards and Newton, 1997a); additionally, constructs with an Ala at this position adopt a more open conformation that can become irreversibly associated with the plasma membrane, unless Ca^{2+} is chelated (Feng et al., 2000). Yet another study established that PKC is in a closed conformation in which neither PIP_2 nor DAG can bind in the absence of Ca^{2+} (Corbalan-Garcia et al., 2003). Further evidence for intramolecular autoinhibitory contacts comes from

studies by Mochly-Rosen and colleagues that revealed that Receptor for Activated C-kinase 1 (RACK1) binds to both the C2 domain and C-terminal tail of PKCβII (Ron et al., 1995; Stebbins and Mochly-Rosen, 2001), suggesting that these domains interface. They then went on to show that the RACK-binding site within the C-terminal tail interacts with a sequence in the C2 domain that mimics the PKC binding site on RACK (pseudo-RACK), maintaining PKC in an inactive conformation (Banci et al., 2002). In addition, RNA aptamers selected to inhibit PKCβII inhibit neither the isolated kinase domain nor PKCβI, which differs only in the C-terminal tail, suggesting the aptamer is targeting a surface comprising determinants both in the C-terminal tail and the regulatory moiety (Conrad et al., 1994). All these studies are consistent with the C2 domain of PKC interacting with the C-terminal tail in order to maintain PKC in a closed conformation and thus unresponsive to basal levels of agonists.

The C2 domain of a related PKC, PKCα, has also be reported to contribute to autoinhibition of the enzyme, in addition to the autoinhibition imparted by the pseudosubstrate and C1 domains (Parissenti et al., 1998; Riedel et al., 1993). For example, deletion of 20 amino acids within the C2 domain induced constitutive activity of PKCα, indicating autoinhibition by this domain (Rotenberg et al., 1998). Larsson and coworkers (Stensman and Larsson, 2007) went on to show that this autoinhibitory interaction, which maintained PKC in a DAG-insensitive conformation, was mediated by negatively charged residues in the C-terminal tail of PKCα and a lysine-rich cluster in the C2 domain. Consistent with our work on PKCβII, reversing the charge of either of these interacting residues resulted in a higher sensitivity to DAG and thus enhanced membrane translocation, whereas simultaneously reversing both charges rescued the enhanced translocation phenotype (Stensman and Larsson, 2007). Although this group mutated three residues within the tail or four within the C2 domain and tested their effect simultaneously, two of the residues (PKCα K209E and D652K, the

equivalent of E655K in PKCβII) were homologous to the ones we tested independently. Taken together, these findings further substantiate our results and suggest that the C2 domain of PKCα has a similar placement to that of PKCβII, with conservation of charge at these critical residues within the interfacing surfaces.

We also show that mutation of the key Zn^{2+}-coordinating residue, Cys70, in the C1A domain results in a constitutively active PKC, revealing that the pseudosubstrate is pulled out of the substrate-binding cavity because of the unfolded C1A domain. This accounts for the lack of electron density of not only the C1A domain, but also the pseudosubstrate, in the crystal packing of the PKCβII SEC mutant (C70S/C217S/C622S) crystals. Deletion of the C1A domain of PKCδ has been shown to result in constitutive activation of the enzyme in *in vitro* kinase assays, leading Blumberg and colleagues (Pu et al., 2009) to propose that the C1A domain contributes to maintaining PKC in an inactive state by stabilizing the pseudosubstrate in the substrate-binding cavity. Taken together, mutation of Cys70 would not have allowed the C1A to fold, preventing insertion of the pseudosubstrate in the substrate-binding cavity. Curiously, Leonard et al. (2011) reported close to 4 mol Zn^{2+} bound to the PKC used for crystallization and reported phorbol ester-stimulated activity. It is difficult to reconcile the lack of electron density, lack of pseudosubstrate binding, and mutation of a key Zn^{2+}-coordinating residue, all suggesting a misfolded C1A domain, with the biochemical characterization presented, unless the analysis was performed on wild-type PKCβII, which was also crystallized, and not the PKCβII SEC mutant for which the crystal packing is presented. Moreover, the potential for a misfolded C1A domain brings into question whether the C1B domain is occupying a functionally relevant position. We note that the assay the authors used to assess unclamping of the C1B and kinase domain was actually monitoring the loss of PKC from the cytosolic fraction. Because destabilizing mutations such as F629D

increase the phosphatase sensitivity of PKC (Gould et al., 2011), the first step in the down-regulation of PKC, this is not an appropriate assay for membrane binding.

The structure proposed by Leonard et al. (2011) suggests the presence of a large flexible linker between the C1B and C2 domains. Yet under no condition tested (absence or presence of Ca^{2+}, with or without anionic membranes) does limited proteolysis of pure PKCβII result in cleavage between these two domains (Keranen and Newton, 1997). In fact, in the absence of cofactors, PKC adopts a compact conformation that is relatively resistant to limited proteolysis. One region becomes proteolytically labile upon membrane binding and another upon activation. As noted above, Ca^{2+}-dependent binding to membranes results in unmasking of the hinge separating the C2 domain from the kinase domain (Keranen and Newton, 1997); subsequent activation results in exposure of the pseudosubstrate segment (Orr et al., 1992). The large exposed linker assigned between the C1B and C2 domains proposed by Leonard et al., (2011) is inconsistent with limited proteolysis data.

A key conclusion by Hurley and colleagues was that the NFD serves as the linchpin for activation of PKC; they proposed that the C1B domain binds the helix to position Phe629 away from the ATP binding site, reducing catalysis. However, we show that mutation of this Phe to Ala results in a PKC whose activity in cells is indistinguishable from that of wild-type enzyme. It is noteworthy that mutation of the corresponding residue in PKA (Phe327) to Ala resulted in only a modest decrease in k_{cat} (from 26 sec^{-1} to 20 sec^{-}) and although the K_m for ATP was increased approximately 10-fold (from 20 μM to 249 μM) (Yang et al., 2009), this is 20-fold lower than the intracellular concentration of ATP, suggesting limited biological relevance. Based on this linchpin mechanism, the authors proposed an intermediate step in the activation of PKC in which the pseudosubstrate is released from the active site but the enzyme is inactive because the C1B is still bound to the kinase domain, positioning Phe629 away from

the ATP binding site. However, release of the pseudosubstrate correlates with the activation of PKC under all conditions examined, including activation by anomalous conditions such as occurs with short-chained phosphatidylcholine or protamine sulfate (Orr et al., 1992; Orr and Newton, 1994). Thus, the NFD helix of PKCβII is not a key regulator of kinase activity; rather release of the pseudosubstrate is the key determinant for activation.

Figure 18 presents a model for the regulation of PKC that takes into account the conformational sensing by the C2 domain. We have previously shown that newly-synthesized PKC (Figure 18A) is in an open conformation in which the membrane-targeting modules are fully exposed and the pseudosubstrate is out of the substrate-binding cavity. Upon maturation by phosphorylation, the enzyme undergoes conformational rearrangements that mask the C1A domain, thus reducing the apparent affinity for DAG of the mature PKC so there is no binding to basal DAG, and position the pseudosubstrate in the substrate-binding cavity. We now build on this model of autoinhibition to show that the C2 domain clamps over the kinase domain, tethering the pseudosubstrate in place for even more effective autoinhibition than previously proposed (Figure 18B). Note that this clamping of the C2 domain revealed by the structure provides a molecular explanation for why the activation loop Thr500 is inaccessible to both PDK-1 and phosphatases in the autoinhibited conformation (Dutil and Newton, 2000). Upon elevation of intracellular Ca^{2+}, conformational selection allows the Ca^{2+}-bound C2 domain to engage on the membrane, trapping PKC in the membrane-bound conformation that is accompanied by a large hinge motion that renders the segment connecting the C2 domain and kinase domain 100-fold more sensitive to limited proteolysis (Figure 18C) (Keranen and Newton, 1997). This membrane-bound species is now able to bind its membrane-embedded ligand, DAG, via the C1B domain, an event that pulls the pseudosubstrate out of the substrate-binding cavity to allow full activation of PKC (Figure 18D).

Our model of PKC activation (Figure 18) shows only one C1 domain binding DAG or phorbol esters, in contrast to the model by Hurley and coworkers that proposes sequential binding of the C1A and then C1B. Seminal studies by Nishizuka and Blumberg originally established that the stoichiometry of ligand binding of full-length PKC is one mole DAG or one mole phorbol ester per mole of PKC (Kikkawa et al., 1983; Konig et al., 1985b), a finding that has been confirmed many times (Giorgione et al., 2003; Hannun et al., 1985; Quest and Bell, 1994). Consistent with this, no binding cooperativity is evident with respect to DAG or PDBu, as would be expected from the reduction in dimensionality of engaging one C1 domain onto the membrane (Hannun and Bell, 1986; Mosior and Newton, 1998b; Newton and Koshland, 1989), nor are dimeric phorbol esters efficient at engaging both C1 domains, an event that can be forced but is highly unfavorable (Giorgione and Newton, 2003). Moreover, three-dimensional reconstructions of PKCδ from two-dimensional crystals also revealed that PKCδ only binds membranes through a single C1 domain, not both (Solodukhin et al., 2007). The multistep activation model for PKCβII that involves sequential engagement of each C1 domain with DAG is inconsistent with the body of literature establishing that only one C1 domain binds ligand.

Two striking features of the PKC structure are now apparent. First, the C2 domain provides an additional layer of autoinhibition to ensure no basal signaling of PKC in the absence of agonists. Thus, activation requires the release of the C2 domain from the kinase domain, followed by the release of the pseudosubstrate from the substrate-binding cavity. Second, intramolecular interactions can now be targeted in therapies. For example, in cancer therapies, where PKC activity should be enhanced (Antal et al., 2015), small molecules or peptides that destabilize the clamped conformation of PKCβII will allow it to be more responsive to second messengers. Conversely, in therapies for degenerative diseases where

PKC activity should be reduced, small molecules or peptides can be designed to stabilize the clamped conformation. Because the C-terminal tails of the PKC isozymes are highly variable, this method could provide a unique isozyme-specific method of regulating the activity of individual isozymes.

EXPERIMENTAL PROCEDURES

Plasmid Constructs, Antibodies, and Reagents

C-terminally tagged rat PKCβII-YFP (Dries et al., 2007) and the membrane-targeted CFP (Violin et al., 2003) have been previously described. Rat PKCβII was RFP-tagged at the C-terminus. All mutants were generated by QuikChange site-directed mutagenesis (Stratagene). The pan anti-phospho-PKC activation loop antibody was previously described (Dutil et al., 1998). The anti-phospho-PKCα/βII (T638/641; 9375S) and pan anti-phospho-PKC (βII S660; 9371S) antibodies were obtained from Cell Signaling, and the anti-PKCβ (610128) antibody was from BD Transduction Laboratories. Phorbol 12,13-dibutyrate (PDBu) and thapsigargin were purchased from Calbiochem.

Cell Culture, Transfection, and Immunoblotting

COS7 cells were cultured in DMEM (Cellgro) containing 10% fetal bovine serum (Atlanta Biologicals) and 1% penicillin/streptomycin (Gibco) at 37 °C in 5% CO_2. Transient transfection was carried out using jetPRIME (PolyPlus Transfection) or FuGENE 6 transfection reagents (Roche Applied Science) for ~24h. Cells were lysed in 50 mM Tris, pH 7.4, 1% Triton X-100, 50 mM NaF, 10 mM $Na_4P_2O_7$, 100 mM NaCl, 5 mM EDTA, 1 mM Na_3VO_4, 1 mM PMSF, and 50 nM Okadaic acid. Whole cell lysates were analyzed by SDS-PAGE and Western blotting via chemiluminescence on a FluorChem Q imaging system (ProteinSimple).

FRET Imaging and Analysis

Cells were imaged as described previously (Gallegos et al., 2006). COS7 cells were co-transfected with the indicated YFP-tagged PKC construct and plasma membrane-targeted CFP at a 1:0.1 ratio of DNA. Base-line images were acquired every 7 or 15 sec for ≥ 2 min before ligand addition. FRET ratios represent mean ± SEM from at least 3 independent experiments. Because the maximal amplitude of translocation of the mutants varied, possibly because changes in the orientation or distance of the fluorophores caused by differential folding of the kinase, the data were normalized to the maximal amplitude of translocation for each cell as assessed following PDBu addition. Normalization was achieved by dividing by the average base-line FRET ratio and then scaling that data from 0 to 100 % of maximal translocation using the equation: $X = (Y-Y_{min})/(Y_{max}-Y_{min})$, where Y = normalized FRET ratio, Y_{min} = minimum value of Y, and Y_{max} is maximum value of Y. The half-time of translocation was calculated by fitting these data to a non-linear regression using a one-phase exponential association equation, with Graph Pad Prism 6.0a (GraphPad Software). Basal PKC activity was measured as previously described (Gallegos and Newton, 2011) by co-transfecting RFP-tagged wild-type or mutant rat PKCβII, or RFP alone, and the C Kinase Activity Reporter (CKAR) (Violin et al., 2003) and treating cells with the PKC inhibitor Gö 6983. Data were normalized to the values for the last minute of the experiment (when PKC activity was lowest). For agonist-dependent PKC activity, data were normalized to the baseline FRET ratios. Statistical significance was determined via a Student's t-test performed in Graph Pad Prism 6.0a (GraphPad Software).

Structure Modeling and Molecular Docking

As the N-terminal pseudosubstrate region of PKCβII has a high level of sequence similarity with the cAMP-dependent protein kinase (PKA) inhibitor (PKI) (Figure 19) we used the structure of PKA:PKI complex (PDBID:1ATP) to model the eleven residues of PKCβII

(aa. 16-26). We then used the C2 domain of PKCβII (PDBID:3PFQ aa. 161-292) for docking to the complex between the PKCβII catalytic core (PDBID:3PFQ aa.339-669) and the pseudosubstrate using ZDOCK server (v. 3.0.2) (Pierce et al., 2014), with no restrictions on the docking interface. Forty two complexes out of fifty contained the C2 domain positioned close to the active site of PKCβII between helices αG and αC similar to the position of the C2 domain from the symmetry mate of 3PFQ structure. Comparing the predicted docking complexes to the symmetry mate C2 domain we selected the most close prediction model with RMSD from the position of the C2 domain in the 3PFQ structure 13Å (1095 atoms). The C1A domain or rat PKCβII was modeled based on the solution structure of the human PKCγ C1A

AUTHOR CONTRIBUTIONS

C.E.A and J.A.C. performed the experiments. C.E.A and A.C.N wrote the manuscript. A.P.K. performed the modeling and docking. S.S.T. and A.C.N. conceived the project.

ACKNOWLEDGMENTS

We thank Emily Kang for experimental assistance and the Newton and Taylor labs for helpful discussions. This work was supported by NIH GM43154 to A.C.N. and DK54441 to S.S.T. C.E.A. was supported in part by the UCSD Graduate Training Program in Cellular and Molecular Pharmacology (T32 GM007752) and the NSF Graduate Research Fellowship (DGE1144086).

Chapter 3, in full, has been submitted for publication of the material as it may appear in *Cell*, 2015, by Corina Antal, Julia Callender, Alexandr Kornev, Susan Taylor, and Alexandra C. Newton. The dissertation author was the primary investigator and author of the material.

FIGURES

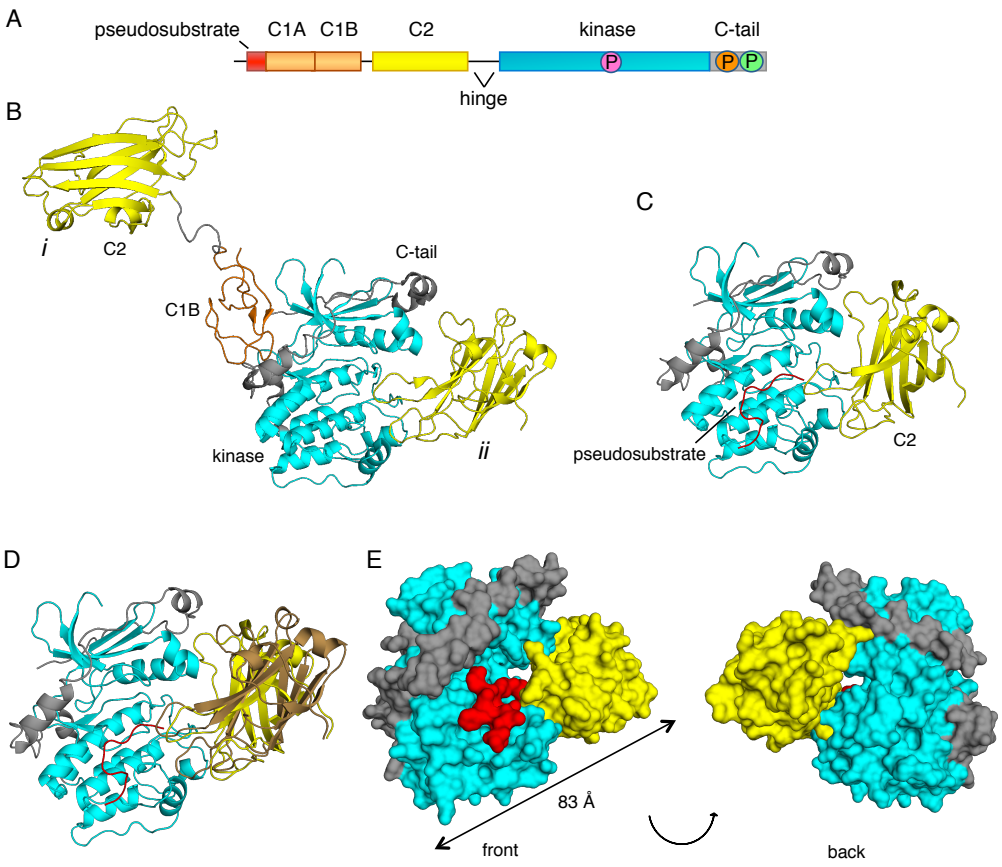

Figure 13. The C2 Domain of PKCβII Interacts with the Kinase Domain and C-Terminal Tail
(A) Schematic of the primary structure of PKCβII showing pseudosubstrate (red), tandem C1A and C1B (orange), C2 (yellow) in the regulatory moiety and the kinase domain (cyan) and C-terminal tail (gray); also indicated are the priming phosphorylation sites (activation loop in pink, turn motif in orange, and hydrophobic motif in green) and the proteolytically-labile hinge that separates the regulatory and catalytic moieties. (B) Crystal structure of PKCβII (PDBID:3PFQ) showing the original interpretation of the location of the C2 domain that traces polypeptide from the C1B to the C2 (mode i) and the alternative interpretation in which the C2 domain binds the kinase domain by an intramolecular interaction (mode ii). The crystal packing shows both modes. (C) C2 domain (yellow) docked onto a complex of the PKCβII kinase domain (cyan) and the modeled pseudosubstrate (red). (D) Complex of the PKCβII kinase domain (cyan) and the mode ii C2 domain (yellow) from the crystal packing with the modeled pseudosubstrate (red), superimposed with the docked C2 domain (brown). (E) Structure of the kinase domain:C2 domain:pseudosubstrate complex showing the opening between the kinase domain (cyan) and the C2 domain (yellow), through which the pseudosubstrate:C1A linker (red) can be threaded through.

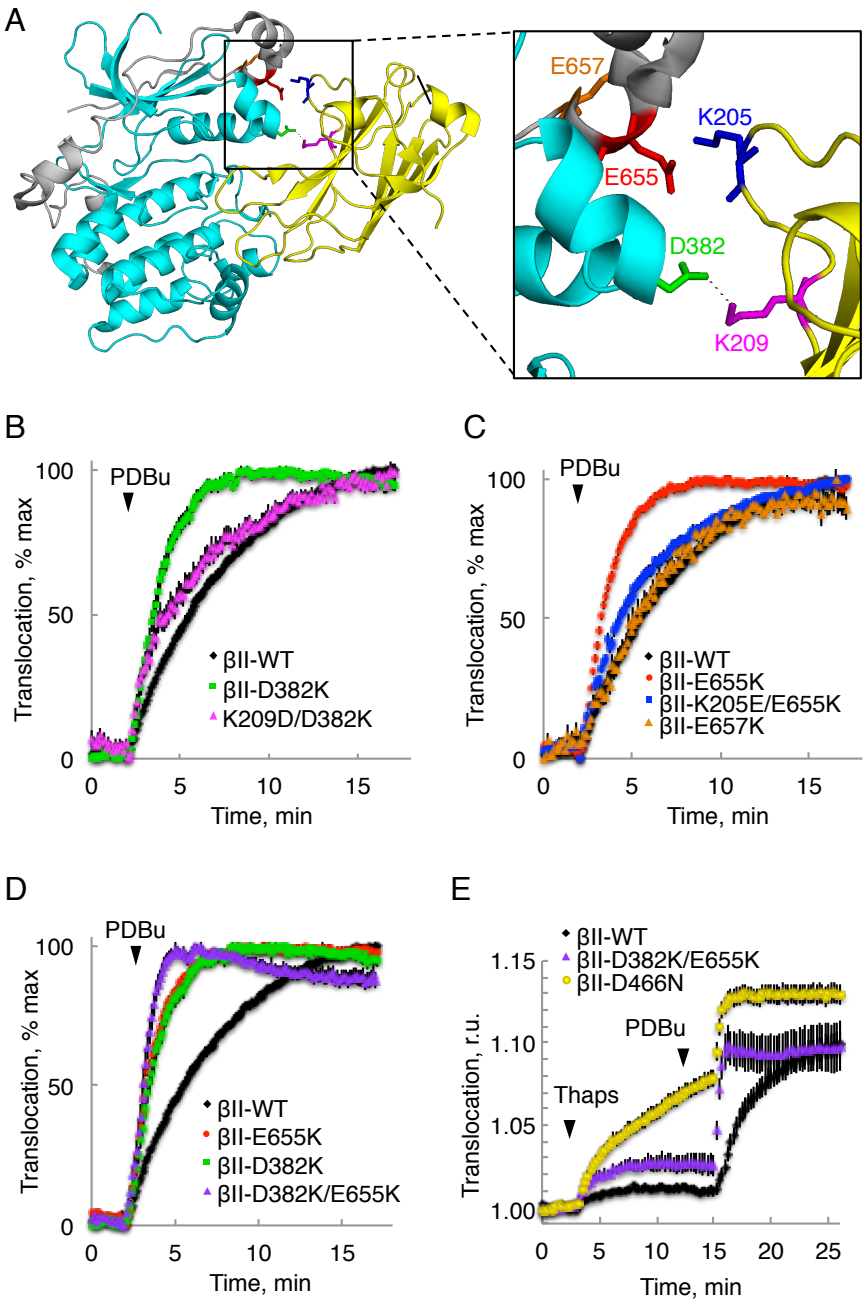

Figure 14. Mutational Analysis Corroborates a C2:Kinase Domain Interface
(A) Crystal structure of PKCβII (PDBID:3PFQ) showing predicted ion pairs between the kinase domain (cyan) or the C-terminal tail (gray) and the C2 domain (yellow). (B-D) Normalized FRET ratio changes (mean ± SEM) representing PDBu- (200 nM) induced PKC translocation in COS7 cells co-expressing YFP-tagged PKCβII WT or mutants and plasma membrane-targeted CFP. (E) FRET-ratio changes (mean ± SEM) representing thapsigargin- (5μM) followed by PDBu- (200 nM) induced PKC translocation in COS7 cells co-expressing YFP-tagged PKCβII WT or mutant and plasma membrane-targeted CFP.

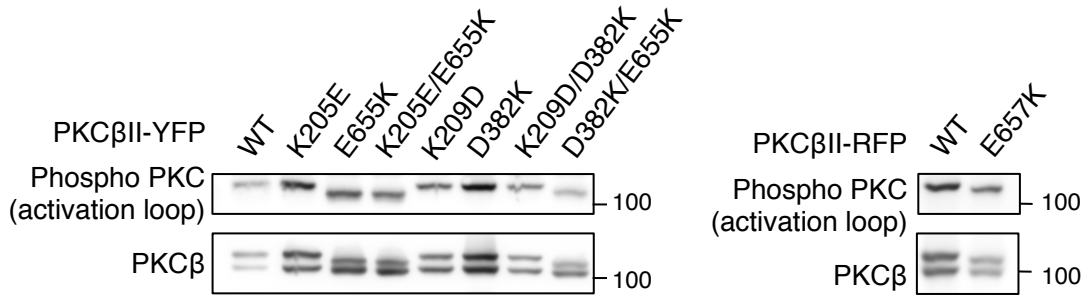

Figure 15. C2 and Kinase Domain Mutants Are Processed by Phosphorylation
Immunoblot showing the phosphorylation state of the indicated YFP-tagged PKCβII proteins. The upper band in the PKCβ blot represents phosphorylated PKCβII, while the lower band represents unphosphorylated PKCβII. The band shift in the Glu/Lys mutants is induced by mutation of the Glu, and not by a difference in phosphorylation.

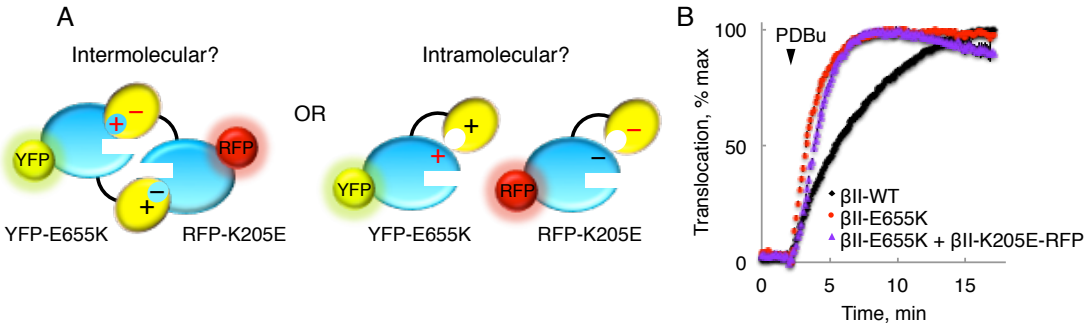

Figure 16. The PKCβII Kinase Domain Binds the C2 Domain through an Intramolecular Interaction
(A) Charge reversal of the ion pair partner in the C2 domain (K205E) would rescue the fast translocation kinetics of the E655K C-terminal tail mutation in the case of an intermolecular (left) but not intramolecular (right) C2:kinase interaction. (B) Normalized FRET ratio changes (mean ± SEM) representing PDBu- (200 nM) induced PKC translocation in COS7 cells co-expressing plasma membrane-targeted CFP and either YFP-PKCβII-WT, YFP-PKCβII-E655K, or both YFP-PKCβII-E655K and RFP-PKCβII-K205E.

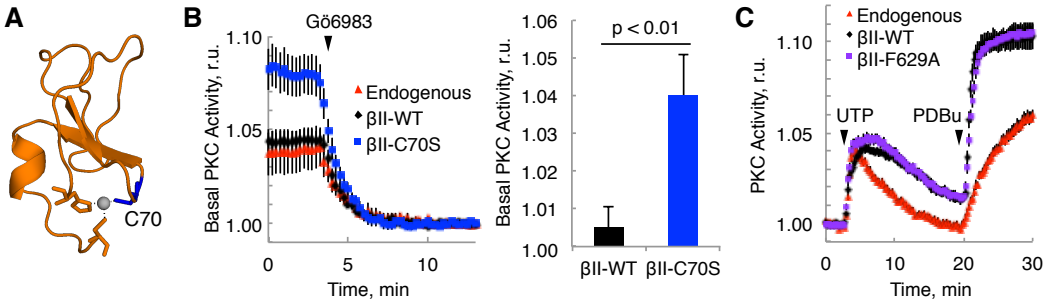

Figure 17. Mutation of Cys70 Dysregulates PKC by Releasing the Pseudosubstrate, whereas Mutation of Phe629 Does not Affect PKC Activation

(A) Modeled structure of the C1A domain of PKCβII showing coordination of Zn^{2+} (gray sphere) by Cys70 (blue). (B) Left: Normalized FRET ratio changes (mean ± SEM) showing basal PKC activity of the indicated RFP-tagged PKCβII constructs or RFP control (endogenous) in COS7 cells co-expressing CKAR that were treated with 6 μM of PKC inhibitor Gö 6983. Right: Quantification of the basal activity of the indicated overexpressed PKC relative to that of endogenous PKC isozymes (RFP alone) in COS7 cells. (C) Normalized FRET ratio changes (mean ± SEM) showing agonist-dependent PKC activity of the indicated RFP-tagged PKCβII constructs or RFP control (endogenous) in COS7 cells co-expressing CKAR.

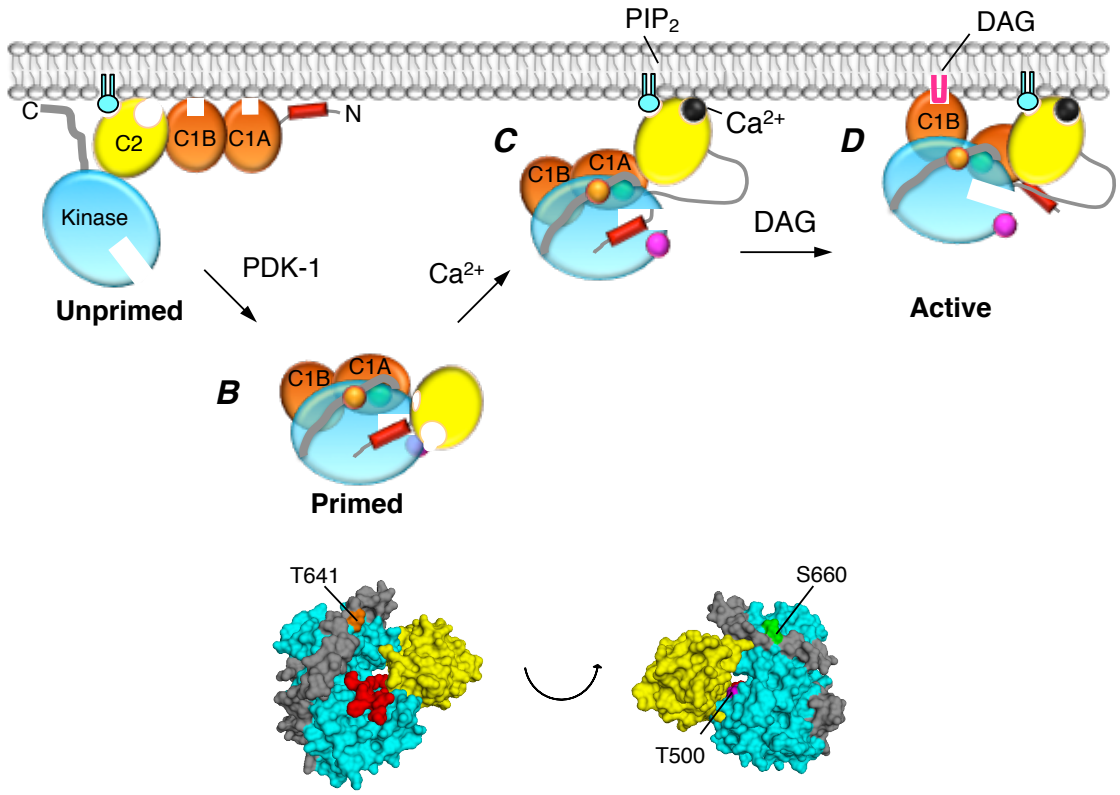

Figure 18. Model of PKCβII Activation

(A) Unprimed cPKC is in a membrane-associated, open conformation in which its C1A, C1B, and C2 domains are fully exposed and the pseudosubstrate and C-terminal tail are unmasked. In this open conformation, the upstream kinase PDK-1 has access to its target, T500, in the activation loop. (B) Upon priming phosphorylation at its activation loop (T500, magenta) by PDK-1, followed by autophosphorylation at the turn motif (T641, orange) and the hydrophobic motif (S660, green), cPKC matures into a closed conformation in which the C2 domain interfaces with the kinase domain, both C1domains become masked, the pseudosubstrate binds the substrate-binding site, and the primed enzyme localizes to the cytosol. (C) In response to agonists that promote PIP_2 hydrolysis, Ca^{2+} binds cytosolic PKCβII via a low affinity interaction such that upon the next diffusion-controlled membrane encounter, the Ca^{2+}-bound C2 domain is retained at the plasma membrane via Ca^{2+}-bridging to anionic lipids and binding to PIP_2 on a surface distal to the Ca^{2+} binding site. (D) Pre-targeted PKC binds the membrane-embedded ligand, DAG, predominantly via the C1B domain, resulting in release of the pseudosubstrate from the substrate-binding cavity, thereby activating PKC. Only one of the C1 domains binds DAG in the membrane at a time.

Figure 19. Sequence Alignment of PKCβII Pseudosubstrate and PKI
Sequence alignment between the PKCβII pseudosubstrate (aa.16-26) and PKIα (aa. 11-22).

CHAPTER 4 − CANCER-ASSOCIATED PROTEIN KINASE C MUTATIONS REVEAL KINASE'S ROLE AS TUMOR SUPPRESSOR

ABSTRACT

Protein kinase C (PKC) isozymes have remained elusive cancer targets despite the unambiguous tumor promoting function of their potent ligands, phorbol esters, and the prevalence of their mutations. We analyzed 8% of PKC mutations identified in human cancers and found that, surprisingly, most were loss-of-function and none were activating. Loss-of-function mutations occurred in all PKC subgroups and impeded second messenger binding, phosphorylation, or catalysis. Correction of a loss-of-function PKCβ mutation by CRISPR-mediated genome editing in a patient-derived colon cancer cell line suppressed anchorage-independent growth and reduced tumor growth in a xenograft model. Hemizygous deletion promoted anchorage-independent growth, revealing PKCβ is haploinsufficient for tumor suppression. Several mutations were dominant-negative, suppressing global PKC signaling output, and bioinformatic analysis suggested that PKC mutations cooperate with co-occurring mutations in cancer drivers. These data establish that PKC isozymes generally function as tumor suppressors, indicating that therapies should focus on restoring, not inhibiting, PKC activity.

INTRODUCTION

The protein kinase C (PKC) family has been intensely investigated in the context of cancer since the discovery that it is a receptor for the tumor-promoting phorbol esters (Castagna et al., 1982). This led to the dogma that activation of PKC by phorbol esters promotes carcinogen-induced tumorigenesis (Griner and Kazanietz, 2007b); yet targeting PKC in cancer has been unsuccessful.

The PKC family contains 9 genes that have many targets and thus diverse cellular functions, including cell survival, proliferation, apoptosis, and migration (Dempsey et al.,

2000). PKC isozymes comprise 3 classes: conventional (cPKC: α, β, γ), novel (nPKC: δ, ε, η, θ), and atypical (aPKC: ζ, ι). cPKC and nPKC isozymes are constitutively phosphorylated at 3 priming sites (activation loop, turn motif, and hydrophobic motif) to structure PKC for catalysis (Newton, 2003). A pseudosubstrate segment maintains PKC in an autoinhibited conformation that is relieved by second messenger binding. cPKC isozymes are activated by binding to diacylglycerol (DAG) and Ca^{2+}, whereas nPKC isozymes are activated solely by DAG, events that engage PKC at membranes. Thus, these PKC isozymes have two prerequisites for activation: constitutive processing phosphorylations and second messenger-dependent relocalization to membranes. Prolonged activation of cPKC and nPKC isozymes with phorbol esters, leads to their dephosphorylation and subsequent degradation, a process referred to as downregulation (Hansra et al., 1996; Young et al., 1987). aPKC isozymes bind neither Ca^{2+} nor DAG.

PKC has proved an intractable target in cancer therapeutics (Kang, 2014). PKCι was proposed to be an oncogene in lung and ovarian cancers (Justilien et al., 2014; Regala et al., 2005; Zhang et al., 2006), and PKCε was categorized as an oncogene because of its ability to transform cells (Cacace et al., 1993). However, for most PKC isozymes there is conflicting evidence as to whether they act as oncogenes or as tumor suppressors. For example, PKCδ is considered a tumor suppressor because of its pro-apoptotic effects (Reyland, 2007). However, it promotes tumor progression of lung and pancreatic cancers in certain contexts (Mauro et al., 2010; Symonds et al., 2011). Similarly, both overexpression and loss of PKCζ in colon cancer cells have been reported to decrease tumorigenicity in nude mice or cell lines, respectively (Luna-Ulloa et al., 2011; Ma et al., 2013). Likewise, PKCα was reported to both induce (Walsh et al., 2004; Wu et al., 2013) and suppress colon cancer cell proliferation (Gwak et al., 2009) and to suppress colon tumor formation in the $APC^{Min/+}$ model (Oster and Leitges, 2006).

Based on the dogma that PKC isozymes contribute positively to cancer progression, many PKC inhibitors have entered clinical trials; however, they have been ineffective (Mackay and Twelves, 2007). In fact, a recent meta-analysis of controlled trials of PKC inhibitors combined with chemotherapy versus chemotherapy alone revealed that PKC inhibitors significantly decreased response rates and disease control rates in non-small cell lung cancer (Zhang et al., 2014). Why has inhibiting PKC failed in the clinic? It has been well established that prolonged or repetitive treatment with phorbol esters depletes cPKC and nPKC isozymes from cells (Blumberg, 1980; Nelson and Alkon, 2009), bringing into question whether loss of PKC, rather than its activation, promotes tumorigenesis.

PKC is frequently mutated in human cancers. To uncover whether loss or gain of PKC function contributes to cancer progression, we selected mutations throughout the primary sequence and family membership and assessed their functional impact. Specifically, we asked how these cancer-associated mutations alter the signaling output of PKC using our genetically-encoded reporter, C Kinase Activity Reporter (CKAR) (Violin et al., 2003). Characterization of 46 of these mutations revealed that most reduced or abolished PKC activity and none were activating. Bioinformatic analysis of all PKC mutations revealed that they may cooperate with co-occurring mutations in oncogenes and tumor suppressors known to be regulated by PKC. Correction of one patient-identified, heterozygous, loss-of-function (LOF) PKCβ mutation in a colon cancer cell line significantly decreased tumor size in mouse xenografts, indicating that loss of PKC function enhances tumor growth. Our data are consistent with PKC isozymes functioning generally as tumor suppressors, reversing the paradigm that their hyperactivation promotes tumor growth.

RESULTS

A Multitude of Cancer-Associated Mutations Have Been Identified within the 9 PKC Genes

554 mutations (as of October 2014), of which most are heterozygous, have been identified in diverse cancers (Cerami et al., 2012b; Gao et al., 2013a) within cPKC (242), nPKC (236), and aPKC (76) isozymes (Figure 20). These mutations reside throughout the entire coding region, with no apparent mutational hotspots. Therefore, we conducted a comprehensive study of mutations within PKC domains and within interdomain regions to determine how they affect PKC signaling to contribute to cancer pathogenesis. 46 mutations of both conserved and non-conserved residues were selected from all 3 classes of PKC isozymes (Tables 1 and 2).

PKC Mutations in the Regulatory C1 and C2 Domains Are LOF

The C1 domains of cPKC and nPKC isozymes are critical for their activation because they mediate PKC translocation to membranes via binding to DAG. Thus, we investigated how C1 domain mutations alter PKC translocation and activation. To measure agonist-dependent PKC activity, COS7 cells co-expressing the FRET-based PKC reporter (CKAR) and equal levels of either wild-type (WT) or mutant mCherry-tagged PKC were stimulated with the cell-permeable DAG, DiC8, or the phorbol ester, phorbol 12,13- dibutyrate (PDBu), and phosphorylation-dependent FRET ratio changes were recorded. Phorbol esters serve as an effective, although non-physiological, tool to maximally activate PKC because bind with 100-fold higher affinity to C1 domains compared to DAG (Mosior and Newton, 1998a). A mutation identified in a colorectal cancer tumor altered a residue (PKCα H75Q) required for coordination of Zn^{2+} and thus for folding of the C1 domain (Figure 21A). This mutation ablated agonist-stimulated activity, as evidenced by a lower FRET ratio trace compared with that of cells containing only endogenous PKC (Figure 21B). This lower agonist-induced and

basal activity (Figure 21A) suggests the mutant is dominant-negative towards global PKC output. Within a head and neck cancer patient, a mutation altered a critical residue (PKCα W58L) required for controlling the affinity for DAG, but not phorbol ester (Dries et al., 2007) (Figure 21A). This mutation also abolished DiC8-induced activity but retained some PDBu-induced activity, consistent with this residue selectively regulating DAG affinity. Because membrane translocation is a prerequisite for activation of cPKC isozymes, we compared the translocation of YFP-tagged WT and mutant PKC to membrane-targeted CFP using FRET (Antal et al., 2014). Mutation of either residue impaired translocation upon stimulation with DiC8, phorbol ester (Figure 21C), or the natural agonist UTP (Figure 21D), accounting for the inability of these agonists to activate the mutants. Lastly, we asked how these mutations affected the processing phosphorylations of PKC. PKCα H75Q, but not W58L, was unphosphorylated, likely because the misfolded C1A domain of the H75Q mutant prevented its processing (Figure 21E). Three additional mutations within the C1A domains of PKCα (G61W), PKCβ (G61W), and PKCγ (Q62H) also exhibited reduced agonist-induced PKC activity (Figure 22B-D). Our analysis of 9 C1 domain mutations revealed that 5 reduced or abolished activity whilst none were hyperactivating (Tables 1 and 2). Inactivation occurred by altering 2 key inputs required for PKC function: disruption of binding to DAG or processing by phosphorylations.

The C2 domain of cPKC isozymes is also critical for activation as it mediates Ca^{2+}-dependent pre-targeting to plasma membrane, where these isozymes bind DAG and become activated (Newton, 2003). One mutation identified within the C2 domain of PKCγ (D193N) was present in colorectal and ovarian cancers and in melanoma. Another (D254N) was found in endometrial and ovarian cancers. Because both of these Asp residues (Figure 21F) coordinate Ca^{2+} (Medkova and Cho, 1998), we monitored their activation upon elevation of

intracellular Ca^{2+} with thapsigargin, a sarco/endoplasmic reticulum Ca^{2+}-ATPase inhibitor (Rogers et al., 1995). In contrast to WT PKCγ, neither mutant was activated (Figure 21G) nor translocated to the plasma membrane (Figure 21H) following thapsigargin addition, consistent with impaired Ca^{2+} binding. However, both mutants retained full responses to phorbol esters, consistent with unimpaired C1 domains. To further substantiate the inability of the mutants to bind Ca^{2+}, we monitored PKC oscillatory translocation stimulated by histamine-induced oscillatory Ca^{2+} release in HeLa cells (Violin et al., 2003). Whereas WT PKCγ exhibited oscillatory translocation in some cells, the C2 domain mutants were unresponsive to histamine (Figure 21I). Thus, these C2 domain mutations dampen PKCγ activity because they impede Ca^{2+} binding. Mutation of 2 other C2 domain residues that are not directly involved in Ca^{2+}-binding (PKCα G257V and PKCγ T218M) also caused LOF (Figure 22D and 14E); PKCα G257V was LOF because it was not processed by phosphorylation (Figure 22F), whereas the remaining C2 domain mutants were (data not shown). Our analysis of 6 C2 domain mutations revealed 4 LOF mutations and no hyperactivating ones (Tables 1 and 2).

PKC Mutations in the Kinase Domain Are LOF

We next evaluated 21 kinase domain mutations, 2 of which were within PKCδ: D530G in colorectal cancer and P568A in head and neck cancer (Figure 23A). Asp530 functions as an anchor for the kinase regulatory spine, a highly conserved structural element of eukaryotic kinases (Kornev et al., 2006; Kornev et al., 2008); not surprisingly, the D530G mutant was kinase-dead and not primed by phosphorylation (Figure 23B and 23C). Mutation of the conserved Pro568 to Ala also prevented a response to natural agonist stimulation, but maintained some PDBu-stimulated activity, as a small pool of this mutant was phosphorylated (Figure 23B and 23C).

Strikingly, all 3 PKCη mutations examined (K591E, R596H, and G598V) altered its subcellular localization by pre-localizing it at the plasma membrane prior to stimulation (Figure 23D). However, despite constitutive membrane association, these mutants had reduced basal and stimulated activity as read out by a phospho-(Ser) PKC substrate antibody (Figure 23E) because they were not processed by phosphorylation (Figure 23F). We have previously shown that unprocessed nPKC isozymes have exposed C1 domains that induce constitutive membrane association (Antal et al., 2014).

A number of mutations were present within the highly conserved APE motif that is involved in substrate binding and allosteric activation of kinases (Kornev et al., 2008). PKCγ P524R and PKCβ A509V mutations ablated activity by preventing processing phosphorylations, and both exhibited dominant-negative roles (Figure 22G-J). PKCβ A509T (colorectal cancer) also showed loss of function in response to UTP, but was modestly activated by the potent ligand PDBu (Figure 22I), likely because a small pool of it was phosphorylated (Figure 22J). A LOF mutation that prevented processing of the atypical PKCζ was also found within the APE motif (E421K; Figure 21G).

Further analysis revealed that 16 out of 21 kinase domain mutations we analyzed (Tables 1 and 2) resulted in full or partial LOF, with the majority preventing processing by phosphorylation. For example, PKCα F435C, PKCα A444V, PKCβII Y417H, PKCβII G585S, and PKCγ G450C had impaired phosphorylation and reduced activity (Figure 22C-F, 21H, and 21I). However, partial LOF mutations were also observed in cases where phosphorylation was maintained: PKCα D481E (Figure 22B and 22F) and PKCγ F362L (Figure 22D and 22J), suggesting that these mutations likely decrease PKC's intrinsic catalytic activity.

The Majority of Cancer-Associated PKC Mutations Are LOF

Our analysis of 46 mutations present within 8 of the PKC genes revealed that ~61% (28) of them were LOF and none were activating (Figure 24A). A lack of identification of activating mutations is not an artifact of our assays, as activating PKC mutations that increase PKC affinity for DAG or decrease autoinhibition are readily detectable (data not shown). LOF mutations were identified within cPKC (α, β, γ), nPKC (δ, ε, η), and aPKC (ζ) isozymes and occurred within the C1, C2, and kinase domains as well as the pseudosubstrate and C-terminal tail (Figure 24B). For example, the PKCγ G23E pseudosubstrate mutation was not processed by phosphorylation (Figure 22J) and thus lacked any UTP-stimulated activity (Figure 22D) and the PKCε R162H pseudosubstrate mutation showed reduced agonist-stimulated and basal activity (Figure 22K and 22L). The PKCβ P619Q C-terminal tail mutation, residing within a conserved PXXP motif required for processing (Gould et al., 2009), was also LOF as it prevented PKC phosphorylation (Figure 22H). Overall, PKC LOF occurred by diverse mechanisms, most commonly by preventing processing phosphorylations or ligand binding, and as such, there were no mutational hotspots for loss of function. However, we identified 7 LOF mutation "warmspots" (Sun et al., 2007) that fell within highly conserved regions of PKC, 1 within the pseudosubstrate and 6 within the kinase domain (Figure 24C). Thus, inactivating mutations targeted conserved regulatory elements and frequently hit the same residue, whereas mutations that exhibited no difference from WT occurred more randomly (Table 2).

Analysis of cancer types most frequently harboring PKC mutations revealed that, although PKC isozymes are mutated across many cancers, PKC mutations are enriched in certain cancers (Figure 24D). Namely, PKC isozymes are mutated in 20-25% of melanomas, colorectal cancers, or lung squamous cell carcinomas, but mutated in <5% of ovarian cancers,

glioblastoma, or breast cancers (Cerami et al., 2012b; Gao et al., 2013a). Additionally, nPKC isozymes are most commonly mutated in gastrointestinal cancers (pancreatic, stomach, and colorectal), which have a lower mutation burden than melanomas and lung cancers, highlighting their importance in this type of cancer (Figure 24D). The majority of PKC mutations are heterozygous, with an allele frequency varying from 0.05 to 0.67 for the mutations characterized (Tables 1 and 2). This indicates that PKC mutations can be truncal events in regards to tumor heterogeneity and exist in a majority of the cells within a tumor, or be branchal events acquired later in tumorigenesis as the tumor progresses to a more aggressive stage. This is consistent with PKC mutations being co-driver events that enhance tumorigenesis mediated by primary drivers such as Kras.

Dominant-Negative PKCβ Mutation Confers a Tumor Growth Advantage

Because the majority of PKC mutations examined were LOF, we tested whether we could rescue HCT116 colon cancer cells that have a heterozygous LOF frameshift mutation in the C2 domain of PKCβ, by overexpressing WT PKCβII. This resulted in a dramatic reduction in anchorage-independent growth (Figure 25A), a hallmark of cellular transformation. Thus we next used CRISPR/Cas9-mediated genome editing to ask whether reverting an endogenous LOF allele to WT would also rescue cell growth. We used DLD1 colon cancer cells, because they harbor a PKCβ A509T LOF mutation (Figure 23I), to assess whether a heterozygous LOF PKC mutation could confer a survival advantage, as most cancer-associated PKC mutations are heterozygous. We reverted the mutation to WT in 3 isogenic clones (Figure 25B and 24C), and confirmed that no sequence alterations existed within the top 2 most likely predicted off-targets (data not shown). Correction of the A509T mutation in the endogenous PKCβ (*PRKCB*) allele caused a slight, but reproducible, increase in the PKCβ levels and a >2-fold increase in PKCα levels, although neither reached statistical significance (Figure 26A).

Immunoblot analysis with a phospho-(Ser) PKC substrate antibody revealed significantly higher basal PKC activity in the corrected cells (Figure 26B). This is consistent with the DLD1 parental cells having reduced PKC activity because of the LOF PKCβ mutation and the lower PKCα levels. We next tested the ability of these cells to grow in suspension. Consistent with having higher PKC activity and a more tumor suppressive phenotype, the corrected cells were less viable in suspension (Figure 26C) because they were less capable of forming compact multicellular aggregates as the DLD1 parental cells formed (Figure 26D). Moreover, the corrected clones had decreased anchorage-independent growth potential (Figure 26E). These results corroborate those obtained from the HCT116 cells overexpressing PKCβII, demonstrating that partial loss of PKCβ activity is necessary for growth in soft agar. However, in a 2D proliferation assay, the DLD1 corrected cells proliferated at similar rates to the DLD1 parental cells (Figure 25D), indicating that it is not the proliferation rates that differ between these cells but rather their ability to grow in the absence of anchorage.

To determine whether PKC displays haploinsufficiency, we knocked out the mutant PKCβ allele in DLD1 cells by creating a frameshift deletion using genome engineering (Figure 25E). This hemizygous clone (WT/- 23), containing only 1 WT allele and thus expressing lower PKCβII levels (Figure 25F), exhibited significantly increased anchorage-independent growth potential compared to those containing 2 WT alleles, indicating that PKCβII is haploinsufficient for tumor suppression (Figure 26E). Additionally, the PKCβ hemizygous cells did not grow as well as the PKCβ A509T mutated cells in soft agar, indicating that this mutation had a dominant-negative effect.

To definitively establish whether a heterozygous LOF PKCβ mutation facilitates tumor growth *in vivo*, the DLD1 parental or corrected cells were subcutaneously injected into the flanks of nude mice and tumor growth was monitored. Consistent with our cellular data,

the tumors derived from the corrected cells were significantly smaller than those from the DLD1 parental cells (Figure 26F and 24G). This reduced growth correlated with increased apoptosis as assessed by TUNEL staining of tumor sections (Figure 26G). These data demonstrate that a heterozygous, dominant-negative PKCβ mutation can significantly increase tumor growth, thus establishing PKCβ as a tumor suppressor.

DISCUSSION

Here we establish that clinical trials targeting PKC have been based on the wrong assumption; it is not inactivation of PKC, but rather activation, that suppresses tumor growth. Thus, we propose that therapies should target mechanisms to restore the PKC signaling output rather than reduce it. Our comprehensive analysis revealed that 61% of the PKC mutations characterized were LOF and none were activating. We did not account for nonsense mutations or deletions, so an even higher proportion of PKC mutations are LOF. Corroborating our data, 3 other LOF PKC mutations have been previously described. A LOF PKCα mutation (D294G in C2 domain) was identified in 3 types of cancer (Alvaro et al., 1993; Prevostel et al., 1997; Zhu et al., 2005) and a LOF PKCζ mutation (S514F in the kinase domain) was identified in colorectal cancer (Galvez et al., 2009). A partial LOF mutation in PKCι (R471C), present in 3 distinct cancers, disrupted substrate binding and induced abnormal epithelial polarity (Linch et al., 2013). To our knowledge, no gain-of-function PKC mutations have been observed in cancer. The identification of LOF mutations throughout the PKC family and in diverse cancers supports a general role for PKC isozymes as tumor suppressors.

Strikingly, several LOF PKC mutations (e.g. PKCβ A509V, PKCγ P524R, and PKCα W58L, H75Q, and G257V) acted in a dominant-negative manner by decreasing global endogenous PKC activity. Moreover, the presence of mutant PKCβ A509T protein in DLD1

cells reduced PKCα levels. One mechanism for this cross-PKC dominant-negative effect is that the LOF PKC impairs the priming phosphorylations of other PKCs, thus reducing their steady-state levels. This is supported by a prior study demonstrating that unprocessed kinase-dead PKC isozymes prevent the phosphorylation of other PKC isozymes, likely because their phosphorylation requires common titratable components (Garcia-Paramio et al., 1998). This dominant-negative role of LOF mutations is corroborated by studies showing that kinase-dead PKC isozymes function in a dominant-negative manner to exhibit tumorigenic effects on cells (Galvez et al., 2009; Hirai et al., 1994; Kim et al., 2013; Lu et al., 1997). Importantly, although some PKC mutations were dominant-negative, loss of PKC such as would occur from nonsense mutations or gene deletions, also conferred a growth advantage (Figure 26E), indicating PKC is haploinsufficient for tumor suppression.

A tumor suppressive role of PKC is supported by PKC gene knockout mouse models and cellular studies. PKCα-deficient (*Prkca*$^{-/-}$) mice develop spontaneous intestinal tumors (Oster and Leitges, 2006). In an APC$^{Min/+}$ background, loss of PKCα induces more aggressive tumors and decreases survival (Oster and Leitges, 2006) and, in the context of oncogenic Kras, PKCα deletion increases lung tumor formation (Hill et al., 2014). Deletion of PKCζ in mice that are PTEN haploinsufficient results in larger, more invasive prostate tumors and enhances intestinal tumorigenesis in an APC$^{Min/+}$ background (Ma et al., 2013). Knock-down of PKCδ in colon cancer cells increases tumor growth in nude mice (Hernandez-Maqueda et al., 2013). Conversely, overexpression of PKC reveals a protective role. Re-expression of PKCβI in colon cancer cells (Choi et al., 1990), of PKCδ in keratinocytes (D'Costa et al., 2006), or overexpression of PKCζ in colon cancer cells (Ma et al., 2013) or in Ras-transformed fibroblasts (Galvez et al., 2009) decreased tumorigenicity in nude mice.

Clinical data reveal lower PKC protein levels and activity in tumor tissue compared with cognate normal tissue, also supporting a tumor suppressive role for PKC. Total PKC activity was significantly lower in human colorectal cancers versus normal mucosa because of decreased PKCβ and PKCδ (Craven and DeRubertis, 1994) or PKCβ and PKCε protein levels (Pongracz et al., 1995). PKCα protein was downregulated in 60% of human colorectal cancers (Suga et al., 1998), and PKCζ was downregulated in renal cell carcinoma (Pu et al., 2012) and non-small cell lung cancer (Galvez et al., 2009). Decreased PKCβ and PKCδ levels correlated with increased grade in bladder cancer (Koren et al., 2000; Langzam et al., 2001; Varga et al., 2004), and decreased PKCδ levels correlated with increased grade in endometrial cancer and glioma (Reno et al., 2008); (Mandil et al., 2001). PKCη was downregulated in colon and hepatocellular carcinomas and lower PKCη expression was associated with poorer long-term survival (Davidson et al., 1994; Lu et al., 2009). However, increased PKCι protein and DNA copy number levels have been observed in certain cancers (Perry et al., 2014; Regala et al., 2005). PKCι is part of the 3q26 amplicon and its increased DNA copy number levels correlate with increased mRNA expression (Figure 27). However, DNA copy number and mRNA levels do not correlate for cPKC genes (Figure 27). In fact, for PKCα, copy number levels inversely correlate with protein levels in breast cancer (Myhre et al., 2013), the cancer in which PKCα is most amplified (Cerami et al., 2012b; Gao et al., 2013a). A number of studies reported increased mRNA expression of other PKC genes in cancer; however, mRNA expression and protein levels often poorly correlate (Myhre et al., 2013). Thus, clinical data of this sort are consistent with a tumor suppressive function of PKC isozymes, although there might be context specific exceptions for PKCι.

The recent discovery that germline LOF mutations in PKCδ are causal drivers of autoimmune lymphoproliferative syndrome and systemic lupus erythematosus, disorders

associated with the acquisition of cancer-associated phenotypes, supports a bona fide tumor suppressive role of PKC in humans (Belot et al., 2013; Kuehn et al., 2013; Salzer et al., 2013). Both diseases are characterized by increased proliferation and decreased apoptosis of B-cells (Belot et al., 2013; Kuehn et al., 2013), and patients frequently develop lymphomas (Bernatsky et al., 2005; Mellemkjaer et al., 1997). Moreover, we found that siblings homozygous for a LOF PKCδ mutation have reduced levels of PKCζ (data not shown), supporting a dominant-negative role of LOF mutations.

How could decreased PKC activity enhance tumorigenesis? One possibility is that PKC isozymes suppress oncogenic signaling by repressing signaling from oncogenes or stabilizing tumor suppressors. Supporting this, unbiased bioinformatic analysis of tumor samples harboring PKC LOF mutations revealed that *TP53* (p53) is one of most frequently mutated genes in tumors harboring LOF mutations for each PKC isozyme (Table 3). PKC might promote the tumor suppressive function of p53 by stabilizing the WT protein. Considerable evidence suggests that phosphorylation by PKCδ stabilizes p53 thus promoting apoptosis (Abbas et al., 2004; Yoshida et al., 2006), but the role of other PKC isozymes is less clear. *KRAS* was also among the top 10 genes mutated in cancers harboring PKC mutations for 7 of the PKC isozymes (Table 3), specifically with mutation at Gly12 (Table 4). This argues that PKC might suppress Kras signaling, such that loss of PKC would be required for Kras to exert its full oncogenic potential. Consistent with this, PKC modulates both the activity and localization of Kras through phosphorylation of Ser181 (Bivona et al., 2006). Although the role of this phosphorylation site in tumors remains controversial (Barcelo et al., 2014), our analysis is consistent with loss of PKC enhancing its oncogenic potential. In fact, the DLD1 and HCT116 cells used in our assays contained an oncogenic Kras mutation (G13D) that is necessary for the ability of these cells to grow in soft agar (data not shown). This suggests that

LOF PKC mutations are not major cancer drivers, but rather co-drivers that contribute to cancer progression.

We also analyzed which kinase or Cancer Census genes (genes implicated in cancer) are significantly more commonly mutated (>15-fold) in tumors harboring PKC mutations versus tumors lacking PKC mutations (Table 5). This allowed us to identify novel proteins that might be important co-drivers or represent novel genetic dependencies for PKC. The tumor suppressor LATS2, which inhibits the Hippo pathway, and the kinases ROCK1 and ROCK2, which are required for the anchorage independent growth and invasion of non-small cell lung cancer cells, were among the top 20 mutated proteins that were significantly enriched in tumors harboring PKC mutations (Table 5). Our analysis reveals that gain-of-function mutations in these genes might be required to promote tumorigenesis in the absence of PKC signaling. We also performed an analysis of cancer-specific genes frequently co-mutated with PKC in lung, colorectal, and melanoma. This revealed very little overlap in co-mutated genes between the 3 cancers and also between the 3 classes of PKC isozymes (Table 6), suggesting that the individual PKC isozymes regulate distinct pathways in different cancers. Interestingly, cancers with a high PKC mutation burden, such as melanoma and colorectal cancers, show little PKC amplification. Conversely, cancers that have higher PKC amplification rates, such as breast and ovarian cancers, have few PKC mutations(Cerami et al., 2012b; Gao et al., 2013a), consistent with PKC mutations having a smaller or different role in breast and ovarian cancers.

The foregoing data provide a mechanism for why inhibiting PKC has proved unsuccessful, and in fact, detrimental, in cancer clinical trials: it is not gain of function, but rather LOF that confers a survival advantage. Therefore, therapeutic strategies should target ways to restore PKC activity. Bryostatin-1, a PKC agonist, also failed as a therapeutic and, in

fact, exhibited counter-therapeutic effects in cervical cancer (Nezhat et al., 2004), likely because it downregulates PKC (Szallasi et al., 1994). Therefore, novel strategies to activate PKC without downregulating it hold significant clinical potential. An important ramification of this study is that drugs that inhibit proteins involved in the processing of PKC cause loss of PKC. Notably, both mTOR and HSP90 inhibitors, currently in use in the clinic (Don and Zheng, 2011; Neckers and Workman, 2012), prevent processing of PKC (Gould et al., 2009; Guertin et al., 2006) and would thus have the detrimental effect of removing its tumor suppressive function. Restoring PKC activity would have to accompany other chemotherapeutics given that PKC isozymes act as the brakes, not the primary drivers, to oncogenic signaling. Our finding that decreased PKC activity enhances tumor growth challenges the concept of inhibiting PKC isozymes in cancer and underscores the need for therapies that restore or stabilize PKC activity in cells.

EXPERIMENTAL PROCEDURES

FRET Imaging and Analysis

Cells were imaged as described previously (Gallegos et al., 2006). For activity measurements, cells were co-transfected with the indicated mCherry-tagged PKC and CKAR or plasma membrane-targeted CKAR, as indicated. For translocation experiments, cells were co-transfected with the indicated YFP-tagged PKC and membrane-targeted CFP.

Generation of CRISPR Cell Lines

The CRISPR/Cas9 genome-editing system was employed to generate DLD1 cell lines in which the PKCβ A509T mutation was reverted to WT or knocked out. For the nuclease method, DLD1 cells were transiently transfected with the hSpCas9 vector containing the gRNA PKCβ-a, the PAGE-purified 70-mer ssODN (Figure 25B), and pMAX-GFP. For the

double nickase method, DLD1 cells were transfected with 2 hSpCas9n vectors containing the gRNA PKCβ-a, or PKCβ-b, the ssODN, and pMAX-GFP. GFP^+ cells were sorted 72 hr later. To reduce off-target mutagenesis, one of the clones (WT/WT 53) was made using a double nicking approach that requires the cooperation between two nickase Cas9 enzymes (Ran et al., 2013). CRISPR-targeted clones were expanded and gDNA was extracted using a Quick-gDNA MiniPrep Kit (Zymo Research Corporation) and screened for the presence of 2 wild-type alleles by PCR using primers spanning the A509 locus, followed by restriction digest with BtgZI. This restriction site was only present in the WT allele and correction of the A509T mutation introduced this site into the other allele. The presence a WT allele at both loci was confirmed by Sanger sequencing (Eton Bioscience).

Xenograft Model

Athymic Nude-*Foxn1*^{nu} mice (Harlan) were housed in compliance with the University of California San Diego Institutional Animal Core and Use Committee. 3 x 10^6 DLD1 cells in 100 μl PBS were injected subcutaneously into the right flank of each 4-week old, female mouse. Tumor dimensions were recorded twice weekly and tumor volume was calculated as 1/2 × length × width^2. Mice were euthanized 43 days after injection and tumors were excised. One tumor was excluded as it did not engraft well (DLD1p) and another was excluded as it was not subcutaneous (WT/WT 31).

Plasmid Constructs

The C Kinase Activity Reporter (CKAR), the membrane-targeted CFP (Violin et al., 2003) and the plasma membrane-localized PKCδ reporter, PM-δCKAR (Kajimoto et al., 2010) were previously described. pENTR clones of DNA encoding human PKCα, βII, δ, ε, η, θ, and ζ were from the Ultimate Human ORF Library (Life Technologies). These were N-

terminally tagged with mCherry via Gateway cloning (Life Technologies) into pDEST-mCherry, which was generated from pcDNA3 (Life Technologies) with mCherry DNA (gift from Roger Tsien) subcloned into the HindIII and EcoRV sites and blunt ligation of the Reading Frame Cassette A (Life Technologies) into the EcoRV site of pcDNA3. PKC isozymes were also N-terminally tagged with YFP via Gateway cloning generated as above. Human PKCζ was N-terminally HA-tagged via Gateway cloning into pDEST-HA generated from ligating the Reading Frame Cassette C into the EcoRV site of pcDNA3-HA. Rat PKCγ was subcloned into pcDNA3 with a RFP tag at the C-terminus. Plasmid vectors encoding the nuclease hSpCas9 (pX330) and the nickase hSpCas9n (pX335) were obtained from the Addgene repository (www.addgene.org/CRISPR). pMAX-GFP was acquired from Lonza.

Antibodies and Reagents

The pan anti-phospho-PKC activation loop antibody was previously described (Dutil et al., 1998). The anti-phospho-PKCα/βII (T638/641; 9375S), anti-phospho-(Ser) PKC substrate (2261S), pan anti-phospho-PKC (βII S660; 9371S), anti-phospho-PKCζ/λ (T410/403; 9378A), and anti-GAPDH (14C10) antibodies were purchased from Cell Signaling. The anti-PKCα (610108), PKCβ (610128), and PKCδ (610397) antibodies were from BD Transduction Laboratories, and the anti-PKCγ (13-3800) antibody was from Zymed. The anti-β-actin antibody (A2228) was purchased from Sigma-Aldrich and the anti-α-tubulin (T6074) antibody was from Sigma. The anti-PKCβII (sc-210) and anti-PKCη (sc-215) antibodies were obtained from Santa Cruz, the anti-HA antibody (HA.11, clone 16B12) from Covance, and the anti-phospho-PKCη (T655; ab5798) was from Abcam. Phorbol 12,13-dibutyrate (PDBu), 1,2-Dioctanoyl-sn-glycerol (DiC8), Uridine-5′-triphosphate (UTP)

trisodium salt, thapsigargin, and Gö6976 were obtained from Calbiochem and histamine was from Sigma-Aldrich.

Cell Culture, Transfection, and Immunoblotting

All cells were maintained in DMEM (Corning) containing 10% fetal bovine serum (Atlanta Biologicals) and penicillin/streptomycin (Corning) at 37 °C, in 5% CO_2. HCT116 and DLD1 cells were supplemented with GlutaMAX (Life Technologies). Tetracycline-inducible, PKCβ-expressing HCT116 cells were also supplemented with Geneticin (10 μg ml^{-1}; Life Technologies) and Blasticidin (500μg ml^{-1}; Fisher Scientific). For the soft agar experiments, the media was supplemented with Non-Essential Amino Acids. Transient transfection of COS7 was carried out using the jetPRIME transfection reagent (PolyPlus Transfection) or the FuGENE 6 transfection reagent (Roche) for ~24h. Cells were lysed in 50 mM Tris, pH 7.4, 1% Triton X-100, 50 mM NaF, 10 mM Na4P2O7, 100mM NaCl, 5mM EDTA, 1 mM Na3VO4, 1 mM PMSF, and 50 nM okadaic acid. Whole cell lysates were analyzed by SDS-PAGE and immunoblotting via chemiluminescence on a FluorChemQ imaging system (Alpha Innotech).

Generation of CRISPR Constructs

Plasmid vectors expressing hSpCas9 (pX330) or the nickase hSpCas9n (pX335) and a chimeric guide RNA (gRNA) were used for cloning of CRISPR/Cas9 targeting constructs. Briefly, the gRNAs were designed using publically available software tools (crispr.genome-engineering.org) that predict unique target sites throughout the human genome. Complementary oligonucleotides (ValueGene) containing the PKCβ gRNA target sequence (Figure 25B) were annealed and cloned into the BbsI site of pX330 and pX335 vectors.

Growth in Suspension

To assess growth in suspension, 5 x 105 cells/well were seeded in an Ultra Low Attachment Surface 6-well plate (Corning) and maintained in suspension for up to 72 hr. Viable cell count was determined using a trypan blue exclusion assay.

Anchorage-independent Growth in Soft Agar

Anchorage-independent growth was measured using soft agar colony formation assays. DLD1 cells were seeded in triplicate in 0.4% Bacto Agar (BD) at 15,000 cells/well in 6-well plates, on top of a 0.6% agar layer. Media was changed every 4 days. 10 images per well at 10X magnification were randomly acquired with an Olympus DP-12 microscope and mean colony area for colonies ≥ 50 μm was quantified using ImageJ. Data represent average ± SEM of 3-6 independent experiments. HCT116 PKCβII stably-expressing cells were made using pLenti6.3/TO/V5-DEST PKCβII and pLenti3.3/TR and selected using 500 μg ml^{-1} Blasticidin and 10 μg ml^{-1} Geneticin. HCT116 cells were seeded in triplicate at 20,000 cells/well in 6-well plates. Media, with or without 1 μg ml^{-1} tetracycline (Sigma-Aldrich), was changed every 3 days. Cells were fixed in ice-cold methanol for 20 min after 25 days and stained with crystal violet (0.005% in H_2O, 20% (v/v) methanol) for 2.5 hr at room temperature. The number of colonies with a diameter ≥ 100 μm was quantified from the entire well using ImageJ 1.49b (National Institutes of Health). Data represent the average ± SEM of 3 independent experiments.

Cell Proliferation Assay

10,000 cells/well were plated in triplicate, in a 12-well plate. Cells were fixed every 2 days with 4% paraformaldehyde in PBS for 15 min, stained with crystal violet (0.1% in H_2O, 10% (v/v) ethanol) for 20 min, lysed in 10% acetic acid, and absorbance was measured at 590 nm in an Infinite M200 PRO Tecan plate reader. Growth rates were normalized to the values

at day 0 and plotted on a log scale. Data represent the mean ± SEM of at least 3 independent experiments.

TUNEL Immunohistochemistry

For immunohistochemistry, tumor tissue was fixed in 10% Neutral buffered formalin over night at 4°C. Tumors were rinsed in 70% EtOH, placed in histology cassettes and paraffin embedded. Cellular DNA fragmentation of tumor sections, as a measure for apoptosis, was detected by terminal deoxynucleotidyl transferase (TdT)–mediated nick end labeling (TUNEL) staining using the ApopTag Peroxidase In Situ Apoptosis Detection Kit (Chemicon). Briefly, paraffin-embedded tumors were rehydrated in decreasing concentrations of ethanol, pre-treated with Proteinase K, quenched in 0.3% hydrogen peroxide in PBS for 30min, and equilibrated. Samples were then treated with the TdT enzyme solution for 60 min in a humidified chamber at 37°C. After application of the Stop-Wash buffer, samples were treated with anti-digoxigenin HRP conjugate for 30 min at room temperature and then developed with a peroxidase substrate Chromagen AEC (3-amino-9-ethylcarbazole) reagent (Vector Labs) for 20 min. Slides were counterstained with Mayer's Hematoxylin (Sigma-Aldrich) for 1 min and coverslips were mounted using VectaMount Mounting Medium (Vector Labs). Images of tissue sections were captured at 4x magnification to create a merged image of the entire section and at 40x magnification for quantification of TUNEL-positive nuclei, using a Keyance BZ-9000 microscope. Relative apoptosis was quantified by determining the percentage of TUNEL-positive cells from 5 random fields, per section, from each tumor in the group, and normalized to the tumors derived from the DLD1 parental cells. Data were analyzed statistically with one-way ANOVA followed by a post hoc Dunnett's Multiple Comparison test (Prism, version 6.0e, GraphPad Software Inc., San Diego, CA),

where ***$p < 0.001$ was considered significant as compared with the DLD1 parental cell group.

Statistical Analysis

All statistical tests were performed using Prism software version 6.0e for Mac (GraphPad Software).

Bioinformatic Analysis

PKC gene mutations and co-occurring mutations were identified using The Cancer Genome Atlas (TCGA) unrestricted and publically available data via the cBio portal (Cerami et al., 2012a; Gao et al., 2013b). Datasets analyzed are listed in Table 7. Only cases with a 'TCGA' prefix were analyzed. All cases with at least one mutation in any protein-coding gene were evaluated giving 5674 cases in total. When multiple datasets for the same cancer subtype were present, the published dataset was assessed initially. If a mutation was recorded in a published case, the corresponding case in a provisional dataset was not analyzed. Cases included in a provisional data set but not the corresponding published dataset were then analyzed for mutations to increase the study population. In any single case, multiple mutations of a specific gene were only recorded as one occurrence of that gene being mutated. Cancer subtype was recorded as the name of study that the case occurred in.

CRAN package 'cgdsr' was used to query cBio databases for mutation and copy number data (available at http://CRAN.R-project.org/package=cgdsr) (Jacobsen, 2013). The bioconductor package 'annmap' was used to map from genes to proteins in order to perform length corrections (available at http://annmap.cruk.manchester.ac.uk) (Yates, 2011). The longest protein annotated (Ensembl db v76) was used to make length corrections. Fisher's Exact Test was used to evaluate the significance of co-occurring mutations. Fisher.test from

the core R package stats (R-Core-Team, 2014) was used to calculate p-values and Bioconductor package 'qvalue' was used to calculate 'q-values' (Dabney, 2014). Cancer Census and kinase genes were filtered using a previously published list (Futreal et al., 2004; Hudson et al., 2014). Effect size was calculated using the proportion of mutation positive cases in study population against the proportion of mutations in the whole population of cases. Proportion of isozyme mutations from different cancer subtypes were calculated using the number of cancer subtype cases with appropriate mutation corrected for the total number of cases of each subtype in the dataset.

Copy number analysis GISTIC (Mermel et al., 2011) score and mRNA expression levels were taken from cBio databases using all TCGA cases (5818) from the previously listed studies that have data for both variables. As with the mutational analysis, data from published cases was used first and unpublished data only used if the published data did not exist. Copy number analysis plots were done using ggplot2 (Wickham, 2009). Correlation scores were calculated using the core R package stats (R-Core-Team, 2014).

AUTHOR CONTRIBUTIONS

L.L.G, J.B., A.C.N, and T.H. initiated the study. C.E.A and A.C.N conceived the experiments and wrote the manuscript. C.E.A performed the experiments with assistance from E.K. for imaging and immunoblots and from C.Z. for the xenograft model. F.B.F. advised on the use of the xenograft model. A.M.H, C.W., C.J.M., and J.B. performed the bioinformatic analysis. N.L.S and E.W.T made the tetracycline-inducible PKCβII HCT116 cells.

ACKNOWLEDGMENTS

We thank the Moores Cancer Center Histology Core for the TUNEL staining, Meghdad Rahdar for cell sorting, and Jack Dixon for equipment use. This work was supported by NIH GM43154 to A.C.N., NIH NS080939 and the James S. McDonnell Foundation to F.B.F., and NIH CA82683 to T.H. C.E.A. was supported by the UCSD Graduate Training Program in Cellular and Molecular Pharmacology (T32 GM007752) and the NSF Graduate Research Fellowship (DGE1144086). A.M.H., C.W., N.L.S,. E.W.T., C.J.M., and J.B. were supported by Cancer Research UK. T.H. is a Frank and Else Schilling American Cancer Society Professor and holds the Renato Dulbecco Chair in Cancer Research.

Chapter 4, in full, is a reprint of material that appears in "Cancer-associated Protein Kinase C Mutations Reveal Kinase's Role as Tumor Suppressor" by Corina E. Antal, Andrew M. Hudson, Emily Kang, Ciro Zanca, Christopher Wirth, Natlaie N. Stephenson, Emily W. Trotter, Lissa L. Gallegos, Crispin J. Miller, Frank B. Furnari, Tony Hunter, John Brognard, and Alexandra C. Newton as published in *Cell in* 2015. The dissertation author was the primary investigator and author of the material.

FIGURES

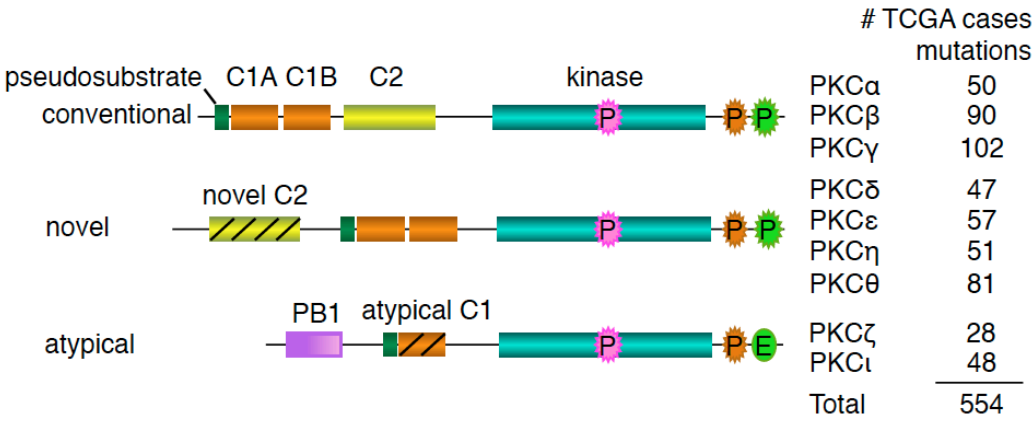

Figure 20. A Multitude of Cancer-Associated Mutations Have Been Identified within the 9 PKC Genes
Left: domain structure of conventional (α, β, γ), novel (δ, ε, η, θ), and atypical (ι, ζ) PKC members showing priming phosphorylation sites: activation loop (pink), turn motif (orange), and hydrophobic motif (green). Right: Number of TCGA cases with cancer-associated mutations (missense, nonsense, insertions, deletions, splice site, or translation start site) identified within each of the PKC isozymes.

Figure 21. PKC Mutations in the Regulatory C1 and C2 Domains Are LOF
(A) Solution structure of the C1A domain of PKCγ (PDB 2E73) showing the corresponding PKCα His75 residue that coordinates Zn2+ and PKCα Trp58. (B) Normalized FRET ratio changes (mean ± SEM) representing DiC8- (10 μM) followed by PDBu- (200 nM) induced PKC activity as read out by CKAR in COS7 cells co-expressing CKAR and either mCherry-tagged WT, mutant PKCα, or no exogenous PKC (endogenous). (C) Left: representative YFP images of the indicated PKC isozymes under basal and PDBu-treated conditions (200 nM; 15 min) showing relocalization of WT but not mutant PKCα to membranes. Right: normalized FRET ratio changes (mean ± SEM) quantifying translocation of YFP-tagged PKCα proteins towards a membrane-targeted CFP upon stimulation with 10μM DiC8, followed by 200 nM PDBu. (D) Normalized FRET ratio changes (mean ± SEM) showing PKC translocation following UTP (100 μM) stimulation. (E) Immunoblot showing the phosphorylation state of the indicated YFP-tagged PKCα proteins. (F) Crystal structure of the C2 domain of PKCγ (PDB 2UZP) highlighting Asp193 and Asp254 residues involved in Ca^{2+}-binding. (G) Normalized FRET ratio changes (mean ± SEM) showing PKC activity as read out by CKAR upon elevation of intracellular Ca2+ stimulated by thapsigargin (5 μM), followed by PDBu (200 nM). (H) Normalized FRET ratio changes (mean ± SEM) showing translocation of YFP-tagged PKCγ constructs towards membrane-localized CFP upon stimulation of COS7 cells with thapsigargin (5 μM) followed by PDBu (200 nM). Data were normalized to the maximal amplitude of translocation for each cell and then scaled from 0 to 1 using the equation: X = (Y-Ymin)/(Ymax-Ymin), where Y = normalized FRET ratio, Ymin = minimum value of Y, and Ymax is maximum value of Y. (I) Normalized FRET ratio changes (mean ± SEM) displaying oscillatory translocation of YFP-tagged WT PKCγ, but not PKCγ mutants D193N and D254N, in HeLa cells co-expressing membrane-targeted CFP and stimulated with 10 μM histamine. Data are representative traces from individual cells of 3 independent experiments.

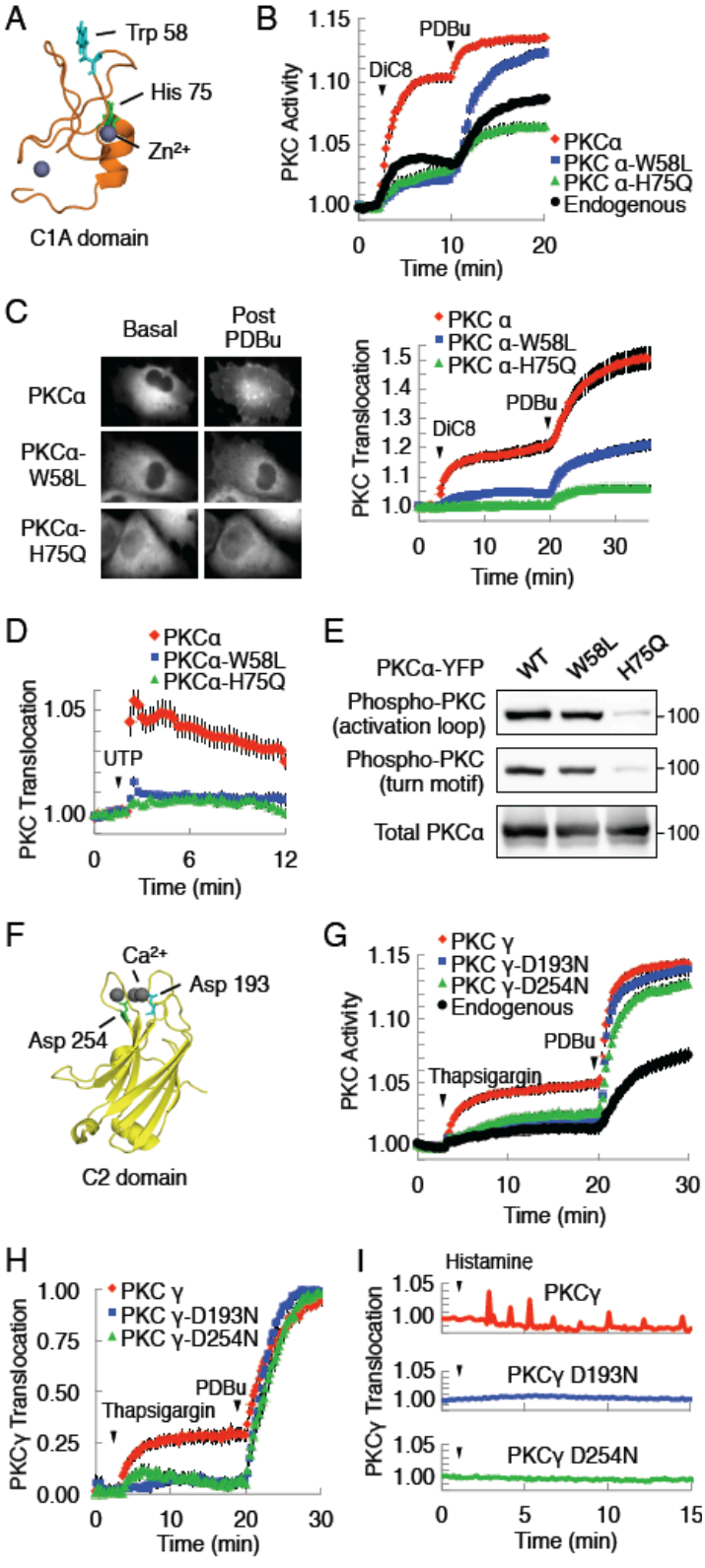
A
Trp 58
His 75
Zn2+
C1A domain
B
PDBu
DiC8
PKC Activity
1.15
1.10
1.05
1.00
0
10
20
Time (min)
PKCα
PKC α-W58L
PKC α-H75Q
Endogenous
C
Basal
Post PDBu
PKCα
PKCα-W58L
PKCα-H75Q
PKC α
PKC α-W58L
PKC α-H75Q
PKC Translocation
1.5
1.4
1.3
1.2
1.1
1.0
PDBu
DiC8
0
10
20
30
Time (min)
D
PKCα
PKCα-W58L
PKCα-H75Q
PKC Translocation
1.05
1.00
UTP
0
6
12
Time (min)
E
PKCα-YFP
WT
W58L
H75Q
Phospho-PKC (activation loop)
Phospho-PKC (turn motif)
Total PKCα
100
100
100
F
Ca2+
Asp 193
Asp 254
C2 domain
G
PKC γ
PKC γ-D193N
PKC γ-D254N
Endogenous
PKC Activity
1.15
1.10
1.05
1.00
PDBu
Thapsigargin
0
10
20
30
Time (min)
H
PKC γ
PKC γ-D193N
PKC γ-D254N
PKCγ Translocation
1.00
0.75
0.50
0.25
0.00
PDBu
Thapsigargin
0
10
20
30
Time (min)
I
Histamine
PKCγ
PKCγ D193N
PKCγ D254N
PKCγ Translocation
1.05
1.00
0
5
10
15
Time (min)

Figure 22. PKC Mutations that Reduce Its Activity
(A) Normalized FRET ratio changes showing basal PKC activity of the indicated mCherry-tagged PKCα constructs in COS7 cells co-expressing CKAR that were treated with 1 μM of PKC inhibitor Gö6976. FRET ratios represent mean ± SEM from at least 3 independent experiments. (B) Normalized FRET ratio changes showing PKC activity of the indicated mCherry-tagged PKCα constructs in COS7 cells co-expressing plasma membrane-targeted CKAR that were stimulated with 10 μM DiC8 followed by 200 nM PDBu. FRET ratios represent mean ± SEM from at least 3 independent experiments. (C) Normalized FRET ratio changes showing PKC activity of the indicated mCherry-tagged PKCβII constructs in COS7 cells co-expressing CKAR that were stimulated with 100 μM UTP followed by 200 nM PDBu. FRET ratios represent mean ± SEM from at least 2 independent experiments. (D) Normalized FRET ratio changes showing PKC activity of the indicated RFP-tagged PKCγ constructs in COS7 cells co-expressing CKAR that were stimulated with 100 μM UTP followed by 200 nM PDBu. FRET ratios represent mean ± SEM from at least 3 independent experiments. (E) Normalized FRET ratio changes showing PKC activity of the indicated mCherry-tagged PKCα constructs in COS7 cells co-expressing CKAR that were stimulated with 100 μM UTP followed by 200 nM PDBu. FRET ratios represent mean ± SEM from at least 3 independent experiments. (F) Immunoblot analysis of the phosphorylation state at the activation loop and total levels of indicated mCherry-tagged PKCα constructs overexpressed in COS7 cells. (G) Immunoblot analysis of the phosphorylation state at the activation loop and total levels of HA-tagged PKCζ WT and E421K and empty vector (-) overexpressed in COS7 cells. Arrow shows phospho-PKCζ band and *asterisk* shows endogenous PKC activation loop phosphorylation. (H) Immunoblot showing activation loop phosphorylation and total levels of HA-tagged PKCβII WT and mutants overexpressed in COS7 cells. Blot at the same exposure was cropped to juxtapose WT and G585S. (I) Immunoblot analysis of the phosphorylation state at the activation loop and total levels of mCherry-tagged PKCβII WT and Y417H overexpressed in COS7 cells. (J) Immunoblot analysis of the phosphorylation state at the activation loop and total levels of indicated RFP-tagged PKCγ constructs overexpressed in COS7 cells. (K) Normalized FRET ratio changes showing PKC activity of the indicated mCherry-tagged PKCε constructs in COS7 cells co-expressing CKAR that were stimulated with 100 μM UTP followed by 200 nM PDBu. FRET ratios represent mean ± SEM from at least 4 independent experiments. (L) Normalized FRET ratio changes showing basal PKC activity of the indicated mCherry-tagged PKCε constructs in COS7 cells co-expressing CKAR that were treated with 6 μM of PKC inhibitor Gö6983. FRET ratios represent mean ± SEM from at least 2 independent experiments.

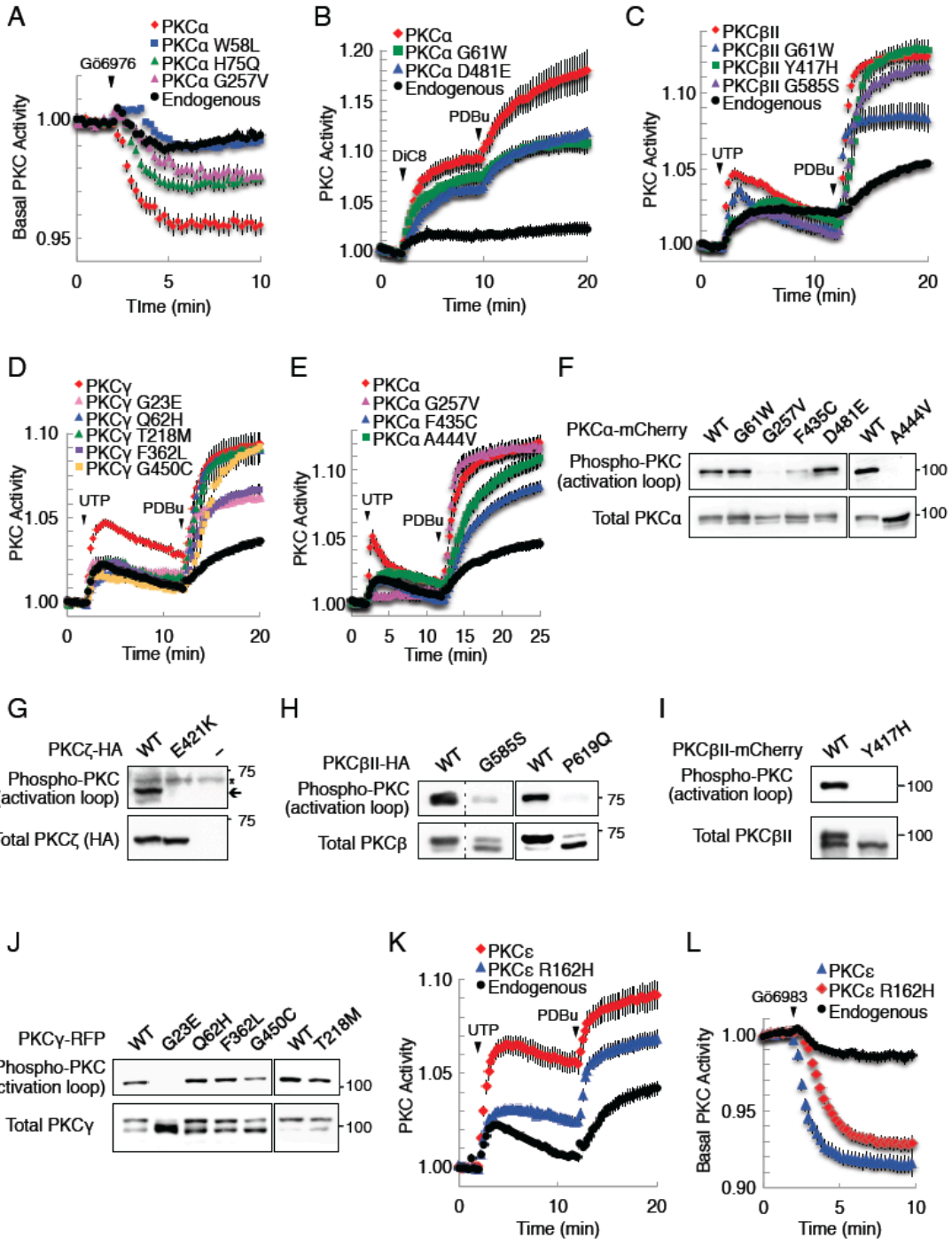
A
PKCα
PKCα W58L
PKCα H75Q
PKCα G257V
Endogenous
Gö6976
Basal PKC Activity
TIme (min)
B
PKCα
PKCα G61W
PKCα D481E
Endogenous
DiC8
PDBu
PKC Activity
Time (min)
C
PKCβII
PKCβII G61W
PKCβII Y417H
PKCβII G585S
Endogenous
UTP
PDBu
PKC Activity
Time (min)
D
PKCγ
PKCγ G23E
PKCγ Q62H
PKCγ T218M
PKCγ F362L
PKCγ G450C
UTP
PDBu
PKC Activity
Time (min)
E
PKCα
PKCα G257V
PKCα F435C
PKCα A444V
UTP
PDBu
PKC Activity
Time (min)
F
PKCα-mCherry
WT
G61W
G257V
F435C
D481E
WT
A444V
Phospho-PKC (activation loop)
Total PKCα
100
G
PKCζ-HA
WT
E421K
–
Phospho-PKC (activation loop)
Total PKCζ (HA)
75
H
PKCβII-HA
WT
G585S
WT
P619Q
Phospho-PKC (activation loop)
Total PKCβ
75
I
PKCβII-mCherry
WT
Y417H
Phospho-PKC (activation loop)
Total PKCβII
100
J
PKCγ-RFP
WT
G23E
Q62H
F362L
G450C
WT
T218M
Phospho-PKC (activation loop)
Total PKCγ
100
K
PKCε
PKCε R162H
Endogenous
UTP
PDBu
PKC Activity
Time (min)
L
PKCε
PKCε R162H
Endogenous
Gö6983
Basal PKC Activity
Time (min)

Figure 23. PKC Mutations in the Kinase Domain Are LOF

(A) Crystal structure of the kinase domain of PKCβII (PDB 2I0E) highlighting cancer-associated residues and the regulatory spine (yellow space filling). (B) Normalized FRET ratio changes (mean ± SEM) showing PKC activity of PKCδ constructs in COS7 cells co-expressing the plasma membrane-targeted, PKCδ specific reporter, PM-δCKAR. Cells were stimulated with UTP (100 μM) followed by PDBu (200 nM). (C) Immunoblot analysis of the phosphorylation state of PKCδ WT and mutants. (D) Representative mCherry images of mCherry-tagged PKCη WT or mutants showing localization under basal conditions and 15 min post 200 nM PDBu addition to COS7 cells. (E) Left: immunoblot showing PKC substrate phosphorylation. COS7 cells overexpressing the indicated constructs were pre-treated with 4 μM Gö6976 for 10 min to inhibit cPKC isozymes and then stimulated or not with 200 nM PDBu to activate nPKC isozymes. Right: immunoblots were quantified and normalized to total PKCη levels and tubulin (right panel). Data represent averages of 3 independent experiments ± SEM. Comparisons for basal and stimulated activity were made using a repeated measure one-way ANOVA followed by post hoc Dunnett's multiple comparison test: *$p < 0.05$ as compared with the WT group. (F) Immunoblot analysis of the phosphorylation state of mCherry-tagged PKCη WT and mutants. (G) Normalized FRET ratio changes (mean ± SEM) showing PKC activity from COS7 cells co-expressing CKAR and RFP-tagged PKCγ mutants stimulated with 200 nM PDBu. (H) Immunoblot depicting PKCγ WT and P524R phosphorylation. The *asterisk* denotes phosphorylated and the *dash* unphosphorylated PKCγ. (I) Normalized FRET ratio changes (mean ± SEM) showing PKC activity of PKCβII constructs in COS7 cells co-expressing CKAR. Cells were stimulated with UTP (100 μM) followed by PDBu (200 nM). (J) Immunoblot depicting mCherry-tagged PKCβII WT and mutant phosphorylation. The *asterisk* denotes phosphorylated and the *dash* unphosphorylated PKCβII.

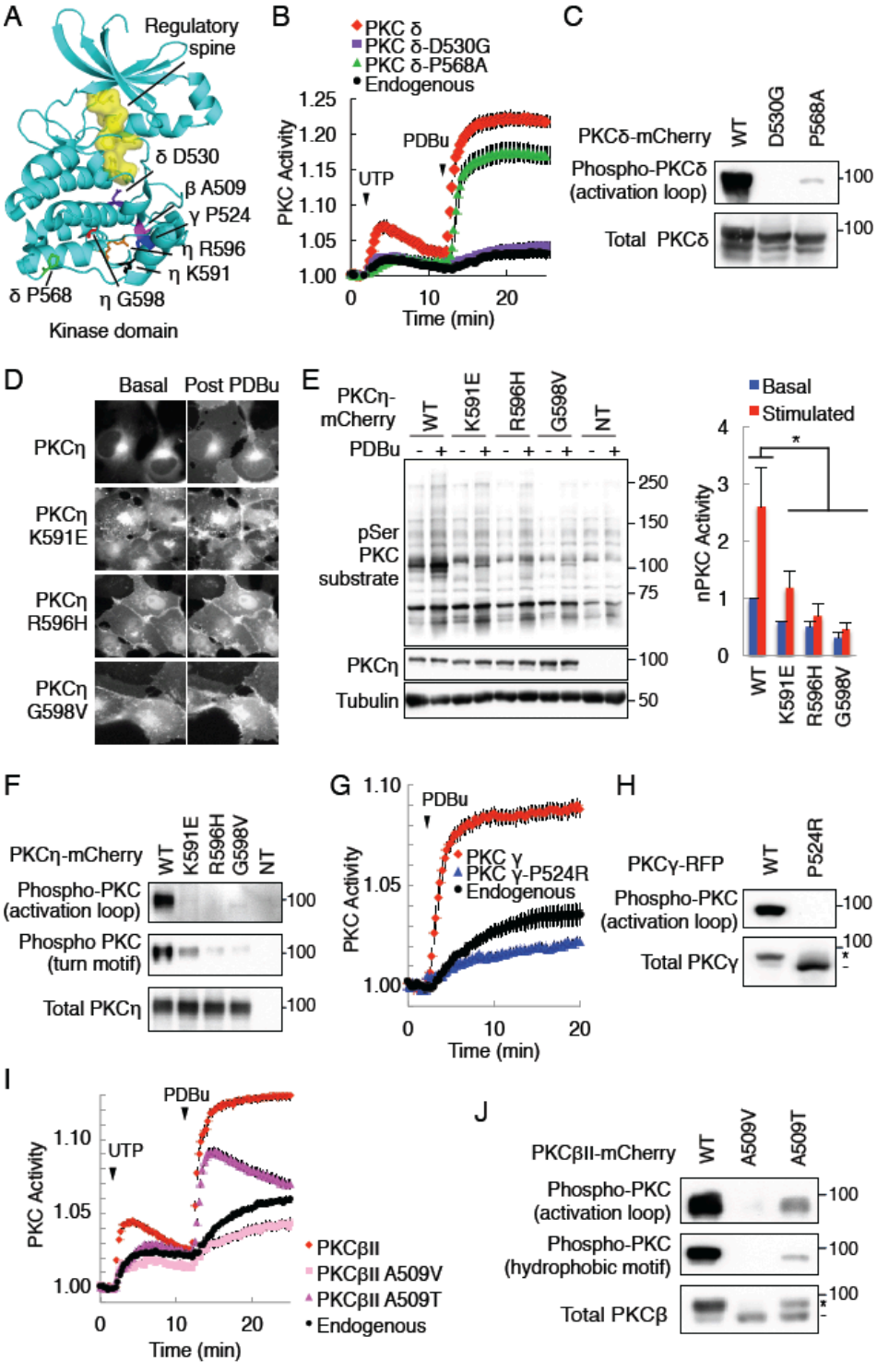
A
Regulatory spine
δ D530
β A509
γ P524
η R596
η K591
δ P568
η G598
Kinase domain
B
PKC δ
PKC δ-D530G
PKC δ-P568A
Endogenous
PKC Activity
PDBu
UTP
Time (min)
C
PKCδ-mCherry
WT
D530G
P568A
Phospho-PKCδ (activation loop)
Total PKCδ
D
Basal
Post PDBu
PKCη
PKCη K591E
PKCη R596H
PKCη G598V
E
PKCη-mCherry
WT
K591E
R596H
G598V
NT
PDBu
pSer PKC substrate
PKCη
Tubulin
Basal
Stimulated
nPKC Activity
F
PKCη-mCherry
Phospho-PKC (activation loop)
Phospho PKC (turn motif)
Total PKCη
G
PKC γ
PKC γ-P524R
Endogenous
H
PKCγ-RFP
P524R
Phospho-PKC (activation loop)
Total PKCγ
I
PKCβII
PKCβII A509V
PKCβII A509T
J
PKCβII-mCherry
A509V
A509T
Phospho-PKC (hydrophobic motif)
Total PKCβ

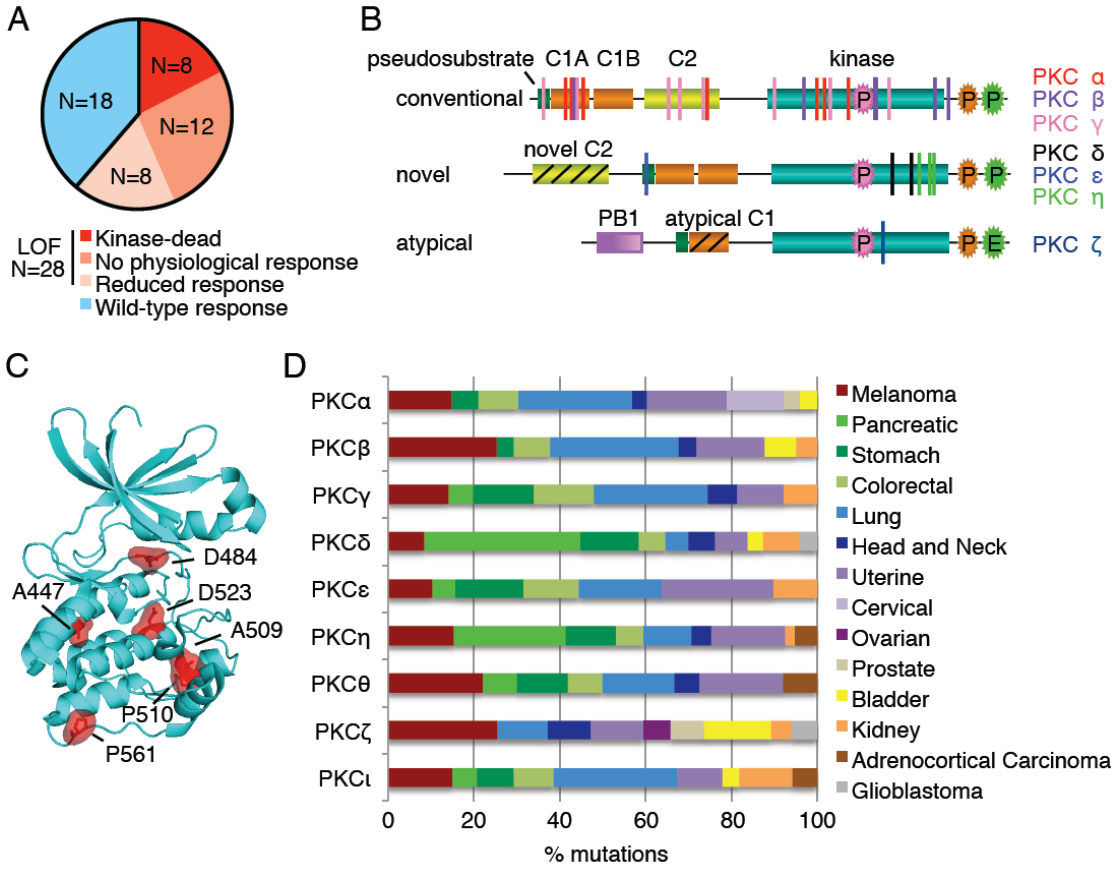

Figure 24. The Majority of PKC Mutations Are Loss-of-Function
(A) Pie chart of the functional impact of the investigated PKC mutations, with bright red representing mutations that lack any activity, medium red representing mutations that show no response to physiological stimuli (DAG or Ca^{2+} elevation) but some response to non-physiological phorbol esters, light red representing mutations that display reduced activity to physiological stimuli compared to the corresponding WT isozyme, and blue representing no difference from the corresponding WT PKC isozyme. (B) Domain structure of cPKC, nPKC, and aPKC isozymes, overlaid with the LOF mutations color-coded by isozyme. (C) Crystal structure of the kinase domain of PKCβII (PDB 2I0E) highlighting "warmspot" residues mutated in at least 4 tumor samples within the various PKC isozymes. (D) Bar graph depicting the % mutations across various cancers for each PKC isozyme.

Figure 25. CRISPR-Mediated Genome Editing of PKCβ A509T Mutation

(A) Immunoblot analysis of PKCβ in HCT116 cells expressing PKCβII under the control of a tetracycline (tet)-inducible promoter and control parental HCT116 cells lacking the PKCβII transgene, in the presence or absence of 1 μg/μl tetracycline (left panel). Colony formation assay in soft agar (middle panel). Transgenic HCT116 cells in the absence of tetracycline and control cells lacking the PKCβII transgene are permissive to colony growth in soft agar. Overexpression of PKCβII upon treatment with 1 μg μl^{-1} tetracycline diminished growth in soft agar. Quantification of number of colonies with a diameter greater than 100 μm (right panel). Graph represents averages ± SEM from 2 independent experiments performed in triplicate. ***, $p < 0.0005$ according to a two-tailed, unpaired Student's t-test. (B) Schematic representation of the PKCβ genomic locus targeted for CRISPR/Cas9-mediated genome editing with the A509T (G:C -> A:T) mutation highlighted in red. The mutant DNA sequence is shown above and the corresponding protein sequence below. Oligonucleotides used as templates for gRNAs, PKCβ-a and PKCβ-b, are underlined in black with the protospacer adjacent motif (PAM) sequence underlined in red. The sites of cleavage are marked by scissors. The sequence for the donor ssODN used is highlighted in green (except it contained the wild-type "G" allele instead of the mutant "A"). BtgZI shows cleavage site used for diagnostic restriction enzyme digest. (C) DNA sequencing results of DLD1 parental cells and the 3 corrected clones with red box highlighting the corrected base pair.(D) Graph showing similar growth rates of DLD1 parental and the 3 corrected clones from a crystal violet proliferation assay. Data represent mean ± SEM from 3 independent experiments performed in triplicate. (E) Sequences of the PKCβ clone WT/- 23 alleles showing the intact WT allele and the mutant allele that was knocked out by a frameshift deletion spanning the exon (capital letters)/intron (lower-case letters) junction and chromatograms depicting deletion are shown. (F) Immunoblot analysis of PKCβII, and ERK levels in the DLD1 cells. (G) Graph showing volume of tumors (day 42; mean ± SEM) obtained from nude mice injected subcutaneously with 3×10^6 DLD1 parental (A509T/WT) or DLD1 corrected (WT/WT 26, WT/WT 31, or WT/WT 53) cells. Comparisons were made using a one-way ANOVA followed by a post hoc Dunnett's multiple comparison test: $*p < 0.05$.

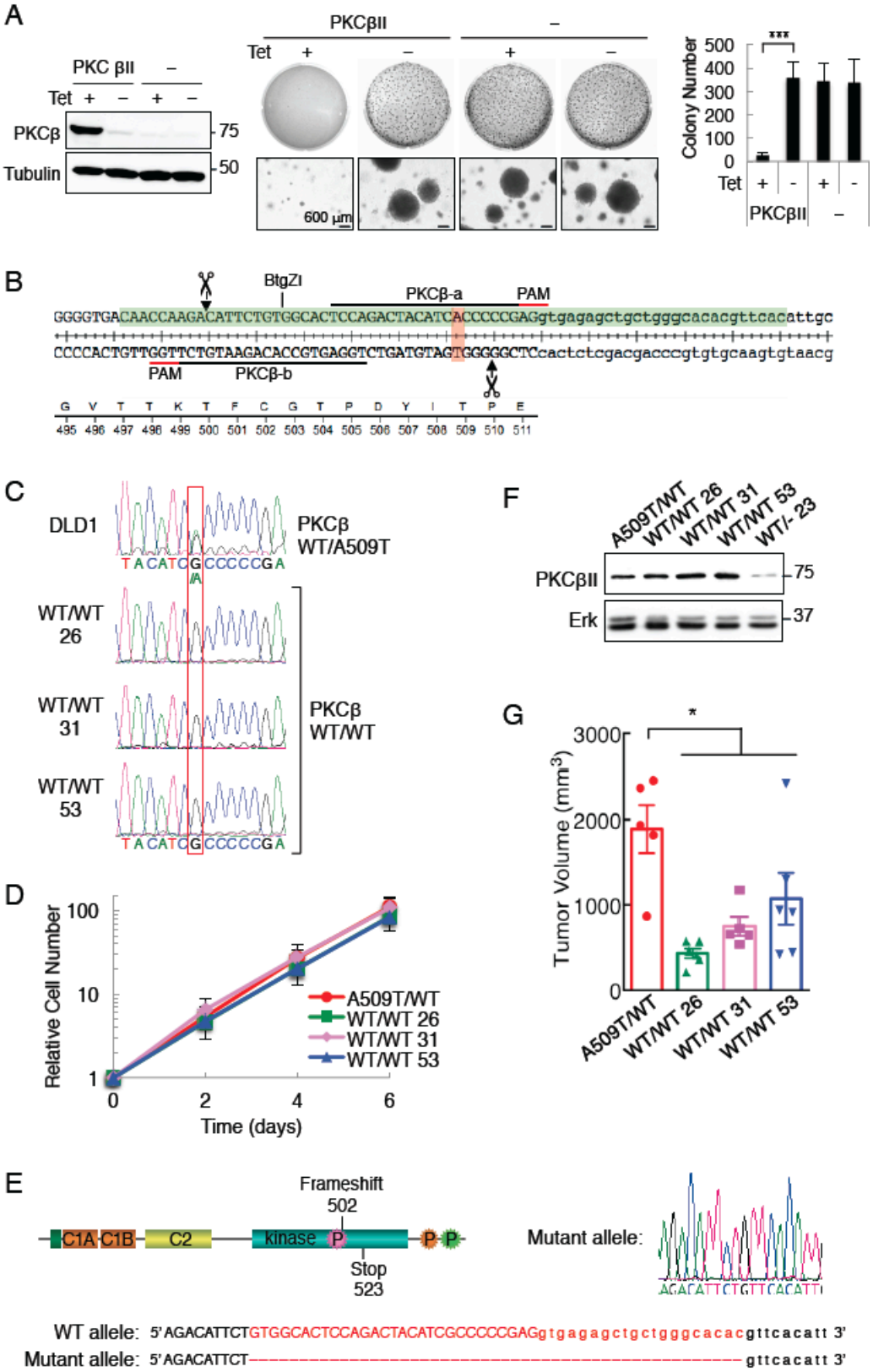
A
PKC βII
Tet
PKCβ
Tubulin
75
50
PKCβII
600 μm
Colony Number
500
400
300
200
100
0
***
B
BtgZI
PKCβ-a
PAM
PKCβ-b
C
DLD1
PKCβ WT/A509T
WT/WT 26
WT/WT 31
WT/WT 53
PKCβ WT/WT
D
Relative Cell Number
100
10
1
Time (days)
A509T/WT
WT/WT 26
WT/WT 31
WT/WT 53
E
Frameshift 502
C1A
C1B
C2
Kinase
P
Stop 523
Mutant allele:
WT allele: 5' AGACATTCTGTGGCACTCCAGACTACATCGCCCCCGAGgtgagagctgctgggcacacgttcacatt 3'
Mutant allele: 5' AGACATTCT gttcacatt 3'
F
A509T/WT
WT/WT 26
WT/WT 31
WT/WT 53
WT/- 23
PKCβII
Erk
75
37
G
Tumor Volume (mm3)
3000
2000
1000
0
*
A509T/WT
WT/WT 26
WT/WT 31
WT/WT 53

Figure 26. Correction of a Heterozygous LOF PKCβ Mutation Reduces Growth in Soft Agar, Suspension, and a Xenograft Model

(A) Immunoblot (left) and quantification (right; mean ± SEM) of PKCβII, PKCα, and GAPDH levels in the DLD1 cells. (B) Immunoblot (left) and quantification (right; mean ± SEM) of phospho-(Ser) PKC substrates. Comparisons were made using a repeated measure one-way ANOVA followed by post hoc Dunnett's multiple comparison test: *$p < 0.05$ as compared with the DLD1 parental cells. Data represent 3 independent experiments ± SEM. (C) Relative viable cell number (mean ± SEM) as assessed by a trypan blue exclusion assay after 72 hr in suspension from 3 independent experiments. Comparisons were made by using a one-way ANOVA followed by post hoc Dunnett's Multiple Comparison test: ***$p < 0.001$ as compared with the DLD1 parental cell group. (D) Representative phase contrast images of DLD1 cells grown in suspension for 24 hr. (E) Left: colony formation assay in soft agar. Right: quantification of colony area (mean ± SEM) for colonies with a diameter ≥ 50 μm from 3-6 independent experiments. Comparisons were made using a one-way ANOVA followed by post hoc Tukey's multiple comparison test: ****$p < 0.0001$ and ***$p < 0.001$ as compared with the DLD1 parental cell group. (F) Tumor growth is presented as the mean tumor volume (mm^3) ± SEM with the red representing data from mice injected with the DLD1 parental cells (A509T/WT; 5 mice) and purple representing the mean of the 3 corrected clones (17 mice total). Comparisons were made using a two-tailed, unpaired Student's t-test for each time point: **$p < 0.005$ and ***$p < 0.0005$. (G) Top: representative fields from TUNEL-stained slides of tumors derived from the DLD1 cells. Bottom: quantification of TUNEL positive nuclei. Comparisons were made using a one-way ANOVA followed by post hoc Dunnett's Multiple Comparison test: ****$p < 0.0001$ as compared with the DLD1 parental cell group.

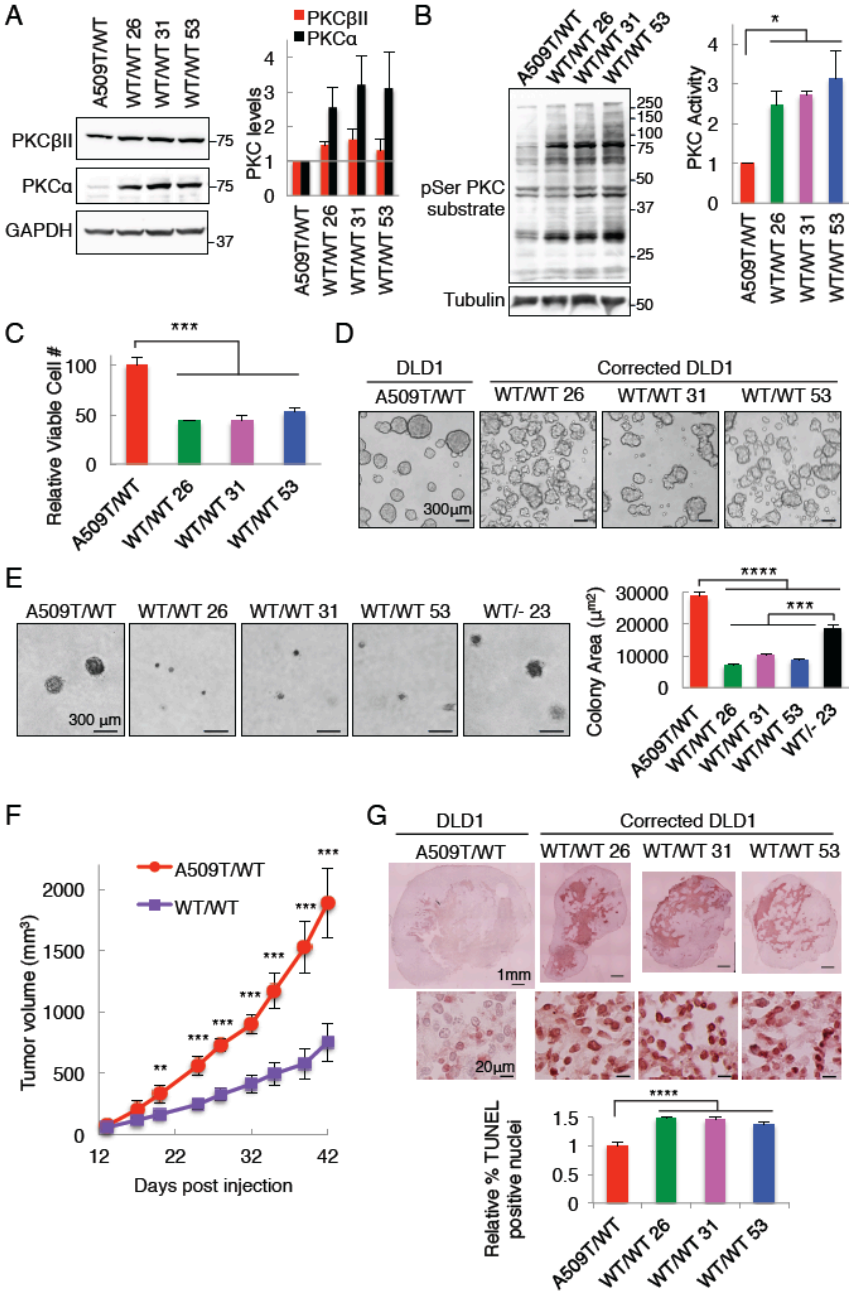
A
A509T/WT
WT/WT 26
WT/WT 31
WT/WT 53
PKCβII
PKCα
GAPDH
75
75
37
PKCβII
PKCα
PKC levels
4
3
2
1
0
B
pSer PKC substrate
Tubulin
250
150
100
75
50
37
25
50
PKC Activity
*
C
***
Relative Viable Cell #
100
50
0
D
DLD1
Corrected DLD1
300μm
E
300 μm
Colony Area (μm²)
30000
20000
10000
****
***
WT/- 23
F
A509T/WT
WT/WT
Tumor volume (mm³)
2000
1500
1000
500
0
12
22
32
42
Days post injection
**
G
1mm
20μm
Relative % TUNEL positive nuclei
1.5
1
0.5
****

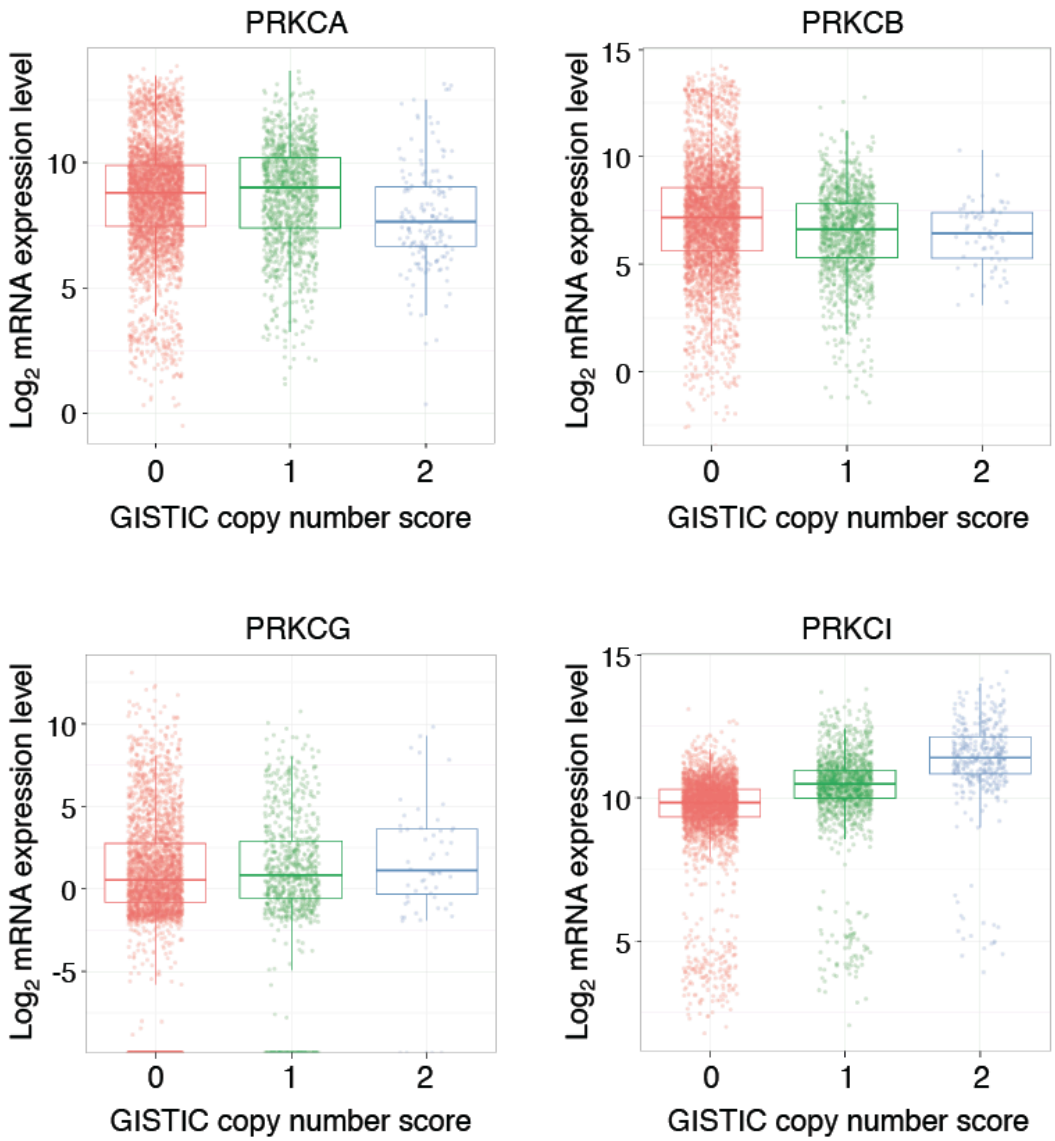

Figure 27. DNA Copy Number Levels and mRNA Expression Correlations
Graphs displaying correlations between log_2 mRNA expression levels and the GISTIC copy number score for the conventional PKC genes: *PRKCA* (PKCα; $r^2 = 0.0017$), *PRKCB* (PKCβ $r^2 = 0.016$), and *PRKCG* (PKCγ $r^2 = 0.00012$), and the atypical *PRKCI* (PKCι $r^2 = 0.23$). 0 represents a diploid gene, 1 represents a single copy gain, and 2 shows high-level amplification or multiple-copy gains. Boxes indicate the median, and the 25th and 75th percentiles; whiskers extend to highest (or lowest) value that falls within 1.5 x the Inter Quartile Range.

TABLES

Table 1. Loss-of-Function PKC Mutations in Cancer
PKC mutations showing no activity with any agonist, no activity with physiological stimuli, or reduced activity in response to physiological stimuli. Allele frequencies were obtained from cBio Portal.

Mutation[a]	Activity	Domain	Cancer(s)	Residue Importance	Allele Frequency	Other Mutations[b]
γ G23E	none[c]	PS	colorectal	adding negative charge to pseudosubstrate	N/A	γ G23W δ G146R ι G128C
ε R162H	low		head and neck	non-conserved	0.15	
α W58L	none[c]	C1A	head and neck	DAG binding; conserved in all C1a domains	0.22	γ W57splice θ W171*
α G61W	low		lung	conserved in cPKC C1a domains	0.05	β G61W
β G61W	low		lung	conserved in cPKC C1a domains	0.06	α G61W
γ Q62H	none[c]		lung	conserved in all PKC isozymes	0.45	α Q63H ε Q197P
α H75Q	none[d]		colorectal	coordinates Zn^{2+}; conserved in all C1 domains	N/A	η H284Y ι H179Y
γ D193N	none[c]	C2	colorectal/melanoma/ovarian	Ca^{2+} binding site	0.28	
γ T218M	none[c]		stomach	non-conserved	0.42	γ T218R
γ D254N	low		endometrial/ovarian	Ca^{2+} binding site	0.43	
α G257V	none[c]		lung	conserved in cPKC isozymes	0.12	
γ F362L	none[c]	Kinase	endometrial	conserved in cPKC and nPKC isozymes	0.21	γ F362fs β F353L
β Y417H	none[c]		liver	conserved in cPKC isozymes	0.67	γ Y431F
ζ E421K	none[d]		breast	APE motif; conserved in most protein kinases	N/A	α E508K ι E423D
α F435C	none[c]		endometrial	conserved in cPKC and nPKC isozymes	0.31	
α A444V	low		endometrial/breast	conserved in cPKC and nPKC isozymes	0.27	β A447T γ A461T γ A461V δ A454V θ A485T ι S359C
γ G450C	none[c]		endometrial/lung/liver	conserved in cPKC isozymes	0.41	ε R502*
α D481E	low		colorectal	DFG motif; conserved in most protein kinases	N/A	β D484N γ D498N ι D396E
β A509V	none[d]		breast	APE motif; conserved in most protein kinases	N/A	α A506V α A506T β A509T
β A509T	none[c]		colorectal	APE motif; conserved in most protein kinases	0.53	α A506V α A506T β A509V
γ P524R	none[d]		pancreatic	APE motif; conserved in most protein kinases	N/A	γ P524L δ P517S ε P576S θ P548S
δ D530G	none[d]		colorectal	anchors the conserved regulatory spine; conserved in all eukaryotic kinases	N/A	β D523N γ D537G γ D537Y
δ P568A	none[c]		head and neck	conserved in all PKC isozymes	0.16	δ P568S β P561H γ P575H
β G585S	low		lung	conserved in all PKC isozymes	N/A	η G598V
η K591E	low		breast	reversal of conserved charge	N/A	η K591N θ R616Q
η R596H	none[d]		colorectal	conserved in all PKC isozymes	0.50	
η G598V	none[d]		lung	conserved in all PKC isozymes	N/A	β G585S
β P619Q	none[d]	C-tail	endometrial	PXXP motif; conserved in AGC kinases	0.48	

[a] Mutations examined in this study
[b] Other mutations present at the same/corresponding residue in the same/other PKC isozymes
[c] Kinase-dead
[d] No response to physiological stimuli

Table 2. PKC Mutations that Showed No Difference from Wild-Type Under Parameters Tested
PKC mutations showing similar activity to their corresponding wild-type isozyme using CKAR as a readout.

Mutation[a]	Domain	Cancer(s)	Residue Importance	Allele Frequency	Other Mutations[b]
δ R67C	C2-like	glioma/colorectal	non-conserved; pTyr binding site	0.44	
α P98S	Interdomain	colorectal	conserved in cPKC isozymes	N/A	
δ V174L	C1A	bladder	non-conserved	0.24	
γ S109R	C1B	lung	non-conserved; putative 14-3-3ε binding site	N/A	α G110R θ K240N
α D116N		colorectal	non-conserved	N/A	
θ K240N		colorectal	non-conserved	0.67	γ S109R
γ R252H	C2	pancreatic/colorectal	conserved in cPKC isozymes	N/A	
β G262R		lung	conserved in cPKC isozymes	0.09	β G262V
β A269T		colorectal	non-conserved	N/A	
α Y286C	Hinge	endometrial	non-conserved	0.42	γ Y286F
δ S302L		melanoma	non-conserved	0.62	
α D467N	Kinase	glioma	conserved in all PKC isozymes	N/A	
ε F476L		ovarian	conserved in all PKC isozymes	N/A	θ F448V
β V496M		glioma	non-conserved; homozygous mutation	N/A	γ T510M θ A534S
γ Y521N		lung	pTyr ; conserved in PKA, B, C	N/A	γ Y521C
ε D541N		lung	conserved in all PKC isozymes	N/A	
δ S645F	C-tail	melanoma	turn motif phosphorylation site	N/A	
α E606K		melanoma	not conserved in nPKC isozymes	0.30	θ E643K

[a] Mutations examined in this study.
[b] Other mutations present at the same/corresponding residue in the same/other PKC isozymes

Table 3. Top 20 Genes with Mutations that Co-Occur with PKC Mutations
Data were normalized based on gene length and the number of co-occurring cases is listed in parentheses. Two genes are highlighted: *TP53* is underlined and *KRAS* is in bold.

PKCα (50)	PKCβ (90)	PKCγ (102)	PKCδ (47)	PKCε (57)	PKCη (51)	PKCθ (81)	PKCι (48)	PKCζ (28)
BLID25 (7)	TP53 (42)	TP53 (52)	**KRAS** (13)	GNG4 (5)	SPINK7 (5)	TP53 (42)	SPRR2G (6)	TNP1 (3)
TP53 (23)	KRTAP6-2 (6)	CDKN2A (17)	TP53 (22)	**KRAS** (11)	RPL39 (3)	CDKN2A (13)	TP53 (26)	TP53 (15)
KRTAP19-5 (4)	PCP4 (4)	**KRAS** (16)	CDKN2A (9)	DEFB114 (4)	**KRAS** (11)	**KRAS** (14)	CDKN2A (10)	CNPY1 (3)
SPRR2E (4)	**KRAS** (12)	HTN1 (4)	CD52 (3)	CNPY1 (5)	DEFB114 (4)	SPANXN5 (5)	BANF1 (5)	SPATA8 (3)
REG3A (8)	OR4A15 (21)	SPRR2G (5)	CNPY1 (4)	SVIP (4)	PLN (3)	DEFB110 (4)	LACRT (7)	SPANXN3 (4)
H3F3C (6)	POM121L12 (18)	DEFB115 (6)	SPINK13 (4)	CXCL10 (5)	DEFB115 (5)	KRTAP15-1 (8)	CXCL9 (6)	KRTAP19-5 (2)
MLLT11 (4)	REG1A (10)	DNAJC5B (12)	ATP5E (2)	KRTAP19-3 (4)	LELP1 (5)	DEFB119 (5)	**KRAS** (9)	VPREB1 (4)
PI3 (5)	NRAS (11)	REG3G (10)	RPL39 (2)	COX7C (3)	DEFB116 (5)	PPIAL4G (9)	RETNLB (5)	GNG4 (2)
SNURF (3)	PLN (3)	SPATA8 (6)	COX7B2 (3)	KRTAP19-8 (3)	KRTAP19-8 (3)	DPPA5 (6)	WFDC10B (4)	ATP6V1G3 (3)
CDKN2A (7)	GNG4 (4)	REG1A (9)	OR4K1 (11)	SPINK7 (4)	IAPP (4)	CRYGB (9)	DEFB110 (3)	CDKN2A (4)
GNG3 (3)	CDKN2A (9)	POM121L12 (16)	FDCSP (3)	TP53 (18)	NPS (4)	SPANXN2 (9)	TMSB15B (2)	DEFB119 (2)
DAOA (6)	DEFA4 (5)	TRAT1 (10)	CARTPT (4)	BANF1 (4)	WFDC10B (4)	KRTAP19-3 (4)	GNG7 (3)	LGALS1 (3)
RPL39 (2)	OR2L13 (16)	HIST1H2AA (7)	DUSP22 (7)	TMSB15B (2)	S100A7L2 (5)	DYNLRB2 (6)	CNPY1 (4)	SCGB1D1 (2)
SVIP (3)	LCE1B (6)	SPINK13 (5)	BANF1 (3)	DEFA4 (4)	CNPY1 (4)	SPATA8 (5)	LSM8 (4)	NANOS2 (3)
PLN (2)	SPANXN3 (7)	CCK (6)	DYNLL2 (3)	POM121L12 (12)	TP53 (17)	KRTAP19-8 (3)	KRTAP19-5 (3)	CCL17 (2)
FAM19A2 (5)	KRTAP19-3 (4)	OR4K1 (16)	LYRM5 (3)	GYPA (6)	DPPA5 (5)	RIPPLY3 (9)	SPANXN5 (3)	NRAS (4)
CPLX4 (6)	TRAT1 (9)	OR4A5 (16)	ATP6V1G3 (4)	DYNLRB2 (5)	DEFB131 (3)	POM121L12 (14)	CSTL1 (6)	CCL1 (2)
SEC22B (8)	IFNB1 (9)	CCL7 (5)	DEFB128 (3)	HIST1H2BB (5)	SPINK13 (4)	OR4N2 (14)	DEFA4 (4)	PATE4 (2)
CTXN3 (3)	KRTAP19-8 (3)	B2M (6)	MAP1LC3B2 (4)	HIST1H2BI (5)	RPL10L (9)	DEFB115 (4)	SPANXD (4)	POM121L12 (6)
KRTAP19-3 (3)	KRTAP8-1 (3)	PCP4 (3)	GPX5 (7)	FGFR1OP2 (10)	SPRR2A (3)	OTOS (4)	EDDM3A (6)	CRIPT (2)

Table 4. Frequently Occurring Specific Mutations in Each PKC Isozyme
List of specific residues of genes mutated in samples that contain PKC mutations and the number of co-occurring cases for each PKC isozyme.

PKCα	Cases	PKCβ	Cases	PKCγ	Cases	PKCδ	Cases	PKCε
PTEN R130Q	5	MS4A8 S3L	5	ACVR2A K435fs	7	PRKCD G432fs	9	ACOT12 R147*
APC R2204*	4	POLE P286R	5	BRAF V600E	7	CIR1 I289fs	5	C20ORF26 R1088Q
DIS3 R382Q	4	PTEN R130Q	5	CBWD1 G144_splice	5	KRAS G12D	4	CBWD1 G144_splice
GPR158 D566N	4	ACOT12 R147*	4	TGFBR2 E125fs	5	OLIG3 H32del	4	EFCAB6 R429*
MFGE8 D170N	4	BRAF V600E	4	CDKN2A Silenced	4	OR10A7 F107del	4	KRAS G12D
NUF2 S340L	4	CEP162 S1242Y	4	ERBB3 V104M	4	TNFSF9 L41del	4	PIK3R1 R348*
ADAMTS17 R1089C	3	KPNA4 R29Q	4	GPR98 R4142W	4	ZMIZ1 P986del	4	RXFP1 S223Y
ALG5 R309*	3	KRAS G12D	4	KRAS G12D	4	ABCB5 R142Q	3	TPTE S423L
ANKDD1A R24H	3	RXFP1 S223Y	4	PIK3CA E545K	4	ACACB R446I	3	ZNF180 R625I
APC R1450*	3	ANKS6 R541*	3	PIK3CA H1047R	4	ACOT12 R147*	3	ZNF675 R220I
ARHGAP29 R647Q	3	ANPEP E636K	3	ACBD3 R223*	3	ADAMDEC1 R200*	3	ACSM2B K195N
ARID1A R1989*	3	ARFGEF1 R1345*	3	AMER1 F173fs	3	AJAP1 T225del	3	ASH1L R1321Q
ATP2B1 R763*	3	ATP2C1 E690K	3	APC R1450*	3	APC R2204*	3	ATP2B1 S1140L
ATP2C1 E690K	3	BRWD3 R1326*	3	ATP2C1 R764H	3	ATP2C1 R764H	3	BCLAF1 E163K
BACH1 E281K	3	C8B S502F	3	ATP9A R290Q	3	CACNA1D MUTATED	3	C1R P216fs
BCL6 R618C	3	CASP8 R68Q	3	BCLAF1 E163K	3	CAMTA1 Q1587fs	3	CCDC36 R209I
BCLAF1 E776*	3	CCDC30 R263*	3	BPI R198Q	3	CBWD1 G144_splice	3	CEP162 S1242Y
BICC1 R200W	3	CCDC36 R209I	3	CASP5 K65fs	3	CCDC36 R209I	3	CLASP1 R1363*
C6 S584L	3	COL17A1 R145*	3	CCDC15 K192fs	3	DHX57 45_46GG>G	3	CMAS R110Q
CASC1 R48Q	3	COPB1 R425C	3	CCDC36 R209I	3	DNAH10 R1888Q	3	COL17A1 R145*
CCDC147 E833*	3	CRYBB1 E65K	3	DHDDS A77T	3	DNAH5 R78Q	3	CSRP2BP R264Q
CCDC30 R263*	3	DCAF16 R91*	3	DISP1 R763C	3	FCN1 S247Y	3	DEFB114 R28C
CCNT2 S530Y	3	DENND4C R1081Q	3	FBXL13 R513Q	3	GPR25 204_205LL>L	3	DENND4C R1081Q
CEACAM5 L640I	3	DNAH5 R3516I	3	FHOD3 P334fs	3	HEATR5B R1025C	3	DNAH7 R3553*
CRTAC1 S344L	3	DNER R666H	3	GDAP2 R187C	3	HERC6 S151L	3	EPX R63H
CUX1 R208*	3	DOCK1 E843K	3	GP2 S41L	3	IFNGR2 F172fs	3	FAT2 S582L
DNAH3 S2226L	3	DSG4 S158L	3	GPR158 D566N	3	KRAS G12V	3	FILIP1 R384*
DNAH5 E3394K	3	EFCAB6 R429*	3	HADHA R291*	3	KRAS G13D	3	FNDC1 K253N
EPHA7 R895*	3	ERCC6L2 L445I	3	HECW2 R1101C	3	MAP2 S285Y	3	FRMPD1 E537K
ERC2 R528C	3	FAM13B R553*	3	HMMR KKK664del	3	MMRN1 Q313del	3	HECW2 R1101C
HERC6 S151L	3	FAM171B D459N	3	ITIH5 R487H	3	MS4A8 S3L	3	HERC5 A1012V
KATNBL1 R66C	3	FBXW7 R658*	3	KCND3 S438L	3	MYO1F R400*	3	HPS3 S133L
KDM3B R1460W	3	FHOD3 A985T	3	KIAA1432 R1186W	3	OAS3 R253Q	3	IL5RA L47I
KIAA2026 R574C	3	FNDC1 K253N	3	KIF18A R17C	3	OR10S1 V229I	3	KBTBD7 R546W
KIF20B E991K	3	GABRG2 S3L	3	KRAS G12C	3	PDE5A R577W	3	KIF14 R598Q
MBOAT2 R43Q	3	GPR98 R4142W	3	KRAS G13D	3	PIK3R1 R348*	3	KIF20B E54K
MSRB2 K56N	3	GRID2 E487K	3	METTL6 F56L	3	POLE P286R	3	KIF23 R150Q
MYO1F R400*	3	GRM6 E363D	3	MS4A8 S3L	3	PON1 R306Q	3	KIF2C A500T
MYOM1 R500*	3	HECW2 R1101C	3	MUC16 P5119S	3	RXFP1 S223Y	3	KIF5A R144C
NF1 R440*	3	ITM2C E167K	3	MYH10 A1893V	3	SGOL2 N645fs	3	KLB F369L
OSBPL10 E513K	3	KDM5B R1461C	3	MYO18B A8T	3	SMARCA2 Q238del	3	KPNA4 R29Q
PLXNA1 E1272K	3	KIF16B R145Q	3	OR51S1 R194C	3	SRP14 A116del	3	KRAS G13D
POLE P286R	3	KIF20B E54K	3	PCDHB15 S314L	3	TMC4 E67del	3	PIK3CA
RAB3GAP1 R231Q	3	KIF5A R144C	3	PGM5 I98V	3	TMEM184A 389_390insG	3	MBOAT2 R43Q
SAP30 R123Q	3	KLHL13 E210K	3	PIK3R1 R348*	3	WRN E510del	3	MS4A8 S3L
SEMA3A D81N	3	LUM E240K	3	POU1F1 R217Q	3	XRCC2 L117fs	3	MYH10 A1893V
SLC30A6 R304*	3	MAP7 S268L	3	PRKCG R205Q	3	YTHDC2 E185K	3	MYO3A R984*
SMC4 R1252*	3	MARK1 R309*	3	PSG9 E404K	3	ZDHHC17 R601*	3	NNMT E233K
SPTY2D1 R301C	3	MAT2B R312Q	3	PTEN R130Q	3	ZMYM5 D59del	3	NPY1R A371T
STXBP6 D92N	3	MBOAT2 R43Q	3	RECQL A248T	3	ZNF560 R694Q	3	NSMCE1 D244N
TECTB L29I	3	MRPL47 E66*	3	RFC5 E82*	3			OBSCN R3596C
TMPRSS4 R175C	3	MS4A6E E89K	3	RGS7 R44C	3			PCDH19 E530K
TOX S354L	3	MUC13 S185L	3	SCAPER R366Q	3			PCDHAC2 S432L
TRIM6-TRIM34 R267C	3	MYH10 A1893V	3	SEC63 L532fs	3			PCDHB7 E398K
TRPM7 R1862C	3	MYO18B A8T	3	SEMA3D R760Q	3			PCLO R5085*
TRPS1 E349K	3	MYO3A R642W	3	SLC22A15 S201L	3			PDZRN4 R708Q
TRPV6 L13I	3	MYOM1 R500*	3	SPATA8 E18K	3			PHF20L1 R126C
TTN L9650I	3	NRAP E327K	3	SPTLC3 R97Q	3			PIK3R5 R741Q
TTN S11984L	3	NRAS Q61R	3	TP53 P152fs	3			PLCL1 R469Q
TXNL1 R234C	3	OR4M1 S268F	3	TP53 R213*	3			POLE P286R
UGT8 E102K	3	OR4M1 S33F	3	UGT8 E102K	3			POLE V411L
XPO1 R749Q	3	OR51S1 R194C	3	UNC45B D71N	3			PRKDC R2522Q
XPO4 R471*	3	OXR1 E122K	3	USH2A R4192C	3			PROX1 R174W
ZIM3 D352N	3	PCDH19 E530K	3	WDR3 E841K	3			PTEN R130Q
ZMAT3 E284D	3	PDE5A R577W	3	XDH R881Q	3			RCOR2 R254Q
ZNF101 R302I	3	PDK4 R161Q	3	XPO4 R471*	3			RSBN1 E572K

Table 4. Frequently Occurring Specific Mutations in Each PKC Isozyme, Continued

PKCα	Cases	PKCβ	Cases	PKCγ	Cases	PKCδ	Cases	PKCε
ZNF117 R185I	3	PIK3R1 R348*	3	ZIM3 D352N	3			RUNDC3B R293*
ZNF136 R156*	3	PIK3R5 R741Q	3					SEMA3D R760Q
ZNF333 R554Q	3	PLCL1 R469Q	3					SLC30A6 R304*
ZNF439 R262I	3	PPM1L R315*	3					STIL S619Y
ZNF610 E32K	3	PREX1 R78H	3					STIL S76L
ZNF610 E376K	3	PRKCB R361Q	3					SULT1C4 R85Q
ZNF678 R509I	3	PTPRT E548K	3					TAP1 R438*
ZNF721 R353I	3	RALA R176*	3					TBC1D4 R684*
ZNF765 S254L	3	RASSF9 E356*	3					TLN2 S208L
		RFC5 E82*	3					TP53 R213*
		SEMA3D R760Q	3					TSSK1B E301K
		SH3GLB2 R145H	3					TTN D16823N
		SIRPB2 S141L	3					UACA E1309*
		SLC22A15 S201L	3					XKR5 R81W
		STK24 A134T	3					YTHDC2 E185K
		SUV420H1 R220Q	3					ZNF14 R575*
		TBC1D4 R684*	3					ZNF266 R512Q
		TCAIM R217C	3					
		THBS1 E1017K	3					
		TMEM164 E232K	3					
		TMEM2 R758*	3					
		TP53 R213*	3					
		TPTE S423L	3					
		TRIM24 R721*	3					
		TRPC5 S490L	3					
		UBAP1 D439N	3					
		WIPI1 A204V	3					
		ZNF180 R401I	3					
		ZNF266 R512Q	3					
		ZNF442 R309Q	3					
		ZNF493 R83Q	3					
		ZNF607 R609I	3					
		ZNF649 R198I	3					
		ZNF678 R313I	3					
		ZNF679 H262Y	3					
		ZNF765 R319I	3					

Table 4. Frequently Occurring Specific Mutations in Each PKC Isozyme, Continued

Cases	PKCη	Cases	PKCθ	Cases	PKCζ	Cases	PKCι	Cases
4	CCDC30 R263*	4	ARMC4 E22K	5	ABCB5 R168Q	2	ARID1A R1989*	5
4	CCDC36 R209I	4	BRAF V600E	4	ABCC2 R911*	2	TOX S354L	5
4	CIR1 I289fs	4	KRAS G12V	4	ACTC1 R212C	2	CNTN4 S1005L	4
4	COL17A1 R145*	4	PCDHB7 E398K	4	ADCYAP1R1 E380K	2	CUX1 R208*	4
4	ISX R86C	4	PIK3CA E545K	4	ALG13 R594*	2	PTEN R130Q	4
4	MS4A8 S3L	4	PIK3R1 R348*	4	AOX1 M55I	2	TP53 R213*	4
4	MYOM1 R500*	4	PTEN R130Q	4	AP4B1 R520C	2	TRPC5 S490L	4
4	NPY1R A371T	4	RUNX1T1 D235N	4	ARAF S214F	2	UGT8 E102K	4
4	POLE P286R	4	ABCA3 R155L	3	ARHGAP36 S212F	2	XPO1 R749Q	4
4	PRKCH P612fs	4	ACBD5 R342C	3	ATP6V0A4 V605I	2	ACSM2B K195N	3
3	ZNF263 R510I	4	ARID1A R1989*	3	BCLAF1 E163K	2	ADAM7 R691C	3
3	ABI1 K445N	3	BMP7 E173K	3	BMP5 G293E	2	ARID2 R314C	3
3	ACOT12 R147*	3	CDKN2A R80*	3	C10ORF71 A426V	2	ATRN R173C	3
3	ANK3 S2871L	3	CDKN2A Silenced	3	CACNA2D4 E156K	2	BRAF V600E	3
3	ATP2C1 E690K	3	CNTNAP2 R483Q	3	CCSER1 Q587*	2	BRWD3 R1326*	3
3	ATP2C1 R764H	3	DNAH10 S2587L	3	CD1A V291I	2	BTBD7 S436L	3
3	BIRC6 R1382Q	3	EFCAB6 R429*	3	CD55 S334F	2	C10ORF129 R151C	3
3	BMP2K QHH486del	3	FAM135B S11L	3	CDKN2A P114L	2	C6 S584L	3
3	BRAF V600E	3	GP2 S41L	3	CEP135 S997L	2	CADPS2 R1246*	3
3	BTN3A2 E153K	3	KCNB2 E223K	3	CEP250 R1045Q	2	CAPRIN2 R215Q	3
3	CDKN2A R80*	3	KCNH5 V263I	3	CFTR Q237*	2	CNTNAP2 R1088*	3
3	COL5A1 E497*	3	KIDINS220 R824L	3	CLEC5A L118F	2	COL4A5 E1637K	3
3	CRTAC1 S344L	3	KIF14 R598Q	3	CRB1 E1058K	2	CR1 R1392C	3
3	CTRL N238fs	3	KLHL13 E210K	3	CTAGE6 R409Q	2	CSTL1 R69*	3
3	CTSC R250*	3	KRAS G12D	3	CUZD1 P114S	2	DCT R499Q	3
3	CUX1 E36K	3	LHCGR E206K	3	DCAF10 E287fs	2	DNAH7 R2961Q	3
3	CYFIP2 R514*	3	MROH2B D1477N	3	DNAJB3 D63N	2	GIGYF2 E66*	3
3	DEFB114 R28C	3	MYO3A R984*	3	DSP G2212E	2	HAUS6 E633*	3
3	DENND3 E1064*	3	OR52J3 R195C	3	DSPP E29K	2	KDR R1032Q	3
3	DHX57 45_46GG>G	3	OR6X1 R225Q	3	EFHC1 R221C	2	KIAA2026 R574C	3
3	DSG4 S285L	3	PCDHAC2 E558K	3	EIF2S2 M6_splice	2	KLHL5 R326C	3
3	ERCC6L2 L445I	3	PCDHAC2 P153S	3	FAM122A K215N	2	MFGE8 D170N	3
3	FHOD3 A985T	3	PCDHAC2 S432L	3	FAM47C Q225E	2	MR1 S46L	3
3	GALP R31Q	3	POLE P286R	3	FLI1 G429E	2	MTF1 R251Q	3
3	GFAP A233T	3	PRKCQ A291V	3	FMN2 F1661L	2	MYH4 A1781T	3
3	GPR155 R764Q	3	RNF133 R270C	3	FNIP2 A725V	2	MYO1F R400*	3
3	GPR98 R4142W	3	RPGRIP1L S886L	3	GIMAP6 E278K	2	MYOM1 R500*	3
3	HECW2 R1101C	3	RPIA A196T	3	GK2 I60S	2	NCAPG R993Q	3
3	HERC5 A1012V	3	SEMA3D R760Q	3	GLRA3 R98C	2	NINL R1366C	3
3	IGF2BP1 R452C	3	SPTLC3 R97Q	3	GLRB E236K	2	OXR1 E122K	3
3	KBTBD7 R546W	3	STIL S76L	3	GNAT2 E276K	2	PARP11 R158Q	3
3	KIAA1432 R1186W	3	TEX15 E511K	3	GPR142 A371V	2	PCDHAC2 P153S	3
3	KIF16B R145Q	3	TP53 G187_splice	3	GPR21 R256Q	2	PCDHAC2 S608L	3
3	KIF20B R1815Q	3	TP53 R175H	3	GSK3A A146T	2	PCDHB7 E398K	3
3	KRAS G12D	3	TRPC5 S490L	3	GUCY1A3 R574Q	2	PIK3CA E545K	3
3	KRAS G12V	3	ZNF14 R575*	3	HCRTR2 R253Q	2	PIK3CA R88Q	3
3	MAGI2 L450M	3	ZNF180 R625I	3	HEPACAM2 G128E	2	PIK3R1 R348*	3
3	MARK1 R309*	3	ZNF649 R198I	3	HS3ST2 R249C	2	PLA2R1 E715D	3
3	MCF2L2 R926Q	3			KIF23 R150Q	2	POLE P286R	3
3	MRPL47 E66*	3			KLHL13 P456_splice	2	POLE V411L	3
3	MSRB2 K56N	3			LGSN G385E	2	POLQ R860Q	3
3	MTMR9 R174W	3			LMTK3 D95N	2	PPM1L R315*	3
3	MYH10 A1893V	3			MAP1B P2164L	2	PRKCI R480C	3
3	MYO18B A8T	3			MCF2 E349K	2	RBL2 E127K	3
3	NF1 R2450*	3			MMEL1 E208K	2	RIMS2 R599Q	3
3	NNMT E233K	3			MNDA S187L	2	SACS R2906Q	3
3	NSMCE1 D244N	3			MUC16 G3177E	2	STIL S76L	3
3	OR4C12 F248L	3			MYO18B E2160K	2	SYNJ1 R573*	3
3	OR5D18 F182L	3			OR12D2 E9K	2	THAP5 S287Y	3
3	PABPC1 R518C	3			OR2A25 G3E	2	THBS1 E1017K	3
3	PANK2 T417fs	3			OR51B2 R261K	2	TNIP3 E156K	3
3	PDZRN4 R708Q	3			OR52R1 S190F	2	TRPS1 E349K	3
3	PUS7L R308Q	3			OR5M8 E172K	2	TXNL1 R234C	3
3	RAF1 V537I	3			PCDH9 D776N	2	WWTR1 R248*	3
3	RALA R176*	3			PDE1C H132Y	2	XPO4 R471*	3
3	RECQL A248T	3			PIK3R1 R348*	2	ZFP3 R273I	3

Table 4. Frequently Occurring Specific Mutations in Each PKC Isozyme, Continued

Cases	PKCη	Cases	PKCθ	Cases	PKCζ	Cases	PKCι	Cases
3	RELN F2722L	3			PMFBP1 G640E	2	ZIM3 D352N	3
3	RFC5 E82*	3			PNPLA1 S422L	2	ZNF583 R344I	3
3	RXFP1 S223Y	3			PPIAL4G R47C	2	ZNF610 E376K	3
3	SEMA3D R760Q	3			PRKCZ R260H	2		
3	SMARCA2 Q238del	3			PSG5 G118E	2		
3	SPARCL1 S282L	3			PTEN R130Q	2		
3	STIL S76L	3			PTPRR G145E	2		
3	TCF7 E164K	3			R3HDM2 R959*	2		
3	TIAM2 E262K	3			RASD2 R202C	2		
3	TMEM161B R315Q	3			RBL1 R159Q	2		
3	TMEM164 E232K	3			RHBG S197L	2		
3	TRIM60 R324Q	3			RXFP1 S223Y	2		
3	TRIO R1276*	3			SAMSN1 D94N	2		
3	TTN D16823N	3			SASH1 R995C	2		
3	UACA E1309*	3			SCN1A G880E	2		
3	XPO4 R471*	3			SCN7A R1622Q	2		
3	ZNF136 R156*	3			SGCG E157K	2		
	ZNF14 R547*	3			SPAG11B V114I	2		
	ZNF32 S62L	3			SRRM4 R144*	2		
	ZNF43 R280C	3			STK19 D89N	2		
	ZNF559 E220K	3			SYNM R517Q	2		
	ZNF678 R313I	3			SYPL2 D177N	2		
	ZNF765 R319I	3			TECPR1 C913*	2		
	ZNF766 E324D	3			TEX15 E511K	2		
					TG R1646Q	2		
					TIAM1 R1332*	2		
					TNP1 S53F	2		
					TP63 E609K	2		
					TRAF5 R393*	2		
					TTN D17130N	2		
					UGT2B15 R174Q	2		
					VPRBP R855Q	2		
					VPS16 R432W	2		
					YTHDC2 E185K	2		
					ZC3H12B R77C	2		
					ZNF560 E177_splice	2		
					ZNF645 R154C	2		
					ZNF709 S322F	2		
					ZNF93 R221I	2		

Table 5. Top 20 Cancer Census and Kinase Genes with Mutations Co-occurring with PKC Mutations

PKCα								
	Gene	q-value	Positive cases	Overall cases	Correction score	%isoform	% family	Effect size
	TLK1	3.45E-12	12	48	0.01525	24.000	0.846	28.37
	SCYL3	1.29E-11	12	57	0.01617	24.000	1.005	23.89
	PRPF4B	5.86E-11	12	67	0.01192	24.000	1.181	20.32
	MAP3K13	5.00E-10	12	84	0.01242	24.000	1.480	16.21
	NCOA1	5.51E-10	12	85	0.00833	24.000	1.498	16.02
	MSH2	1.11E-10	11	54	0.01178	22.000	0.952	23.12
	TRPM7	2.96E-09	11	79	0.00590	22.000	1.392	15.80
	STK24	4.74E-10	10	46	0.02257	20.000	0.811	24.67
	MAPK10	8.61E-10	10	50	0.02155	20.000	0.881	22.70
	NONO	8.61E-10	10	50	0.02123	20.000	0.881	22.70
	DDX10	1.37E-09	10	53	0.01143	20.000	0.934	21.41
	STAT3	3.16E-09	10	59	0.01299	20.000	1.040	19.23
	TRIM33	3.16E-09	10	59	0.00887	20.000	1.040	19.23
	BCL6	1.80E-08	10	74	0.01416	20.000	1.304	15.34
	MAK	5.51E-09	9	45	0.01389	18.000	0.793	22.70
	PTK2B	4.81E-08	9	61	0.00892	18.000	1.075	16.74
	TTBK2	5.34E-08	9	62	0.00546	18.000	1.093	16.47
	CDC73	6.63E-08	9	64	0.01695	18.000	1.128	15.96
	KTN1	8.39E-08	9	66	0.00663	18.000	1.163	15.47
	NPR2	1.02E-07	9	68	0.00860	18.000	1.198	15.02
PKCβ								
	Gene	q-value	Positive cases	Overall cases	Correction score	%isoform	% family	Effect size
	EML4	3.70E-11	13	54	0.01310	14.444	0.952	15.18
	AKT3	6.08E-10	11	43	0.02296	12.222	0.758	16.13
	NR4A3	1.18E-09	11	46	0.01727	12.222	0.811	15.08
	PLK3	2.71E-09	10	38	0.01548	11.111	0.670	16.59
	SGK3	2.23E-09	9	27	0.01815	10.000	0.476	21.01
	CDKL1	2.00E-08	9	35	0.02514	10.000	0.617	16.21
	MAP3K2	2.00E-08	9	35	0.01454	10.000	0.617	16.21
	VRK1	4.16E-08	8	27	0.02020	8.889	0.476	18.68
	UHMK1	5.44E-08	8	28	0.01909	8.889	0.493	18.01
	MLKL	1.83E-07	8	33	0.01699	8.889	0.582	15.28
	NEK7	1.30E-07	7	21	0.02318	7.778	0.370	21.01
	CLK4	6.81E-07	7	27	0.01455	7.778	0.476	16.34
	CAMK2D	8.57E-07	7	28	0.01313	7.778	0.493	15.76
	SSX1	2.38E-06	6	21	0.03191	6.667	0.370	18.01
	LHFP	3.92E-06	6	23	0.03000	6.667	0.405	16.45
	CREB3L1	6.20E-06	6	25	0.01156	6.667	0.441	15.13
	TFEB	6.20E-06	6	25	0.01068	6.667	0.441	15.13
	KDSR	1.38E-05	5	17	0.01506	5.556	0.300	18.54
	TSSK4	1.38E-05	5	17	0.01479	5.556	0.300	18.54
	MSI2	2.92E-05	5	20	0.01524	5.556	0.352	15.76
PKCγ								
	Gene	q-value	Positive cases	Overall cases	Correction score	%isoform	% family	Effect size
	SRPK1	1.64E-10	12	43	0.01453	11.765	0.758	15.52
	MAP4K2	9.90E-10	10	30	0.01220	9.804	0.529	18.54
	CAMKK1	1.33E-09	10	31	0.01880	9.804	0.546	17.94
	CCDC6	1.77E-09	10	32	0.02110	9.804	0.564	17.38
	GNAQ	2.81E-07	7	21	0.01950	6.863	0.370	18.54
	TFG	3.85E-07	7	22	0.01750	6.863	0.388	17.70
	FASTK	2.52E-06	6	19	0.01093	5.882	0.335	17.57
	PHKG1	3.32E-06	6	20	0.01432	5.882	0.352	16.69
	MDM4	3.32E-06	6	20	0.01224	5.882	0.352	16.69
	TSSK3	4.33E-06	6	21	0.02239	5.882	0.370	15.89
	JAZF1	8.96E-06	5	14	0.02058	4.902	0.247	19.87
	CD274	8.96E-06	5	14	0.01724	4.902	0.247	19.87
	CDX2	2.91E-05	5	18	0.01597	4.902	0.317	15.45
	LMO1	2.81E-05	4	9	0.02564	3.922	0.159	24.72
	VTI1A	6.20E-05	4	11	0.01843	3.922	0.194	20.23
	BCL2	8.63E-05	4	12	0.01674	3.922	0.211	18.54
	PDCD1LG2	1.53E-04	4	14	0.01465	3.922	0.247	15.89
	MLLT11	4.46E-04	3	8	0.03333	2.941	0.141	20.86
	TAL2	4.46E-04	3	8	0.02778	2.941	0.141	20.86

Table 5. Top 20 Cancer Census and Kinase Genes with Mutations Co-occurring with PKC Mutations, Continued

PKCδ								
	Gene	q-value	Positive cases	Overall cases	Correction score	%isoform	% family	Effect size
	TIE1	2.83E-09	12	94	0.01054	25.532	1.657	15.41
	BRDT	3.26E-09	12	96	0.01262	25.532	1.692	15.09
	GPC3	5.57E-10	11	57	0.01824	23.404	1.005	23.30
	TSC1	3.26E-09	11	73	0.00945	23.404	1.287	18.19
	BMP2K	4.42E-09	11	77	0.00947	23.404	1.357	17.25
	MLLT10	2.99E-08	10	76	0.00936	21.277	1.339	15.88
	CDK13	3.27E-08	10	77	0.00661	21.277	1.357	15.68
	DYRK1A	4.12E-08	9	57	0.01180	19.149	1.005	19.06
	IKZF1	5.85E-08	9	60	0.01734	19.149	1.057	18.11
	CDC73	8.74E-08	9	64	0.01695	19.149	1.128	16.98
	LATS2	1.57E-07	9	70	0.00827	19.149	1.234	15.52
	NCKIPSD	1.16E-08	8	31	0.01108	17.021	0.546	31.15
	GSK3B	1.41E-08	8	32	0.01848	17.021	0.564	30.18
	DYRK4	3.59E-07	8	55	0.01262	17.021	0.969	17.56
	BUB1B	4.01E-07	8	56	0.00752	17.021	0.987	17.25
	SCYL3	4.51E-07	8	57	0.01078	17.021	1.005	16.94
	EXT1	5.46E-07	8	59	0.01072	17.021	1.040	16.37
	TRIM33	5.46E-07	8	59	0.00710	17.021	1.040	16.37
	ECT2L	6.08E-07	8	60	0.00885	17.021	1.057	16.10
	NPR1	8.99E-07	8	64	0.00754	17.021	1.128	15.09
PKCε								
	Gene	q-value	Positive cases	Overall cases	Correction score	%isoform	% family	Effect size
	ARHGEF12	2.56E-12	15	92	0.00972	26.316	1.621	16.23
	NEK10	1.02E-11	14	85	0.01195	24.561	1.498	16.40
	EPHA8	1.62E-11	14	90	0.01393	24.561	1.586	15.48
	PCM1	1.26E-11	13	69	0.00642	22.807	1.216	18.75
	EML4	1.35E-11	12	54	0.01210	21.053	0.952	22.12
	BMPR2	9.30E-11	12	66	0.01156	21.053	1.163	18.10
	TSC1	2.25E-10	12	73	0.01031	21.053	1.287	16.36
	BCL6	2.58E-10	12	74	0.01700	21.053	1.304	16.14
	ROCK2	4.18E-10	12	78	0.00865	21.053	1.375	15.31
	FANCG	6.36E-11	11	48	0.01768	19.298	0.846	22.81
	STK33	9.54E-11	11	50	0.02140	19.298	0.881	21.90
	KIF5B	2.48E-10	11	56	0.01142	19.298	0.987	19.55
	CYLD	1.07E-09	11	67	0.01151	19.298	1.181	16.34
	NPR2	1.22E-09	11	68	0.01051	19.298	1.198	16.10
	STIL	1.39E-09	11	69	0.00854	19.298	1.216	15.87
	TSSK1B	8.47E-10	10	48	0.02725	17.544	0.846	20.74
	ZBTB16	7.84E-09	10	64	0.01486	17.544	1.128	15.55
	ANKK1	4.02E-09	9	42	0.01176	15.789	0.740	21.33
	MAK	6.54E-09	9	45	0.01389	15.789	0.793	19.91
	RPS6KA5	1.21E-08	9	49	0.01115	15.789	0.864	18.28
PKCη								
	Gene	q-value	Positive cases	Overall cases	Correction score	%isoform	% family	Effect size
	LIFR	2.75E-15	18	120	0.01641	35.294	2.115	16.69
	TEX14	5.42E-15	17	105	0.01136	33.333	1.851	18.01
	BRIP1	1.78E-14	16	94	0.01281	31.373	1.657	18.94
	USP6	4.95E-14	16	103	0.01138	31.373	1.815	17.28
	LRRK1	1.60E-13	16	114	0.00794	31.373	2.009	15.61
	CASC5	2.82E-13	15	98	0.00640	29.412	1.727	17.03
	NUP98	8.59E-13	15	108	0.00826	29.412	1.903	15.45
	MLLT4	8.59E-13	15	108	0.00818	29.412	1.903	15.45
	FANCD2	3.39E-13	14	80	0.00952	27.451	1.410	19.47
	CDKL5	4.44E-13	14	82	0.01359	27.451	1.445	18.99
	ARHGEF12	1.60E-12	14	92	0.00907	27.451	1.621	16.93
	BRDT	2.60E-12	14	96	0.01472	27.451	1.692	16.22
	LATS2	1.17E-12	13	70	0.01195	25.490	1.234	20.66
	BMP2K	3.15E-12	13	77	0.01120	25.490	1.357	18.78
	EPHA4	8.69E-12	13	85	0.01318	25.490	1.498	17.02
	DAPK1	8.69E-12	13	85	0.00909	25.490	1.498	17.02
	CDC42BPB	1.10E-11	13	87	0.00760	25.490	1.533	16.62
	IGF1R	1.92E-11	13	92	0.00951	25.490	1.621	15.72
	PASK	2.38E-11	13	94	0.00977	25.490	1.657	15.39
	SCYL3	2.19E-12	12	57	0.01617	23.529	1.005	23.42

Table 5. Top 20 Cancer Census and Kinase Genes with Mutations Co-occurring with PKC Mutations, Continued

PKCθ								
	Gene	q-value	Positive cases	Overall cases	Correction score	%isoform	% family	Effect size
	FAS	8.65E-09	9	32	0.02687	11.111	0.564	19.70
	PDK4	3.39E-08	9	38	0.02190	11.111	0.670	16.59
	LCK	7.42E-08	9	42	0.01670	11.111	0.740	15.01
	MLLT1	5.09E-08	8	28	0.01431	9.877	0.493	20.01
	NRBP1	2.46E-07	8	35	0.01473	9.877	0.617	16.01
	CREB3L1	3.86E-07	7	25	0.01349	8.642	0.441	19.61
	MAP2K6	1.21E-06	7	30	0.02096	8.642	0.529	16.34
	OGG1	1.48E-06	7	31	0.01651	8.642	0.546	15.82
	MAP2K5	5.90E-06	6	25	0.01339	7.407	0.441	16.81
	STK38L	1.08E-05	6	28	0.01293	7.407	0.493	15.01
	IL2	1.82E-05	5	18	0.03268	6.173	0.317	19.46
	LMO2	1.82E-05	5	18	0.02203	6.173	0.317	19.46
	TWF2	2.90E-05	5	20	0.01433	6.173	0.352	17.51
	CAMK1	2.90E-05	5	20	0.01351	6.173	0.352	17.51
	HOXA9	4.45E-05	5	22	0.01838	6.173	0.388	15.92
	MAPK14	4.45E-05	5	22	0.01389	6.173	0.388	15.92
	PAFAH1B2	8.54E-05	4	13	0.01747	4.938	0.229	21.55
	CDK9	0.000145372	4	15	0.01075	4.938	0.264	18.68
	BCL7A	0.000182108	4	16	0.01732	4.938	0.282	17.51
	HOXA13	0.000182108	4	16	0.01031	4.938	0.282	17.51
PKCζ								
	Gene	q-value	Positive cases	Overall cases	Correction score	%isoform	% family	Effect size
	ARAF	6.12E-07	8	47	0.01314	28.571	0.828	34.492
	DYRK4	0.000156942	6	55	0.00946	21.429	0.969	22.106
	NR4A3	0.000468669	5	46	0.00785	17.857	0.811	22.026
	EEF2K	0.000845892	5	58	0.00690	17.857	1.022	17.469
	BRSK1	0.00091573	5	61	0.00630	17.857	1.075	16.610
	LMTK3	0.000975243	5	63	0.00336	17.857	1.110	16.083
	MAP3K8	0.000655374	4	24	0.00857	14.286	0.423	33.774
	CREB3L1	0.00069527	4	25	0.00771	14.286	0.441	32.423
PKCι								
	Gene	q-value	Positive cases	Overall cases	Correction score	%isoform	% family	Effect size
	EPHA7	4.54E-14	17	121	0.01703	35.417	2.133	16.61
	TRPM7	4.54E-14	15	79	0.00804	31.250	1.392	22.44
	MYO3B	5.90E-12	14	102	0.01044	29.167	1.798	16.22
	ULK4	1.17E-11	13	86	0.01020	27.083	1.516	17.87
	BRDT	3.49E-11	13	96	0.01367	27.083	1.692	16.01
	TRIP11	3.80E-11	13	97	0.00657	27.083	1.710	15.84
	FOXP1	1.16E-11	12	66	0.01732	25.000	1.163	21.49
	EPHB2	1.41E-10	12	86	0.01137	25.000	1.516	16.49
	MARK1	2.39E-10	12	91	0.01508	25.000	1.604	15.59
	ROCK1	2.96E-10	12	93	0.00886	25.000	1.639	15.25
	NTRK2	1.41E-10	11	65	0.01313	22.917	1.146	20.00
	CDK13	6.38E-10	11	77	0.00728	22.917	1.357	16.89
	NCOA1	1.54E-09	11	85	0.00763	22.917	1.498	15.30
	TLK1	1.62E-10	10	48	0.01271	20.833	0.846	24.63
	GMPS	2.67E-10	10	51	0.01443	20.833	0.899	23.18
	XPO1	7.74E-10	10	58	0.00934	20.833	1.022	20.38
	EXT1	8.80E-10	10	59	0.01340	20.833	1.040	20.04
	CAMK4	1.54E-09	10	63	0.02114	20.833	1.110	18.76
	LATS2	3.65E-09	10	70	0.00919	20.833	1.234	16.89
	JAK1	6.51E-09	10	75	0.00867	20.833	1.322	15.76

List of genes that are mutated >15-fold in tumors harboring PKC mutations versus tumors lacking PKC mutations, ranked by the number of mutations in each PKC isozyme and with a false discovery rate cutoff of 0.001 or smaller. The q-values represent the False Discovery Rate corrected significance of co-occurrence. Effect size was calculated using the proportion of mutation positive cases in the study population against the proportion of mutations in the whole population of cases.

Table 6. Top 20 Genes Containing Mutations Co-occurring with cPKC, nPKC, or aPKC Mutations in Lung Cancer, Colorectal Cancer, or Melanoma

List of genes and number of cases of co-occurring mutations with cPKC, nPKC, or aPKC isozyme mutations. Data are corrected for gene length.

Lung

	cPKC : gene	cPKC : num co-occuring mutations in lung studies	cPKC : length-corrected score	nPKC : gene	nPKC : num co-occuring mutations in lung studies	nPKC : length-corrected score	aPKC : gene	aPKC : num co-occuring mutations in lung studies	aPKC : length-corrected score
1	TP53	43	0.10941	TP53	22	0.05598	TP53	13	0.03308
2	REG3A	9	0.05143	KRTAP21-2	3	0.03614	REG3A	5	0.02857
3	CDKN2A	7	0.04118	KRTAP6-2	2	0.03226	SPANXN5	2	0.02778
4	REG3G	7	0.04000	DEFB110	2	0.02985	SPRR2G	2	0.02740
5	SMR3B	3	0.03797	KRTAP19-7	2	0.02778	GNG4	2	0.02667
6	OR4A15	13	0.03779	KRAS	5	0.02646	NPS	2	0.02247
7	POM121L12	11	0.03716	DEFB115	2	0.02273	IFNB1	4	0.02139
8	REG1A	6	0.03614	OCLM	1	0.02273	KRAS	4	0.02116
9	C8ORF22	3	0.03571	SPANXN2	4	0.02222	CCL7	2	0.02020
10	SPANXN3	5	0.03546	TEX37	4	0.02222	NDUFA13	3	0.02000
11	C7ORF66	4	0.03478	LEMD1	4	0.02210	CLLU1OS	2	0.01980
12	OR4C15	12	0.03243	PIP	3	0.02055	DEFB116	2	0.01961
13	OR4C6	10	0.03236	NGB	3	0.01987	HTN3	1	0.01961
14	KRTAP6-2	2	0.03226	CLLU1OS	2	0.01980	SNAP25	4	0.01942
15	PCP4	2	0.03226	UBE2A	3	0.01974	GREM2	3	0.01786
16	KRAS	6	0.03175	OR4C46	6	0.01942	UQCR11	1	0.01786
17	DEFB110	2	0.02985	HIST1H4F	2	0.01942	CDKN2A	3	0.01765
18	KRTAP15-1	4	0.02920	OR2M5	6	0.01923	REG3G	3	0.01714
19	ATP5L	3	0.02913	OR2W3	6	0.01911	C5ORF55	2	0.01681
20	OR2M5	9	0.02885	RPL10L	4	0.01869	CLDN12	4	0.01639

Colorectal

	cPKC : gene	cPKC : num co-occuring mutations in colorectal studies	cPKC : length-corrected score	nPKC : gene	nPKC : num co-occuring mutations in colorectal studies	nPKC : length-corrected score	aPKC : gene	aPKC : num co-occuring mutations in colorectal studies	aPKC : length-corrected score
1	B2M	4	0.03279	KRAS	7	0.03704	LYRM5	2	0.02222
2	KRAS	6	0.03175	TCTA	3	0.02913	IL4	3	0.01961
3	NDUFA4	2	0.02469	OSTN	3	0.02256	PRM1	1	0.01961
4	ACVR2A	12	0.02339	SCGB1D1	2	0.02222	RPL39	1	0.01961
5	TMEM105	3	0.02326	CXCL11	2	0.02128	SAA1	2	0.01639
6	CCL18	2	0.02247	CLC	3	0.02113	CXCL9	2	0.01600
7	LYRM5	2	0.02222	KRTAP22-1	1	0.02083	C12ORF54	2	0.01575
8	GYPB	2	0.02198	IL2	3	0.01961	FAM19A2	2	0.01527
9	S100A2	2	0.02062	RPL39	1	0.01961	GNG7	1	0.01471
10	HRSP12	3	0.02027	WBP5	2	0.01923	GOLT1B	2	0.01449
11	DPY30	2	0.02020	PLN	1	0.01923	MT1B	1	0.01429
12	HIGD1B	2	0.02020	IGIP	1	0.01887	SNURF	1	0.01408
13	PRM1	1	0.01961	SERTM1	2	0.01869	KRTAP19-5	1	0.01389
14	RPL39	1	0.01961	REG1A	3	0.01807	SPRR2B	1	0.01389
15	TCTA	2	0.01942	FAM163A	3	0.01796	C6ORF48	1	0.01333
16	PLN	1	0.01923	PTN	3	0.01786	COX6C	1	0.01333
17	C16ORF87	3	0.01863	PTH	2	0.01739	GNG3	1	0.01333
18	BLID	2	0.01852	DNAJC19	2	0.01724	RGS21	2	0.01316
19	REG1A	3	0.01807	KRTAP6-2	1	0.01613	UBE2A	2	0.01316
20	HTN1	1	0.01754	OR6N1	5	0.01603	NMS	2	0.01307

Melanoma

	cPKC : gene	cPKC : num co-occuring mutations in melanoma studies	cPKC : length-corrected score	nPKC : gene	nPKC : num co-occuring mutations in melanoma studies	nPKC : length-corrected score	aPKC : gene	aPKC : num co-occuring mutations in melanoma studies	aPKC : length-corrected score
1	PCP4	4	0.06452	CDKN2A	8	0.04706	TNP1	3	0.05455
2	NRAS	11	0.05820	SMR3A	6	0.04478	SPRR2G	3	0.04110
3	DEFB115	5	0.05682	DEFB110	3	0.04478	RETNLB	4	0.03604
4	SPRR2G	4	0.05479	POM121L12	13	0.04392	WFDC10B	3	0.03371
5	CDKN2A	9	0.05294	DEFA5	4	0.04255	ATP6V1G3	4	0.03226
6	OR10K2	15	0.04808	SPINK13	4	0.04255	DEFB110	2	0.02985
7	POM121L12	14	0.04730	NRAS	8	0.04233	GCSAML	4	0.02963
8	PRB4	11	0.04453	LELP1	4	0.04082	CDKN2A	5	0.02941
9	GCSAML	6	0.04444	ATP6V1G3	5	0.04032	LACRT	4	0.02899
10	TP53	16	0.04071	GYPA	6	0.04000	SPATA8	3	0.02857
11	ATP6V1G3	5	0.04032	PRB2	16	0.03846	COX8C	2	0.02778
12	SPATA8	4	0.03810	DPPA3	6	0.03774	SPANXN5	2	0.02778
13	FAM19A1	5	0.03759	GCSAML	5	0.03704	SPRR2D	2	0.02778
14	OR51S1	12	0.03715	KRTAP19-3	3	0.03704	CLEC5A	5	0.02660
15	TNP1	2	0.03636	RIPPLY3	7	0.03684	DEFB112	3	0.02655
16	OR4K1	11	0.03537	PPIAL4G	6	0.03659	TCL1A	3	0.02632
17	LALBA	5	0.03521	RETNLB	4	0.03604	C7ORF66	3	0.02609
18	OR4M1	11	0.03514	OR4N2	11	0.03583	OR4N2	8	0.02606
19	HTN1	2	0.03509	KRTAP12-4	4	0.03571	LCE1B	3	0.02542
20	LILRA1	17	0.03476	C7ORF66	4	0.03478	KRTAP19-3	2	0.02469

Table 7. TCGA Studies Screened for Mutations
TCGA studies used for the bioinformatic analyses of genes with mutations that co-occur with PKC mutations

Cancer type	TCGA study
Acute Myeloid Leukemia	TCGA, NEJM 2013
Acute Myeloid Leukemia	TCGA, Provisional
Adrenocortical Carcinoma	TCGA, Provisional
Bladder Urothelial Carcinoma	TCGA, Nature 2014
Bladder Urothelial Carcinoma	TCGA, Provisional
Brain Lower Grade Glioma	TCGA, Provisional
Breast Invasive Carcinoma	TCGA, Nature 2012
Breast Invasive Carcinoma	TCGA, Provisional
Cervical Squamous Cell Carcinoma and Endocervical Adenocarcinoma	TCGA, Provisional
Colorectal Adenocarcinoma	TCGA, Nature 2012
Colorectal Adenocarcinoma	TCGA, Provisional
Glioblastoma	TCGA, Cell 2013
Glioblastoma	TCGA, Nature 2008
Glioblastoma Multiforme	TCGA, Provisional
Head and Neck Squamous Cell Carcinoma	TCGA, Provisional
Head and Neck Squamous Cell Carcinoma	TCGA, in revision
Kidney Chromophobe	TCGA, Provisional
Kidney Renal Clear Cell Carcinoma	TCGA, Nature 2013
Kidney Renal Clear Cell Carcinoma	TCGA, Provisional
Kidney Renal Papillary Cell Carcinoma	TCGA, Provisional
Lung Adenocarcinoma	TCGA, Nature, in press
Lung Adenocarcinoma	TCGA, Provisional
Lung Squamous Cell Carcinoma	TCGA, Nature 2012
Lung Squamous Cell Carcinoma	TCGA, Provisional
Ovarian Serous Cystadenocarcinoma	TCGA, Nature 2011
Ovarian Serous Cystadenocarcinoma	TCGA, Provisional
Pancreatic Adenocarcinoma	TCGA, Provisional
Prostate Adenocarcinoma	TCGA, Provisional
Skin Cutaneous Melanoma	TCGA, Provisional
Stomach Adenocarcinoma	TCGA, Provisional
Thyroid Carcinoma	TCGA, Provisional
Uterine Carcinosarcoma	TCGA, Provisional
Uterine Corpus Endometrial Carcinoma	TCGA, Provisional
Uterine Corpus Endometrioid Carcinoma	TCGA, Nature 2013

CHAPTER 5 − SUMMARY AND CONCLUSIONS

The work within this thesis describes mechanisms that contribute to the regulation of PKC as well as to its dysregulation in disease. As PKC activity has to be precisely balanced at every subcellular location, its regulation is under intricate control. This control of the spatial and temporal dynamics of PKC signaling comes from regulation through various mechanisms, such as phosphorylation, binding to second messengers, conformational changes, and binding to scaffolds. Perturbation of any of these mechanisms of control can lead to pathophysiological states. Therefore, understanding all mechanisms through which PKC is regulated is key to developing novel therapeutics to restore PKC activity to physiological levels and to the appropriate subcellular locations. This work enabled us draw two significant conclusions: 1] through the use of FRET-based imaging and biochemical techniques, we elucidated a mechanism through which PKC optimizes its affinity for its activating ligands through conformation transitions and intramolecular interactions, and 2] through the use of FRET-based PKC activity reporters, CRISPR-mediated genome editing methods, and xenograft models, we established that PKC is a tumor suppressor (Figure 28). Thus, the studies described within this dissertation have expanded our knowledge of PKC both at the molecular and functional level.

MATURATION OF PKC MASKS ITS C1 DOMAINS TO OPTIMIZE SIGNALING

Optimal tuning of PKC signaling is essential for maintaining cellular homeostasis. Our FRET-based studies in Chapter 2 established that PKC undergoes conformational transitions as it matures, becomes activated, and is downregulated. These conformational changes tune PKC's affinity for diacylglycerol in order to optimize its dynamic range of signaling. Nascent PKC isozymes adopt an open conformation in which the ligand-binding surfaces of both C1 domains are exposed and thus can readily bind DAG. Upon the acquisition of processing phosphorylations, PKC matures into a closed, but catalytically

competent conformation. This species is maintained in an inactive state until the second messengers, Ca^{2+} and DAG, become available. In the absence of these second messengers, the closed conformation maintains the binding surfaces of both C1 domains masked through intramolecular interactions. This conformation reduces the affinity of the C1 domains for DAG, thus tuning the ability of PKC to become activated in such a way that it is inactive in the absence of these second messengers, but quickly becomes activated upon their production. In the absence of these processing phosphorylations and subsequent conformational changes, PKC would be constitutively active. We further show that for PKCβII, the C1B domain is the primary DAG binder, although the C1A domain can bind DAG as well.

This mechanism of tuning the affinity for ligands through intramolecular interactions is commonly utilized by other multi-domain enzymes. In PKC, these conformational transitions occur through processing phosphorylations. Although the process of PKC maturation is now well known, a number of questions remain to be addressed. For example, although it is known that mTOR plays a role in the maturation of PKC, its exact role in cells remains to be determined. Whether mTOR directly phosphorylates PKC, phosphorylates a chaperone that then binds PKC, or itself acts as a chaperone in order to allow PKC to auto-phosphorylate, is yet to be determined.

THE STRUCTURE OF PKC

Described in Chapter 3, our data support the hypothesis that the C2 domain of PKCβII interacts with the kinase domain and C-terminal tail through intramolecular interactions, maintaining PKC in a closed, autoinhibited conformation, thus reducing its basal binding to membranes. We identified and validated two points of electrostatic interaction of the C2 domain, one with the N-terminal lobe of the kinase domain and one with the C-terminal tail. Although the structures of most PKC domains have been resolved by solution NMR or X-ray

crystallography, the structure of the entire molecule remains elusive. Future work is required to discern the points of interaction of the C1A and C1B domains, as both have been proposed to interact with other domains within the enzyme. Elucidating these interactions is important as it might reveal novel ways of targeting PKC, either by opening it up with small molecules or peptides in order to activate it or by clamping it in the closed conformation in order to inhibit it.

PKC AS A TUMOR SUPPRESSOR

PKC has long been implicated in cancer development and has thus been targeted therapeutically over the last three decades. The work presented in Chapter 4 overturned a 30+-year old dogma that postulated that PKC is hyperactive in cancer and should thus be inhibited. We show that, in fact, the majority of cancer-associated PKC mutations from human tumors are loss-of-function and that a heterozygous loss-of-function PKCβII mutation can provide a growth advantage in cells as well as in a mouse xenograft model. These data suggest that therapeutic strategies should no longer be aimed at inhibiting PKC in cancer, as previously attempted, but instead, should be aimed at increasing or restoring PKC activity. However, much work has to be done in order to identify feasible and practical means of restoring PKC activity or of activating the wild-type PKC allele in patients. For example, PKC activity could be increased by developing PKC agonists that directly recruit PKC to membranes or that allosterically open up the kinase by breaking up intradomain interactions, in order to activate the wild-type PKC isozyme and compensate for the lack of activity of the mutant PKC. However, the agonist must not downregulate PKC after prolonged treatment, as do phorbol esters and Bryostatins. Downregulation could potentially be prevented by inhibiting the isomerization of PKC by Pin1, a step necessary for its dephosphorylation (Abrahamsen et al., 2012), or by inhibiting the ability of its hydrophobic motif phosphatase, PHLPP (Gao et al.,

2008), to dephosphorylate PKC. By targeting the PH domain of PHLPP, only its function towards PKC would be affected. Gene therapy could also be used to add a corrected copy of the PKC gene into patient cells. However, for the dominant negative mutations that prevent processing phosphorylation and affect the maturation of other PKCs in the cell, these methods might not work well. In these cases, the mutated gene would have to be replaced with a corrected one. However, caution should be taken when attempting to restore PKC activity as too much PKC activity could be detrimental and could induce other pathophysiologies.

FUTURE DIRECTIONS

One of the limitations on PKC research is the lack of isozyme-specific tools to study individual PKCs. Considering that PKC isozymes have little substrate specificity *in vitro* and that multiple isozymes are expressed in the same cell types, elucidating downstream signaling pathways and subcellular localization of endogenous PKC isozymes poses significant challenges. Developing isozyme-specific PKC modulators has been difficult because of the high homology among the PKC isozymes, as well as among protein kinases in general. Therefore, the specific roles of each PKC isozyme and their redundancy remain to be elucidated. However, the advent of genome editing technologies will facilitate a much more thorough and accurate study of PKC by enabling manipulation of the levels and sequence of the endogenous gene. This technology could be used to increase or repress the expression of individual endogenous PKC genes and to introduce disease-associated mutations within the endogenous protein. Moreover, the use of endogenous tags would allow for determining the subcellular localization of each isozyme. Genome editing technology would thus greatly advance our knowledge of PKC and facilitate the development of drugs to target this enzyme in disease.

FIGURES

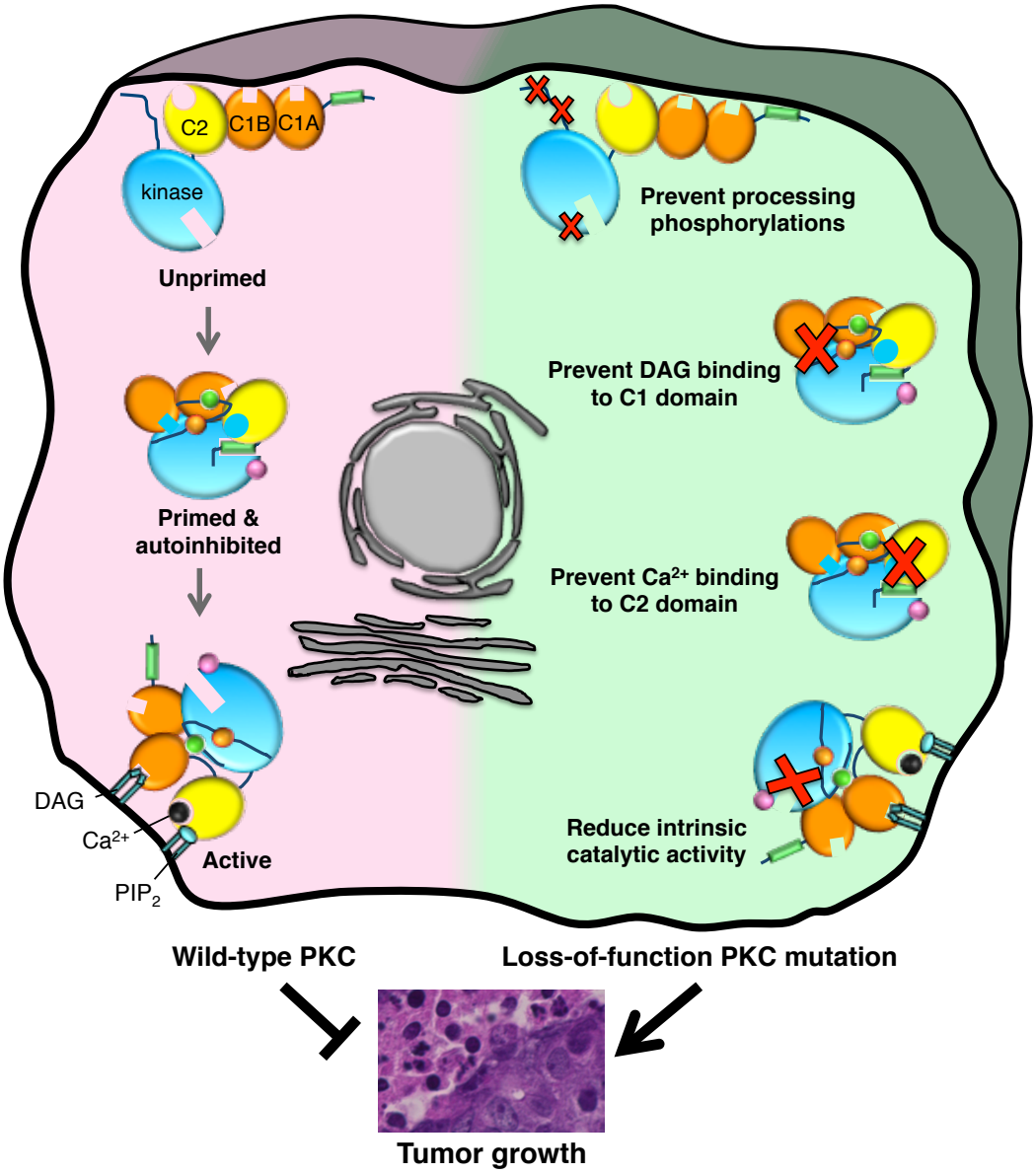

Figure 28. Regulation of PKC and its Dysregulation in Cancer
Left: Model showing processing of PKC. Unprimed cPKC is in a membrane-associated, open conformation. Upon priming phosphorylation at its activation loop (pink circle), turn motif (orange circle), and the hydrophobic motif (green circle), cPKC matures into a closed conformation in which the C1A, C1B, and C2 domains become masked, the pseudosubstrate binds the substrate-binding site, and the primed enzyme localizes to the cytosol. These intradomain interactions maintain PKC in a closed, but autoinhibited conformation until the second messengers DAG and Ca^{2+} are produced and bind to PKC, thus activating it. Wild-type PKC can suppress tumor growth.
Right: Cancer-associated PKC mutations induce loss-of-function by preventing processing phosphorylations, DAG binding to the C1 domain, or Ca2+ binding to the C2 domain, or by reducing the intrinsic catalytic activity of PKC. Inactivating mutations are permissive to tumor growth.

REFERENCES

Abbas, T., White, D., Hui, L., Yoshida, K., Foster, D.A., and Bargonetti, J. (2004). Inhibition of human p53 basal transcription by down-regulation of protein kinase Cdelta. The Journal of biological chemistry *279*, 9970-9977.

Alvaro, V., Levy, L., Dubray, C., Roche, A., Peillon, F., Querat, B., and Joubert, D. (1993). Invasive human pituitary tumors express a point-mutated alpha-protein kinase-C. The Journal of clinical endocrinology and metabolism *77*, 1125-1129.

Antal, C.E., Hudson, A.M., Kang, E., Zanca, C., Wirth, C., Stephenson, N.L., Trotter, E.W., Gallegos, L.L., Miller, C.J., Furnari, F.B., Hunter, T., Brognard, J., and Newton, A.C. (2015). Cancer-Associated Protein Kinase C Mutations Reveal Kinase's Role as Tumor Suppressor. Cell *160*, 489-502.

Antal, C.E., Violin, J.D., Kunkel, M.T., Skovso, S., and Newton, A.C. (2014). Intramolecular conformational changes optimize protein kinase C signaling. Chemistry & biology *21*, 459-469.

Astoul, E., Watton, S., and Cantrell, D. (1999). The dynamics of protein kinase B regulation during B cell antigen receptor engagement. J Cell Biol *145*, 1511-1520.

Banci, L., Cavallaro, G., Kheifets, V., and Mochly-Rosen, D. (2002). Molecular dynamics characterization of the C2 domain of protein kinase Cbeta. The Journal of biological chemistry *277*, 12988-12997.

Barcelo, C., Paco, N., Morell, M., Alvarez-Moya, B., Bota-Rabassedas, N., Jaumot, M., Vilardell, F., Capella, G., and Agell, N. (2014). Phosphorylation at Ser-181 of oncogenic KRAS is required for tumor growth. Cancer research *74*, 1190-1199.

Behn-Krappa, A., and Newton, A.C. (1999). The hydrophobic phosphorylation motif of conventional protein kinase C is regulated by autophosphorylation. Curr Biol *9*, 728-737.

Belin, R.J., Sumandea, M.P., Allen, E.J., Schoenfelt, K., Wang, H., Solaro, R.J., and de Tombe, P.P. (2007). Augmented protein kinase C-alpha-induced myofilament protein phosphorylation contributes to myofilament dysfunction in experimental congestive heart failure. Circulation research *101*, 195-204.

Belot, A., Kasher, P.R., Trotter, E.W., Foray, A.P., Debaud, A.L., Rice, G.I., Szynkiewicz, M., Zabot, M.T., Rouvet, I., Bhaskar, S.S., Daly, S.B., Dickerson, J.E., Mayer, J., O'Sullivan, J., Juillard, L., Urquhart, J.E., Fawdar, S., Marusiak, A.A., Stephenson, N., Waszkowycz, B., M, W.B., Biesecker, L.G., G, C.M.B., Rene, C., Eliaou, J.F., Fabien, N., Ranchin, B., Cochat, P., Gaffney, P.M., Rozenberg, F., Lebon, P., Malcus, C., Crow, Y.J., Brognard, J., and Bonnefoy, N. (2013). Protein kinase cdelta deficiency causes mendelian systemic lupus erythematosus with B cell-defective apoptosis and hyperproliferation. Arthritis and rheumatism *65*, 2161-2171.

Benes, C.H., Wu, N., Elia, A.E., Dharia, T., Cantley, L.C., and Soltoff, S.P. (2005). The C2 domain of PKCdelta is a phosphotyrosine binding domain. Cell *121*, 271-280.

Bernado, P. (2010). Effect of interdomain dynamics on the structure determination of modular proteins by small-angle scattering. Eur Biophys J *39*, 769-780.

Bernatsky, S., Boivin, J.F., Joseph, L., Rajan, R., Zoma, A., Manzi, S., Ginzler, E., Urowitz, M., Gladman, D., Fortin, P.R., Petri, M., Edworthy, S., Barr, S., Gordon, C., Bae, S.C., Sibley, J., Isenberg, D., Rahman, A., Aranow, C., Dooley, M.A., Steinsson, K., Nived, O., Sturfelt, G., Alarcon, G., Senecal, J.L., Zummer, M., Hanly, J., Ensworth, S., Pope, J., El-Gabalawy, H., McCarthy, T., St Pierre, Y.,

Ramsey-Goldman, R., and Clarke, A. (2005). An international cohort study of cancer in systemic lupus erythematosus. Arthritis and rheumatism *52*, 1481-1490.

Berridge, M.J. (1987). Inositol trisphosphate and diacylglycerol: two interacting second messengers. Annual review of biochemistry *56*, 159-193.

Bittova, L., Stahelin, R.V., and Cho, W. (2001). Roles of ionic residues of the C1 domain in protein kinase C-alpha activation and the origin of phosphatidylserine specificity. The Journal of biological chemistry *276*, 4218-4226.

Bivona, T.G., Quatela, S.E., Bodemann, B.O., Ahearn, I.M., Soskis, M.J., Mor, A., Miura, J., Wiener, H.H., Wright, L., Saba, S.G., Yim, D., Fein, A., Perez de Castro, I., Li, C., Thompson, C.B., Cox, A.D., and Philips, M.R. (2006). PKC regulates a farnesyl-electrostatic switch on K-Ras that promotes its association with Bcl-XL on mitochondria and induces apoptosis. Molecular cell *21*, 481-493.

Blumberg, P.M. (1980). In vitro studies on the mode of action of the phorbol esters, potent tumor promoters: part 1. Critical reviews in toxicology *8*, 153-197.

Boggon, T.J., and Eck, M.J. (2004). Structure and regulation of Src family kinases. Oncogene *23*, 7918-7927.

Borner, C., Filipuzzi, I., Wartmann, M., Eppenberger, U., and Fabbro, D. (1989). Biosynthesis and posttranslational modifications of protein kinase C in human breast cancer cells. J Biol Chem *264*, 13902-13909.

Bowling, N., Walsh, R.A., Song, G., Estridge, T., Sandusky, G.E., Fouts, R.L., Mintze, K., Pickard, T., Roden, R., Bristow, M.R., Sabbah, H.N., Mizrahi, J.L., Gromo, G., King, G.L., and Vlahos, C.J. (1999). Increased protein kinase C activity and expression of Ca2+-sensitive isoforms in the failing human heart. Circulation *99*, 384-391.

Braun, D.C., Garfield, S.H., and Blumberg, P.M. (2005). Analysis by fluorescence resonance energy transfer of the interaction between ligands and protein kinase Cdelta in the intact cell. J Biol Chem *280*, 8164-8171.

Buechler, J.A., Vedvick, T.A., and Taylor, S.S. (1989). Differential labeling of the catalytic subunit of cAMP-dependent protein kinase with acetic anhydride: substrate-induced conformational changes. Biochemistry *28*, 3018-3024.

Cacace, A.M., Guadagno, S.N., Krauss, R.S., Fabbro, D., and Weinstein, I.B. (1993). The epsilon isoform of protein kinase C is an oncogene when overexpressed in rat fibroblasts. Oncogene *8*, 2095-2104.

Castagna, M., Takai, Y., Kaibuchi, K., Sano, K., Kikkawa, U., and Nishizuka, Y. (1982). Direct activation of calcium-activated, phospholipid-dependent protein kinase by tumor-promoting phorbol esters. J Biol Chem *257*, 7847-7851.

Cerami, E., Gao, J., Dogrusoz, U., Gross, B.E., Sumer, S.O., Aksoy, B.A., Jacobsen, A., Byrne, C.J., Heuer, M.L., Larsson, E., Antipin, Y., Reva, B., Goldberg, A.P., Sander, C., and Schultz, N. (2012a). The cBio cancer genomics portal: an open platform for exploring multidimensional cancer genomics data. Cancer Discov *2*, 401-404.

Cerami, E., Gao, J., Dogrusoz, U., Gross, B.E., Sumer, S.O., Aksoy, B.A., Jacobsen, A., Byrne, C.J., Heuer, M.L., Larsson, E., Antipin, Y., Reva, B., Goldberg, A.P., Sander, C., and Schultz, N. (2012b).

The cBio cancer genomics portal: an open platform for exploring multidimensional cancer genomics data. Cancer discovery *2*, 401-404.

Cho, W., and Stahelin, R.V. (2006). Membrane binding and subcellular targeting of C2 domains. Biochimica et biophysica acta *1761*, 838-849.

Choi, P.M., Tchou-Wong, K.M., and Weinstein, I.B. (1990). Overexpression of protein kinase C in HT29 colon cancer cells causes growth inhibition and tumor suppression. Molecular and cellular biology *10*, 4650-4657.

Conrad, R., Keranen, L.M., Ellington, A.D., and Newton, A.C. (1994). Isozyme-specific inhibition of protein kinase C by RNA aptamers. The Journal of biological chemistry *269*, 32051-32054.

Corbalan-Garcia, S., Garcia-Garcia, J., Rodriguez-Alfaro, J.A., and Gomez-Fernandez, J.C. (2003). A new phosphatidylinositol 4,5-bisphosphate-binding site located in the C2 domain of protein kinase Calpha. The Journal of biological chemistry *278*, 4972-4980.

Corbin, J.A., Evans, J.H., Landgraf, K.E., and Falke, J.J. (2007). Mechanism of specific membrane targeting by C2 domains: localized pools of target lipids enhance Ca2+ affinity. Biochemistry *46*, 4322-4336.

Craven, P.A., and DeRubertis, F.R. (1994). Loss of protein kinase C delta isozyme immunoreactivity in human adenocarcinomas. Digestive diseases and sciences *39*, 481-489.

Csukai, M., Chen, C.H., De Matteis, M.A., and Mochly-Rosen, D. (1997). The coatomer protein beta'-COP, a selective binding protein (RACK) for protein kinase Cepsilon. J Biol Chem *272*, 29200-29206.

D'Costa, A.M., Robinson, J.K., Maududi, T., Chaturvedi, V., Nickoloff, B.J., and Denning, M.F. (2006). The proapoptotic tumor suppressor protein kinase C-delta is lost in human squamous cell carcinomas. Oncogene *25*, 378-386.

Dabney, A., Storey, J.D. (2014). qvalue: Q-value estimation for false discovery rate control. R package version 1380 edn.

Davidson, L.A., Jiang, Y.H., Derr, J.N., Aukema, H.M., Lupton, J.R., and Chapkin, R.S. (1994). Protein kinase C isoforms in human and rat colonic mucosa. Archives of biochemistry and biophysics *312*, 547-553.

Dempsey, E.C., Newton, A.C., Mochly-Rosen, D., Fields, A.P., Reyland, M.E., Insel, P.A., and Messing, R.O. (2000). Protein kinase C isozymes and the regulation of diverse cell responses. American journal of physiology Lung cellular and molecular physiology *279*, L429-438.

Dev, K.K., Nakajima, Y., Kitano, J., Braithwaite, S.P., Henley, J.M., and Nakanishi, S. (2000). PICK1 interacts with and regulates PKC phosphorylation of mGLUR7. The Journal of neuroscience : the official journal of the Society for Neuroscience *20*, 7252-7257.

Don, A.S., and Zheng, X.F. (2011). Recent clinical trials of mTOR-targeted cancer therapies. Reviews on recent clinical trials *6*, 24-35.

Dries, D.R., Gallegos, L.L., and Newton, A.C. (2007). A single residue in the C1 domain sensitizes novel protein kinase C isoforms to cellular diacylglycerol production. The Journal of biological chemistry *282*, 826-830.

Dries, D.R., and Newton, A.C. (2008). Kinetic analysis of the interaction of the C1 domain of protein kinase C with lipid membranes by stopped-flow spectroscopy. The Journal of biological chemistry *283*, 7885-7893.

Dutil, E.M., and Newton, A.C. (2000). Dual role of pseudosubstrate in the coordinated regulation of protein kinase C by phosphorylation and diacylglycerol. The Journal of biological chemistry *275*, 10697-10701.

Dutil, E.M., Toker, A., and Newton, A.C. (1998). Regulation of conventional protein kinase C isozymes by phosphoinositide-dependent kinase 1 (PDK-1). Current biology : CB *8*, 1366-1375.

Edwards, A.S., Faux, M.C., Scott, J.D., and Newton, A.C. (1999). Carboxyl-terminal phosphorylation regulates the function and subcellular localization of protein kinase C betaII. J Biol Chem *274*, 6461-6468.

Edwards, A.S., and Newton, A.C. (1997a). Phosphorylation at conserved carboxyl-terminal hydrophobic motif regulates the catalytic and regulatory domains of protein kinase C. The Journal of biological chemistry *272*, 18382-18390.

Edwards, A.S., and Newton, A.C. (1997b). Regulation of protein kinase C betaII by its C2 domain. Biochemistry *36*, 15615-15623.

Evans, J.H., Murray, D., Leslie, C.C., and Falke, J.J. (2006). Specific translocation of protein kinase Calpha to the plasma membrane requires both Ca2+ and PIP2 recognition by its C2 domain. Molecular biology of the cell *17*, 56-66.

Facchinetti, V., Ouyang, W., Wei, H., Soto, N., Lazorchak, A., Gould, C., Lowry, C., Newton, A.C., Mao, Y., Miao, R.Q., Sessa, W.C., Qin, J., Zhang, P., Su, B., and Jacinto, E. (2008). The mammalian target of rapamycin complex 2 controls folding and stability of Akt and protein kinase C. The EMBO journal *27*, 1932-1943.

Feng, X., Becker, K.P., Stribling, S.D., Peters, K.G., and Hannun, Y.A. (2000). Regulation of receptor-mediated protein kinase C membrane trafficking by autophosphorylation. The Journal of biological chemistry *275*, 17024-17034.

Ferrer-Orta, C., Agudo, R., Domingo, E., and Verdaguer, N. (2009). Structural insights into replication initiation and elongation processes by the FMDV RNA-dependent RNA polymerase. Current opinion in structural biology *19*, 752-758.

Futreal, P.A., Coin, L., Marshall, M., Down, T., Hubbard, T., Wooster, R., Rahman, N., and Stratton, M.R. (2004). A census of human cancer genes. Nat Rev Cancer *4*, 177-183.

Gallegos, L.L., Kunkel, M.T., and Newton, A.C. (2006). Targeting protein kinase C activity reporter to discrete intracellular regions reveals spatiotemporal differences in agonist-dependent signaling. The Journal of biological chemistry *281*, 30947-30956.

Gallegos, L.L., and Newton, A.C. (2011). Genetically encoded fluorescent reporters to visualize protein kinase C activation in live cells. Methods in molecular biology *756*, 295-310.

Galvez, A.S., Duran, A., Linares, J.F., Pathrose, P., Castilla, E.A., Abu-Baker, S., Leitges, M., Diaz-Meco, M.T., and Moscat, J. (2009). Protein kinase Czeta represses the interleukin-6 promoter and impairs tumorigenesis in vivo. Molecular and cellular biology *29*, 104-115.

Gao, J., Aksoy, B.A., Dogrusoz, U., Dresdner, G., Gross, B., Sumer, S.O., Sun, Y., Jacobsen, A., Sinha, R., Larsson, E., Cerami, E., Sander, C., and Schultz, N. (2013a). Integrative analysis of complex cancer genomics and clinical profiles using the cBioPortal. Science signaling *6*, pl1.

Gao, J., Aksoy, B.A., Dogrusoz, U., Dresdner, G., Gross, B., Sumer, S.O., Sun, Y., Jacobsen, A., Sinha, R., Larsson, E., Cerami, E., Sander, C., and Schultz, N. (2013b). Integrative analysis of complex cancer genomics and clinical profiles using the cBioPortal. Sci Signal *6*, pl1.

Gao, T., Brognard, J., and Newton, A.C. (2008). The phosphatase PHLPP controls the cellular levels of protein kinase C. J Biol Chem *283*, 6300-6311.

Garcia-Paramio, P., Cabrerizo, Y., Bornancin, F., and Parker, P.J. (1998). The broad specificity of dominant inhibitory protein kinase C mutants infers a common step in phosphorylation. The Biochemical journal *333 (Pt 3)*, 631-636.

Giorgione, J., Hysell, M., Harvey, D.F., and Newton, A.C. (2003). Contribution of the C1A and C1B domains to the membrane interaction of protein kinase C. Biochemistry *42*, 11194-11202.

Giorgione, J., and Newton, A.C. (2003). Measuring the binding of protein kinase C to sucrose-loaded vesicles. Methods in molecular biology *233*, 105-113.

Gould, C.M., Antal, C.E., Reyes, G., Kunkel, M.T., Adams, R.A., Ziyar, A., Riveros, T., and Newton, A.C. (2011). Active site inhibitors protect protein kinase C from dephosphorylation and stabilize its mature form. The Journal of biological chemistry *286*, 28922-28930.

Gould, C.M., Kannan, N., Taylor, S.S., and Newton, A.C. (2009). The chaperones Hsp90 and Cdc37 mediate the maturation and stabilization of protein kinase C through a conserved PXXP motif in the C-terminal tail. The Journal of biological chemistry *284*, 4921-4935.

Greenwald, E.C., Redden, J.M., Dodge-Kafka, K.L., and Saucerman, J.J. (2014). Scaffold state switching amplifies, accelerates, and insulates protein kinase C signaling. J Biol Chem *289*, 2353-2360.

Griner, E.M., and Kazanietz, M.G. (2007a). Protein kinase C and other diacylglycerol effectors in cancer. Nat Rev Cancer *7*, 281-294.

Griner, E.M., and Kazanietz, M.G. (2007b). Protein kinase C and other diacylglycerol effectors in cancer. Nature reviews Cancer *7*, 281-294.

Grodsky, N., Li, Y., Bouzida, D., Love, R., Jensen, J., Nodes, B., Nonomiya, J., and Grant, S. (2006). Structure of the catalytic domain of human protein kinase C beta II complexed with a bisindolylmaleimide inhibitor. Biochemistry *45*, 13970-13981.

Guerrero-Valero, M., Ferrer-Orta, C., Querol-Audi, J., Marin-Vicente, C., Fita, I., Gomez-Fernandez, J.C., Verdaguer, N., and Corbalan-Garcia, S. (2009). Structural and mechanistic insights into the association of PKCalpha-C2 domain to PtdIns(4,5)P2. Proceedings of the National Academy of Sciences of the United States of America *106*, 6603-6607.

Guertin, D.A., Stevens, D.M., Thoreen, C.C., Burds, A.A., Kalaany, N.Y., Moffat, J., Brown, M., Fitzgerald, K.J., and Sabatini, D.M. (2006). Ablation in mice of the mTORC components raptor, rictor, or mLST8 reveals that mTORC2 is required for signaling to Akt-FOXO and PKCalpha, but not S6K1. Developmental cell *11*, 859-871.

Guo, J., Cong, L., Rybin, V.O., Gertsberg, Z., and Steinberg, S.F. (2010). Protein kinase C-{delta} regulates the subcellular localization of Shc in H2O2-treated cardiomyocytes. American journal of physiology Cell physiology *299*, C770-778.

Gwak, J., Jung, S.J., Kang, D.I., Kim, E.Y., Kim, D.E., Chung, Y.H., Shin, J.G., and Oh, S. (2009). Stimulation of protein kinase C-alpha suppresses colon cancer cell proliferation by down-regulation of beta-catenin. Journal of cellular and molecular medicine *13*, 2171-2180.

Hannun, Y.A., and Bell, R.M. (1986). Phorbol ester binding and activation of protein kinase C on triton X-100 mixed micelles containing phosphatidylserine. The Journal of biological chemistry *261*, 9341-9347.

Hannun, Y.A., Loomis, C.R., and Bell, R.M. (1985). Activation of protein kinase C by Triton X-100 mixed micelles containing diacylglycerol and phosphatidylserine. The Journal of biological chemistry *260*, 10039-10043.

Hansra, G., Bornancin, F., Whelan, R., Hemmings, B.A., and Parker, P.J. (1996). 12-O-Tetradecanoylphorbol-13-acetate-induced dephosphorylation of protein kinase Calpha correlates with the presence of a membrane-associated protein phosphatase 2A heterotrimer. The Journal of biological chemistry *271*, 32785-32788.

Hauge, C., Antal, T.L., Hirschberg, D., Doehn, U., Thorup, K., Idrissova, L., Hansen, K., Jensen, O.N., Jorgensen, T.J., Biondi, R.M., and Frodin, M. (2007). Mechanism for activation of the growth factor-activated AGC kinases by turn motif phosphorylation. The EMBO journal *26*, 2251-2261.

Hernandez-Maqueda, J.G., Luna-Ulloa, L.B., Santoyo-Ramos, P., Castaneda-Patlan, M.C., and Robles-Flores, M. (2013). Protein kinase C delta negatively modulates canonical Wnt pathway and cell proliferation in colon tumor cell lines. PloS one *8*, e58540.

Hill, K.S., Erdogan, E., Khoor, A., Walsh, M.P., Leitges, M., Murray, N.R., and Fields, A.P. (2014). Protein kinase Calpha suppresses Kras-mediated lung tumor formation through activation of a p38 MAPK-TGFbeta signaling axis. Oncogene *33*, 2134-2144.

Hirai, S., Izumi, Y., Higa, K., Kaibuchi, K., Mizuno, K., Osada, S., Suzuki, K., and Ohno, S. (1994). Ras-dependent signal transduction is indispensable but not sufficient for the activation of AP1/Jun by PKC delta. The EMBO journal *13*, 2331-2340.

Hirsch, A.H., Glantz, S.B., Li, Y., You, Y., and Rubin, C.S. (1992). Cloning and expression of an intron-less gene for AKAP 75, an anchor protein for the regulatory subunit of cAMP-dependent protein kinase II beta. J Biol Chem *267*, 2131-2134.

Hof, P., Pluskey, S., Dhe-Paganon, S., Eck, M.J., and Shoelson, S.E. (1998). Crystal structure of the tyrosine phosphatase SHP-2. Cell *92*, 441-450.

Hommel, U., Zurini, M., and Luyten, M. (1994). Solution structure of a cysteine rich domain of rat protein kinase C. Nature structural biology *1*, 383-387.

Hoshi, N., Langeberg, L.K., Gould, C.M., Newton, A.C., and Scott, J.D. (2010). Interaction with AKAP79 modifies the cellular pharmacology of PKC. Mol Cell *37*, 541-550.

Hudson, A.M., Yates, T., Li, Y., Trotter, E.W., Fawdar, S., Chapman, P., Lorigan, P., Biankin, A., Miller, C.J., and Brognard, J. (2014). Discrepancies in Cancer Genomic Sequencing Highlight Opportunities for Driver Mutation Discovery. Cancer Res.

Ikenoue, T., Inoki, K., Yang, Q., Zhou, X., and Guan, K.L. (2008). Essential function of TORC2 in PKC and Akt turn motif phosphorylation, maturation and signalling. The EMBO journal *27*, 1919-1931.

Jacobsen, A. (2013). cgdsr: R-Based API for accessing the MSKCC Cancer Genomics Data Server (CGDS).

Jacques, D.A., and Trewhella, J. (2010). Small-angle scattering for structural biology--expanding the frontier while avoiding the pitfalls. Protein Sci *19*, 642-657.

Ji, J., Hassler, M.L., Shimobayashi, E., Paka, N., Streit, R., and Kapfhammer, J.P. (2014). Increased protein kinase C gamma activity induces Purkinje cell pathology in a mouse model of spinocerebellar ataxia 14. Neurobiology of disease *70*, 1-11.

Johnson, J.E., Giorgione, J., and Newton, A.C. (2000). The C1 and C2 domains of protein kinase C are independent membrane targeting modules, with specificity for phosphatidylserine conferred by the C1 domain. Biochemistry *39*, 11360-11369.

Justilien, V., Walsh, M.P., Ali, S.A., Thompson, E.A., Murray, N.R., and Fields, A.P. (2014). The PRKCI and SOX2 oncogenes are coamplified and cooperate to activate Hedgehog signaling in lung squamous cell carcinoma. Cancer cell *25*, 139-151.

Kajimoto, T., Sawamura, S., Tohyama, Y., Mori, Y., and Newton, A.C. (2010). Protein kinase C {delta}-specific activity reporter reveals agonist-evoked nuclear activity controlled by Src family of kinases. The Journal of biological chemistry *285*, 41896-41910.

Kang, J.-H. (2014). Protein Kinase C (PKC) Isozymes and Cancer. New Journal of Science *2014*, 36.

Kazanietz, M.G., Bustelo, X.R., Barbacid, M., Kolch, W., Mischak, H., Wong, G., Pettit, G.R., Bruns, J.D., and Blumberg, P.M. (1994). Zinc finger domains and phorbol ester pharmacophore. Analysis of binding to mutated form of protein kinase C zeta and the vav and c-raf proto-oncogene products. J Biol Chem *269*, 11590-11594.

Kazanietz, M.G., Wang, S., Milne, G.W., Lewin, N.E., Liu, H.L., and Blumberg, P.M. (1995). Residues in the second cysteine-rich region of protein kinase C delta relevant to phorbol ester binding as revealed by site-directed mutagenesis. The Journal of biological chemistry *270*, 21852-21859.

Keranen, L.M., Dutil, E.M., and Newton, A.C. (1995). Protein kinase C is regulated in vivo by three functionally distinct phosphorylations. Current biology : CB *5*, 1394-1403.

Keranen, L.M., and Newton, A.C. (1997). Ca2+ differentially regulates conventional protein kinase Cs' membrane interaction and activation. The Journal of biological chemistry *272*, 25959-25967.

Kheifets, V., and Mochly-Rosen, D. (2007). Insight into intra- and inter-molecular interactions of PKC: design of specific modulators of kinase function. Pharmacological research : the official journal of the Italian Pharmacological Society *55*, 467-476.

Kikkawa, U., Takai, Y., Tanaka, Y., Miyake, R., and Nishizuka, Y. (1983). Protein kinase C as a possible receptor protein of tumor-promoting phorbol esters. J Biol Chem *258*, 11442-11445.

Kim, J.Y., Valencia, T., Abu-Baker, S., Linares, J., Lee, S.J., Yajima, T., Chen, J., Eroshkin, A., Castilla, E.A., Brill, L.M., Medvedovic, M., Leitges, M., Moscat, J., and Diaz-Meco, M.T. (2013). c-Myc phosphorylation by PKCzeta represses prostate tumorigenesis. Proceedings of the National Academy of Sciences of the United States of America *110*, 6418-6423.

Kishimoto, A., Kajikawa, N., Shiota, M., and Nishizuka, Y. (1983). Proteolytic activation of calcium-activated, phospholipid-dependent protein kinase by calcium-dependent neutral protease. The Journal of biological chemistry *258*, 1156-1164.

Klauck, T.M., Faux, M.C., Labudda, K., Langeberg, L.K., Jaken, S., and Scott, J.D. (1996). Coordination of three signaling enzymes by AKAP79, a mammalian scaffold protein. Science *271*, 1589-1592.

Konig, B., Di Nitto, P.A., and Blumberg, P.M. (1985a). Phospholipid and Ca++ dependency of phorbol ester receptors. Journal of cellular biochemistry *27*, 255-265.

Konig, B., DiNitto, P.A., and Blumberg, P.M. (1985b). Stoichiometric binding of diacylglycerol to the phorbol ester receptor. Journal of cellular biochemistry *29*, 37-44.

Koren, R., Langzam, L., Paz, A., Livne, P.M., Gal, R., and Sampson, S.R. (2000). Protein kinase C (PKC) isoenzymes immunohistochemistry in lymph node revealing solution-fixed, paraffin-embedded bladder tumors. Applied immunohistochemistry & molecular morphology : AIMM / official publication of the Society for Applied Immunohistochemistry *8*, 166-171.

Kornev, A.P., Haste, N.M., Taylor, S.S., and Eyck, L.F. (2006). Surface comparison of active and inactive protein kinases identifies a conserved activation mechanism. Proceedings of the National Academy of Sciences of the United States of America *103*, 17783-17788.

Kornev, A.P., Taylor, S.S., and Ten Eyck, L.F. (2008). A helix scaffold for the assembly of active protein kinases. Proceedings of the National Academy of Sciences of the United States of America *105*, 14377-14382.

Kuehn, H.S., Niemela, J.E., Rangel-Santos, A., Zhang, M., Pittaluga, S., Stoddard, J.L., Hussey, A.A., Evbuomwan, M.O., Priel, D.A., Kuhns, D.B., Park, C.L., Fleisher, T.A., Uzel, G., and Oliveira, J.B. (2013). Loss-of-function of the protein kinase C delta (PKCdelta) causes a B-cell lymphoproliferative syndrome in humans. Blood *121*, 3117-3125.

Kunkel, M.T., and Newton, A.C. (2010). Calcium transduces plasma membrane receptor signals to produce diacylglycerol at Golgi membranes. J Biol Chem *285*, 22748-22752.

Lamark, T., Perander, M., Outzen, H., Kristiansen, K., Overvatn, A., Michaelsen, E., Bjorkoy, G., and Johansen, T. (2003). Interaction codes within the family of mammalian Phox and Bem1p domain-containing proteins. J Biol Chem *278*, 34568-34581.

Langzam, L., Koren, R., Gal, R., Kugel, V., Paz, A., Farkas, A., and Sampson, S.R. (2001). Patterns of protein kinase C isoenzyme expression in transitional cell carcinoma of bladder. Relation to degree of malignancy. American journal of clinical pathology *116*, 377-385.

Le Good, J.A., Ziegler, W.H., Parekh, D.B., Alessi, D.R., Cohen, P., and Parker, P.J. (1998). Protein kinase C isotypes controlled by phosphoinositide 3-kinase through the protein kinase PDK1. Science *281*, 2042-2045.

Leitges, M., Kovac, J., Plomann, M., and Linden, D.J. (2004). A unique PDZ ligand in PKCalpha confers induction of cerebellar long-term synaptic depression. Neuron *44*, 585-594.

Leonard, T.A., Rozycki, B., Saidi, L.F., Hummer, G., and Hurley, J.H. (2011). Crystal structure and allosteric activation of protein kinase C betaII. Cell *144*, 55-66.

Linch, M., Sanz-Garcia, M., Soriano, E., Zhang, Y., Riou, P., Rosse, C., Cameron, A., Knowles, P., Purkiss, A., Kjaer, S., McDonald, N.Q., and Parker, P.J. (2013). A cancer-associated mutation in atypical protein kinase Ciota occurs in a substrate-specific recruitment motif. Science signaling *6*, ra82.

Lu, H.C., Chou, F.P., Yeh, K.T., Chang, Y.S., Hsu, N.C., and Chang, J.G. (2009). Analysing the expression of protein kinase C eta in human hepatocellular carcinoma. Pathology *41*, 626-629.

Lu, Z., Hornia, A., Jiang, Y.W., Zang, Q., Ohno, S., and Foster, D.A. (1997). Tumor promotion by depleting cells of protein kinase C delta. Molecular and cellular biology *17*, 3418-3428.

Luna-Ulloa, L.B., Hernandez-Maqueda, J.G., Santoyo-Ramos, P., Castaneda-Patlan, M.C., and Robles-Flores, M. (2011). Protein kinase C zeta is a positive modulator of canonical Wnt signaling pathway in tumoral colon cell lines. Carcinogenesis *32*, 1615-1624.

Ma, L., Tao, Y., Duran, A., Llado, V., Galvez, A., Barger, J.F., Castilla, E.A., Chen, J., Yajima, T., Porollo, A., Medvedovic, M., Brill, L.M., Plas, D.R., Riedl, S.J., Leitges, M., Diaz-Meco, M.T., Richardson, A.D., and Moscat, J. (2013). Control of nutrient stress-induced metabolic reprogramming by PKCzeta in tumorigenesis. Cell *152*, 599-611.

Mackay, H.J., and Twelves, C.J. (2007). Targeting the protein kinase C family: are we there yet? Nature reviews Cancer *7*, 554-562.

Mandil, R., Ashkenazi, E., Blass, M., Kronfeld, I., Kazimirsky, G., Rosenthal, G., Umansky, F., Lorenzo, P.S., Blumberg, P.M., and Brodie, C. (2001). Protein kinase Calpha and protein kinase Cdelta play opposite roles in the proliferation and apoptosis of glioma cells. Cancer research *61*, 4612-4619.

Marin-Vicente, C., Gomez-Fernandez, J.C., and Corbalan-Garcia, S. (2005). The ATP-dependent membrane localization of protein kinase Calpha is regulated by Ca2+ influx and phosphatidylinositol 4,5-bisphosphate in differentiated PC12 cells. Molecular biology of the cell *16*, 2848-2861.

Mauro, L.V., Grossoni, V.C., Urtreger, A.J., Yang, C., Colombo, L.L., Morandi, A., Pallotta, M.G., Kazanietz, M.G., Bal de Kier Joffe, E.D., and Puricelli, L.L. (2010). PKC Delta (PKCdelta) promotes tumoral progression of human ductal pancreatic cancer. Pancreas *39*, e31-41.

Medkova, M., and Cho, W. (1998). Mutagenesis of the C2 domain of protein kinase C-alpha. Differential roles of Ca2+ ligands and membrane binding residues. The Journal of biological chemistry *273*, 17544-17552.

Mellemkjaer, L., Andersen, V., Linet, M.S., Gridley, G., Hoover, R., and Olsen, J.H. (1997). Non-Hodgkin's lymphoma and other cancers among a cohort of patients with systemic lupus erythematosus. Arthritis and rheumatism *40*, 761-768.

Mermel, C.H., Schumacher, S.E., Hill, B., Meyerson, M.L., Beroukhim, R., and Getz, G. (2011). GISTIC2.0 facilitates sensitive and confident localization of the targets of focal somatic copy-number alteration in human cancers. Genome biology *12*, R41.

Moore, P.B. (1980). Small-Angle Scattering - Information-Content and Error Analysis. Journal of Applied Crystallography *13*, 168-175.

Mosior, M., and McLaughlin, S. (1991). Peptides that mimic the pseudosubstrate region of protein kinase C bind to acidic lipids in membranes. Biophysical journal *60*, 149-159.

Mosior, M., and Newton, A.C. (1998a). Mechanism of the apparent cooperativity in the interaction of protein kinase C with phosphatidylserine. Biochemistry *37*, 17271-17279.

Mosior, M., and Newton, A.C. (1998b). Mechanism of the apparent cooperativity in the interaction of protein kinase C with phosphatidylserine. Biochemistry *37*, 17271-17279.

Myhre, S., Lingjaerde, O.C., Hennessy, B.T., Aure, M.R., Carey, M.S., Alsner, J., Tramm, T., Overgaard, J., Mills, G.B., Borresen-Dale, A.L., and Sorlie, T. (2013). Influence of DNA copy number and mRNA levels on the expression of breast cancer related proteins. Molecular oncology *7*, 704-718.

Nalefski, E.A., and Falke, J.J. (1996). The C2 domain calcium-binding motif: structural and functional diversity. Protein science : a publication of the Protein Society *5*, 2375-2390.

Nalefski, E.A., and Newton, A.C. (2001). Membrane binding kinetics of protein kinase C betaII mediated by the C2 domain. Biochemistry *40*, 13216-13229.

Neckers, L., and Workman, P. (2012). Hsp90 molecular chaperone inhibitors: are we there yet? Clinical cancer research : an official journal of the American Association for Cancer Research *18*, 64-76.

Nelson, T.J., and Alkon, D.L. (2009). Neuroprotective versus tumorigenic protein kinase C activators. Trends Biochem Sci *34*, 136-145.

Newton, A. (2010). Protein kinase C: poised to signal. American journal of physiology Endocrinology and metabolism *298*, 402.

Newton, A.C. (1995). Protein kinase C. Seeing two domains. Curr Biol *5*, 973-976.

Newton, A.C. (2001). Protein kinase C: structural and spatial regulation by phosphorylation, cofactors, and macromolecular interactions. Chemical reviews *101*, 2353-2364.

Newton, A.C. (2003). Regulation of the ABC kinases by phosphorylation: protein kinase C as a paradigm. Biochem J *370*, 361-371.

Newton, A.C., and Koshland, D.E., Jr. (1989). High cooperativity, specificity, and multiplicity in the protein kinase C-lipid interaction. The Journal of biological chemistry *264*, 14909-14915.

Nezhat, F., Wadler, S., Muggia, F., Mandeli, J., Goldberg, G., Rahaman, J., Runowicz, C., Murgo, A.J., and Gardner, G.J. (2004). Phase II trial of the combination of bryostatin-1 and cisplatin in advanced or recurrent carcinoma of the cervix: a New York Gynecologic Oncology Group study. Gynecologic oncology *93*, 144-148.

Nishizuka, Y. (1995). Protein kinase C and lipid signaling for sustained cellular responses. Faseb J *9*, 484-496.

O'Neill, A.K., Gallegos, L.L., Justilien, V., Garcia, E.L., Leitges, M., Fields, A.P., Hall, R.A., and Newton, A.C. (2011). Protein kinase Calpha promotes cell migration through a PDZ-dependent interaction with its novel substrate discs large homolog 1 (DLG1). The Journal of biological chemistry *286*, 43559-43568.

Oancea, E., and Meyer, T. (1998). Protein Kinase C as a Molecular Machine for Decoding Calcium and Diacylglycerol Signals. Cell *95*, 307-318.

Ohno, S., Konno, Y., Akita, Y., Yano, A., and Suzuki, K. (1990). A point mutation at the putative ATP-binding site of protein kinase C alpha abolishes the kinase activity and renders it down-regulation-insensitive. A molecular link between autophosphorylation and down-regulation. The Journal of biological chemistry *265*, 6296-6300.

Ono, Y., Fujii, T., Igarashi, K., Kuno, T., Tanaka, C., Kikkawa, U., and Nishizuka, Y. (1989). Phorbol ester binding to protein kinase C requires a cysteine-rich zinc-finger-like sequence. Proceedings of the National Academy of Sciences of the United States of America *86*, 4868-4871.

Orr, J.W., Keranen, L.M., and Newton, A.C. (1992). Reversible exposure of the pseudosubstrate domain of protein kinase C by phosphatidylserine and diacylglycerol. The Journal of biological chemistry *267*, 15263-15266.

Orr, J.W., and Newton, A.C. (1992). Interaction of protein kinase C with phosphatidylserine. 1. Cooperativity in lipid binding. Biochemistry *31*, 4661-4667.

Orr, J.W., and Newton, A.C. (1994). Intrapeptide regulation of protein kinase C. The Journal of biological chemistry *269*, 8383-8387.

Oster, H., and Leitges, M. (2006). Protein kinase C alpha but not PKCzeta suppresses intestinal tumor formation in ApcMin/+ mice. Cancer research *66*, 6955-6963.

Parissenti, A.M., Kirwan, A.F., Kim, S.A., Colantonio, C.M., and Schimmer, B.P. (1998). Inhibitory properties of the regulatory domains of human protein kinase Calpha and mouse protein kinase Cepsilon. The Journal of biological chemistry *273*, 8940-8945.

Parker, P.J., and Murray-Rust, J. (2004). PKC at a glance. Journal of cell science *117*, 131-132.

Pawson, T. (1995). Protein modules and signalling networks. Nature *373*, 573-580.

Pawson, T. (2007). Dynamic control of signaling by modular adaptor proteins. Current opinion in cell biology *19*, 112-116.

Perez, J.L., Khatri, L., Chang, C., Srivastava, S., Osten, P., and Ziff, E.B. (2001). PICK1 targets activated protein kinase Calpha to AMPA receptor clusters in spines of hippocampal neurons and reduces surface levels of the AMPA-type glutamate receptor subunit 2. The Journal of neuroscience : the official journal of the Society for Neuroscience *21*, 5417-5428.

Perry, A.S., Furusato, B., Nagle, R.B., and Ghosh, S. (2014). Increased aPKC Expression Correlates with Prostatic Adenocarcinoma Gleason Score and Tumor Stage in the Japanese Population. Prostate cancer *2014*, 481697.

Pierce, B.G., Wiehe, K., Hwang, H., Kim, B.H., Vreven, T., and Weng, Z. (2014). ZDOCK server: interactive docking prediction of protein-protein complexes and symmetric multimers. Bioinformatics *30*, 1771-1773.

Pongracz, J., Clark, P., Neoptolemos, J.P., and Lord, J.M. (1995). Expression of protein kinase C isoenzymes in colorectal cancer tissue and their differential activation by different bile acids. International journal of cancer Journal international du cancer *61*, 35-39.

Prevostel, C., Martin, A., Alvaro, V., Jaffiol, C., and Joubert, D. (1997). Protein kinase C alpha and tumorigenesis of the endocrine gland. Hormone research *47*, 140-144.

Pu, Y., Garfield, S.H., Kedei, N., and Blumberg, P.M. (2009). Characterization of the differential roles of the twin C1a and C1b domains of protein kinase C-delta. J Biol Chem *284*, 1302-1312.

Pu, Y.S., Huang, C.Y., Chen, J.Y., Kang, W.Y., Lin, Y.C., Shiu, Y.S., Chuang, S.J., Yu, H.J., Lai, M.K., Tsai, Y.C., Wu, W.J., and Hour, T.C. (2012). Down-regulation of PKCzeta in renal cell carcinoma and its clinicopathological implications. Journal of biomedical science *19*, 39.

Quest, A.F., and Bell, R.M. (1994). The regulatory region of protein kinase C gamma. Studies of phorbol ester binding to individual and combined functional segments expressed as glutathione S-transferase fusion proteins indicate a complex mechanism of regulation by phospholipids, phorbol esters, and divalent cations. The Journal of biological chemistry *269*, 20000-20012.

Quest, A.F., Bloomenthal, J., Bardes, E.S., and Bell, R.M. (1992). The regulatory domain of protein kinase C coordinates four atoms of zinc. The Journal of biological chemistry *267*, 10193-10197.

R-Core-Team (2014). R: A language and environment for statistical computing. R Foundation for Statistical Computing. (Vienna, Austria.).

Ran, F.A., Hsu, P.D., Lin, C.Y., Gootenberg, J.S., Konermann, S., Trevino, A.E., Scott, D.A., Inoue, A., Matoba, S., Zhang, Y., and Zhang, F. (2013). Double nicking by RNA-guided CRISPR Cas9 for enhanced genome editing specificity. Cell *154*, 1380-1389.

Regala, R.P., Weems, C., Jamieson, L., Khoor, A., Edell, E.S., Lohse, C.M., and Fields, A.P. (2005). Atypical protein kinase C iota is an oncogene in human non-small cell lung cancer. Cancer research *65*, 8905-8911.

Reno, E.M., Haughian, J.M., Dimitrova, I.K., Jackson, T.A., Shroyer, K.R., and Bradford, A.P. (2008). Analysis of protein kinase C delta (PKC delta) expression in endometrial tumors. Human pathology *39*, 21-29.

Reyland, M.E. (2007). Protein kinase Cdelta and apoptosis. Biochemical Society transactions *35*, 1001-1004.

Riedel, H., Su, L., and Hansen, H. (1993). Yeast phenotype classifies mammalian protein kinase C cDNA mutants. Molecular and cellular biology *13*, 4728-4735.

Rogers, T.B., Inesi, G., Wade, R., and Lederer, W.J. (1995). Use of thapsigargin to study Ca2+ homeostasis in cardiac cells. Bioscience reports *15*, 341-349.

Ron, D., Chen, C.H., Caldwell, J., Jamieson, L., Orr, E., and Mochly-Rosen, D. (1994). Cloning of an intracellular receptor for protein kinase C: a homolog of the beta subunit of G proteins. Proceedings of the National Academy of Sciences of the United States of America *91*, 839-843.

Ron, D., Luo, J., and Mochly-Rosen, D. (1995). C2 region-derived peptides inhibit translocation and function of beta protein kinase C in vivo. The Journal of biological chemistry *270*, 24180-24187.

Rotenberg, S.A., Zhu, J., Hansen, H., Li, X.D., Sun, X.G., Michels, C.A., and Riedel, H. (1998). Deletion analysis of protein kinase Calpha reveals a novel regulatory segment. Journal of biochemistry *124*, 756-763.

Salzer, E., Santos-Valente, E., Klaver, S., Ban, S.A., Emminger, W., Prengemann, N.K., Garncarz, W., Mullauer, L., Kain, R., Boztug, H., Heitger, A., Arbeiter, K., Eitelberger, F., Seidel, M.G., Holter, W.,

Pollak, A., Pickl, W.F., Forster-Waldl, E., and Boztug, K. (2013). B-cell deficiency and severe autoimmunity caused by deficiency of protein kinase C delta. Blood *121*, 3112-3116.

Schleifenbaum, A., Stier, G., Gasch, A., Sattler, M., and Schultz, C. (2004). Genetically encoded FRET probe for PKC activity based on pleckstrin. Journal of the American Chemical Society *126*, 11786-11787.

Scott, A.M., Antal, C.E., and Newton, A.C. (2013). Electrostatic and Hydrophobic Interactions Differentially Tune Membrane Binding Kinetics of the C2 Domain of Protein Kinase Calpha. J Biol Chem.

Scott, J.D., and Newton, A.C. (2012). Shedding light on local kinase activation. BMC biology *10*, 61.

Sharkey, N.A., Leach, K.L., and Blumberg, P.M. (1984). Competitive inhibition by diacylglycerol of specific phorbol ester binding. Proceedings of the National Academy of Sciences of the United States of America *81*, 607-610.

Shi, F., Telesco, S.E., Liu, Y., Radhakrishnan, R., and Lemmon, M.A. (2010). ErbB3/HER3 intracellular domain is competent to bind ATP and catalyze autophosphorylation. Proceedings of the National Academy of Sciences of the United States of America *107*, 7692-7697.

Sieber, F.E., Traystman, R.J., Brown, P.R., and Martin, L.J. (1998). Protein kinase C expression and activity after global incomplete cerebral ischemia in dogs. Stroke; a journal of cerebral circulation *29*, 1445-1452; discussion 1452-1443.

Solodukhin, A.S., Kretsinger, R.H., and Sando, J.J. (2007). Initial three-dimensional reconstructions of protein kinase C delta from two-dimensional crystals on lipid monolayers. Cellular signalling *19*, 2035-2045.

Sonnenburg, E.D., Gao, T., and Newton, A.C. (2001). The Phosphoinositide-dependent Kinase, PDK-1, Phosphorylates Conventional Protein Kinase C Isozymes by a Mechanism That Is Independent of Phosphoinositide 3-Kinase. Journal of Biological Chemistry *276*, 45289-45297.

Stahelin, R.V., and Cho, W. (2001). Roles of calcium ions in the membrane binding of C2 domains. Biochem J *359*, 679-685.

Stahelin, R.V., Digman, M.A., Medkova, M., Ananthanarayanan, B., Rafter, J.D., Melowic, H.R., and Cho, W. (2004). Mechanism of diacylglycerol-induced membrane targeting and activation of protein kinase Cdelta. J Biol Chem *279*, 29501-29512.

Stahelin, R.V., Kong, K.F., Raha, S., Tian, W., Melowic, H.R., Ward, K.E., Murray, D., Altman, A., and Cho, W. (2012). Protein kinase Ctheta C2 domain is a phosphotyrosine binding module that plays a key role in its activation. J Biol Chem *287*, 30518-30528.

Staudinger, J., Lu, J., and Olson, E.N. (1997). Specific interaction of the PDZ domain protein PICK1 with the COOH terminus of protein kinase C-alpha. J Biol Chem *272*, 32019-32024.

Staudinger, J., Zhou, J., Burgess, R., Elledge, S.J., and Olson, E.N. (1995). PICK1: a perinuclear binding protein and substrate for protein kinase C isolated by the yeast two-hybrid system. J Cell Biol *128*, 263-271.

Stebbins, E.G., and Mochly-Rosen, D. (2001). Binding specificity for RACK1 resides in the V5 region of beta II protein kinase C. The Journal of biological chemistry *276*, 29644-29650.

Stensman, H., and Larsson, C. (2007). Identification of acidic amino acid residues in the protein kinase C alpha V5 domain that contribute to its insensitivity to diacylglycerol. The Journal of biological chemistry *282*, 28627-28638.

Stensman, H., Raghunath, A., and Larsson, C. (2004). Autophosphorylation suppresses whereas kinase inhibition augments the translocation of protein kinase Calpha in response to diacylglycerol. The Journal of biological chemistry *279*, 40576-40583.

Stewart, M.D., Morgan, B., Massi, F., and Igumenova, T.I. (2011). Probing the determinants of diacylglycerol binding affinity in the C1B domain of protein kinase Calpha. Journal of molecular biology *408*, 949-970.

Suga, K., Sugimoto, I., Ito, H., and Hashimoto, E. (1998). Down-regulation of protein kinase C-alpha detected in human colorectal cancer. Biochemistry and molecular biology international *44*, 523-528.

Sun, S., Schiller, J.H., and Gazdar, A.F. (2007). Lung cancer in never smokers--a different disease. Nature reviews Cancer *7*, 778-790.

Symonds, J.M., Ohm, A.M., Carter, C.J., Heasley, L.E., Boyle, T.A., Franklin, W.A., and Reyland, M.E. (2011). Protein kinase C delta is a downstream effector of oncogenic K-ras in lung tumors. Cancer research *71*, 2087-2097.

Szallasi, Z., Bogi, K., Gohari, S., Biro, T., Acs, P., and Blumberg, P.M. (1996). Non-equivalent roles for the first and second zinc fingers of protein kinase Cdelta. Effect of their mutation on phorbol ester-induced translocation in NIH 3T3 cells. J Biol Chem *271*, 18299-18301.

Szallasi, Z., Smith, C.B., Pettit, G.R., and Blumberg, P.M. (1994). Differential regulation of protein kinase C isozymes by bryostatin 1 and phorbol 12-myristate 13-acetate in NIH 3T3 fibroblasts. J Biol Chem *269*, 2118-2124.

Takahashi, M., Mukai, H., Oishi, K., Isagawa, T., and Ono, Y. (2000). Association of immature hypophosphorylated protein kinase cepsilon with an anchoring protein CG-NAP. J Biol Chem *275*, 34592-34596.

Takahashi, M., Shibata, H., Shimakawa, M., Miyamoto, M., Mukai, H., and Ono, Y. (1999). Characterization of a novel giant scaffolding protein, CG-NAP, that anchors multiple signaling enzymes to centrosome and the golgi apparatus. J Biol Chem *274*, 17267-17274.

Takeishi, Y., Ping, P., Bolli, R., Kirkpatrick, D.L., Hoit, B.D., and Walsh, R.A. (2000). Transgenic overexpression of constitutively active protein kinase C epsilon causes concentric cardiac hypertrophy. Circulation research *86*, 1218-1223.

Varga, A., Czifra, G., Tallai, B., Nemeth, T., Kovacs, I., Kovacs, L., and Biro, T. (2004). Tumor grade-dependent alterations in the protein kinase C isoform pattern in urinary bladder carcinomas. European urology *46*, 462-465.

Verbeek, D.S., Knight, M.A., Harmison, G.G., Fischbeck, K.H., and Howell, B.W. (2005). Protein kinase C gamma mutations in spinocerebellar ataxia 14 increase kinase activity and alter membrane targeting. Brain : a journal of neurology *128*, 436-442.

Violin, J.D., Zhang, J., Tsien, R.Y., and Newton, A.C. (2003). A genetically encoded fluorescent reporter reveals oscillatory phosphorylation by protein kinase C. The Journal of cell biology *161*, 899-909.

Walsh, M.F., Woo, R.K., Gomez, R., and Basson, M.D. (2004). Extracellular pressure stimulates colon cancer cell proliferation via a mechanism requiring PKC and tyrosine kinase signals. Cell proliferation *37*, 427-441.

Wickham, H. (2009). ggplot2: elegant graphics for data analysis (Springer New York).

Wu, B., Zhou, H., Hu, L., Mu, Y., and Wu, Y. (2013). Involvement of PKCalpha activation in TF/VIIa/PAR2-induced proliferation, migration, and survival of colon cancer cell SW620. Tumour biology : the journal of the International Society for Oncodevelopmental Biology and Medicine *34*, 837-846.

Wu-Zhang, A.X., Murphy, A.N., Bachman, M., and Newton, A.C. (2012). Isozyme-specific interaction of protein kinase Cdelta with mitochondria dissected using live cell fluorescence imaging. J Biol Chem *287*, 37891-37906.

Wynne, J.P., Wu, J., Su, W., Mor, A., Patsoukis, N., Boussiotis, V.A., Hubbard, S.R., and Philips, M.R. (2012). Rap1-interacting adapter molecule (RIAM) associates with the plasma membrane via a proximity detector. J Cell Biol *199*, 317-330.

Xu, R.X., Pawelczyk, T., Xia, T.H., and Brown, S.C. (1997). NMR structure of a protein kinase C-gamma phorbol-binding domain and study of protein-lipid micelle interactions. Biochemistry *36*, 10709-10717.

Yang, J., Cron, P., Thompson, V., Good, V.M., Hess, D., Hemmings, B.A., and Barford, D. (2002). Molecular mechanism for the regulation of protein kinase B/Akt by hydrophobic motif phosphorylation. Mol Cell *9*, 1227-1240.

Yang, J., Kennedy, E.J., Wu, J., Deal, M.S., Pennypacker, J., Ghosh, G., and Taylor, S.S. (2009). Contribution of non-catalytic core residues to activity and regulation in protein kinase A. The Journal of biological chemistry *284*, 6241-6248.

Yang, Y., and Igumenova, T.I. (2013). The C-terminal v5 domain of protein kinase calpha is intrinsically disordered, with propensity to associate with a membrane mimetic. PloS one *8*, e65699.

Yates, T. (2011). annmap: Genome annotation and visualisation package pertaining to Affymetrix arrays and NGS analysis.

Yoshida, K., Liu, H., and Miki, Y. (2006). Protein kinase C delta regulates Ser46 phosphorylation of p53 tumor suppressor in the apoptotic response to DNA damage. The Journal of biological chemistry *281*, 5734-5740.

Young, S., Parker, P.J., Ullrich, A., and Stabel, S. (1987). Down-regulation of protein kinase C is due to an increased rate of degradation. The Biochemical journal *244*, 775-779.

Young, S., Rothbard, J., and Parker, P.J. (1988). A monoclonal antibody recognising the site of limited proteolysis of protein kinase C. Inhibition of down-regulation in vivo. European journal of biochemistry / FEBS *173*, 247-252.

Zhang, L., Huang, J., Yang, N., Liang, S., Barchetti, A., Giannakakis, A., Cadungog, M.G., O'Brien-Jenkins, A., Massobrio, M., Roby, K.F., Katsaros, D., Gimotty, P., Butzow, R., Weber, B.L., and Coukos, G. (2006). Integrative genomic analysis of protein kinase C (PKC) family identifies PKCiota as a biomarker and potential oncogene in ovarian carcinoma. Cancer research *66*, 4627-4635.

Zhang, L.L., Cao, F.F., Wang, Y., Meng, F.L., Zhang, Y., Zhong, D.S., and Zhou, Q.H. (2014). The protein kinase C (PKC) inhibitors combined with chemotherapy in the treatment of advanced non-small cell lung cancer: meta-analysis of randomized controlled trials. Clinical & translational oncology : official publication of the Federation of Spanish Oncology Societies and of the National Cancer Institute of Mexico.

Zheng, Y., Zhang, L., Jia, X., Wang, H., and Hu, Y. (2012). Interaction of protein inhibitor of activated STAT 2 (PIAS2) with receptor of activated C kinase 1, RACK1. FEBS letters *586*, 122-126.

Zhu, Y., Dong, Q., Tan, B.J., Lim, W.G., Zhou, S., and Duan, W. (2005). The PKCalpha-D294G mutant found in pituitary and thyroid tumors fails to transduce extracellular signals. Cancer Res *65*, 4520-4524.